The Role of Hydro-Climatic Changes on Paleolandscape Evolution and on Prehistoric Settlement During the Last Humid-Arid Cycle in the Horn of Africa

(VOLUME B, Supplementary Materials)

Carlo Mologni

Géoazur UMR 7329

Contents

Chapter BI

Supplementary materials

BI.1 Chapter-IV Supplementary Materials

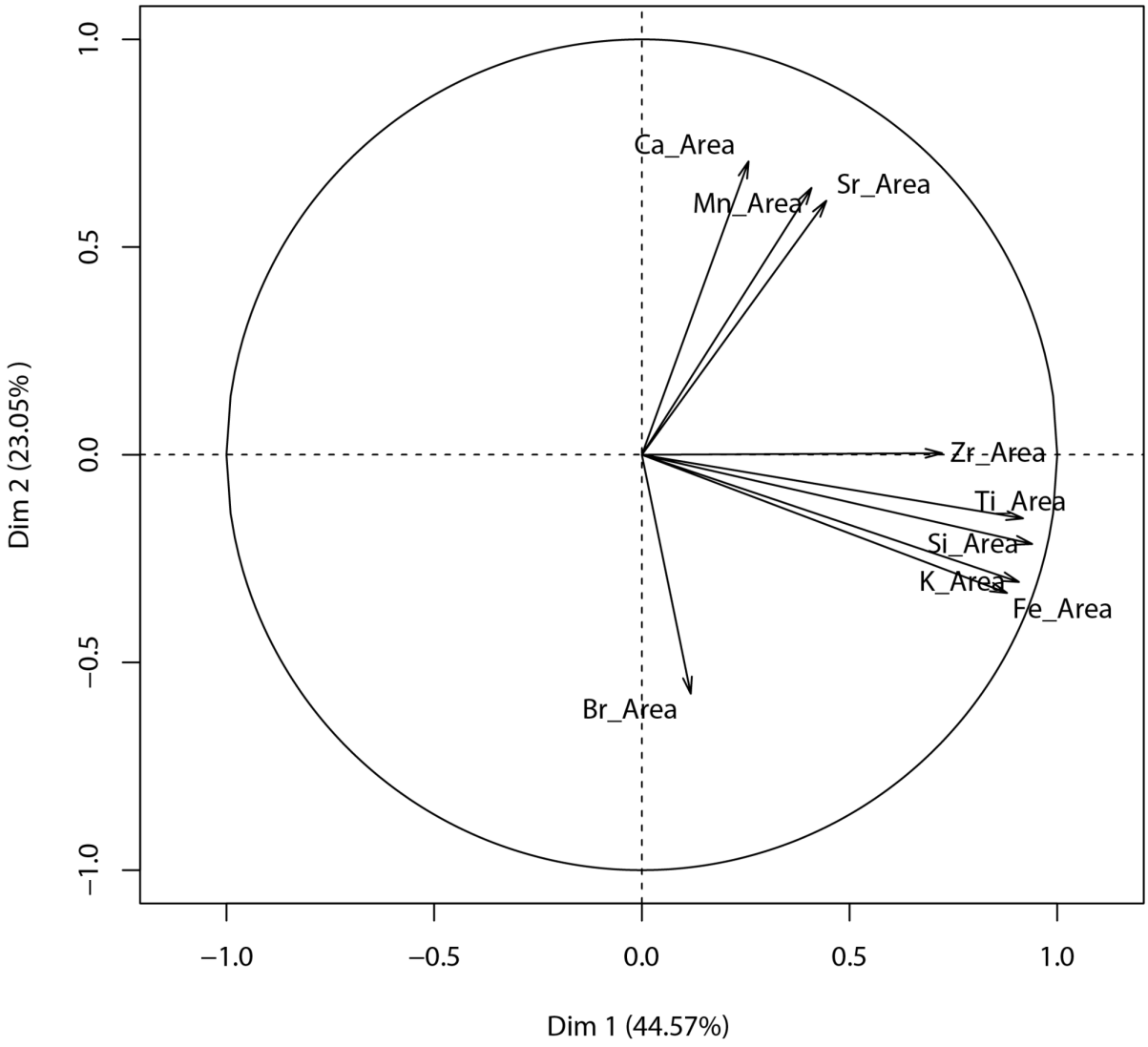

Figure BI.1: Principal components analysys variables on T1 event-layers from the core MD04-2726, which cleary differentiatng the terrigenous elemental components (Zr, Ti, Si, K, Fr) and the authigenic (Mn, redox processes) or marine primary productivity (Ca, Sr) elemental components.

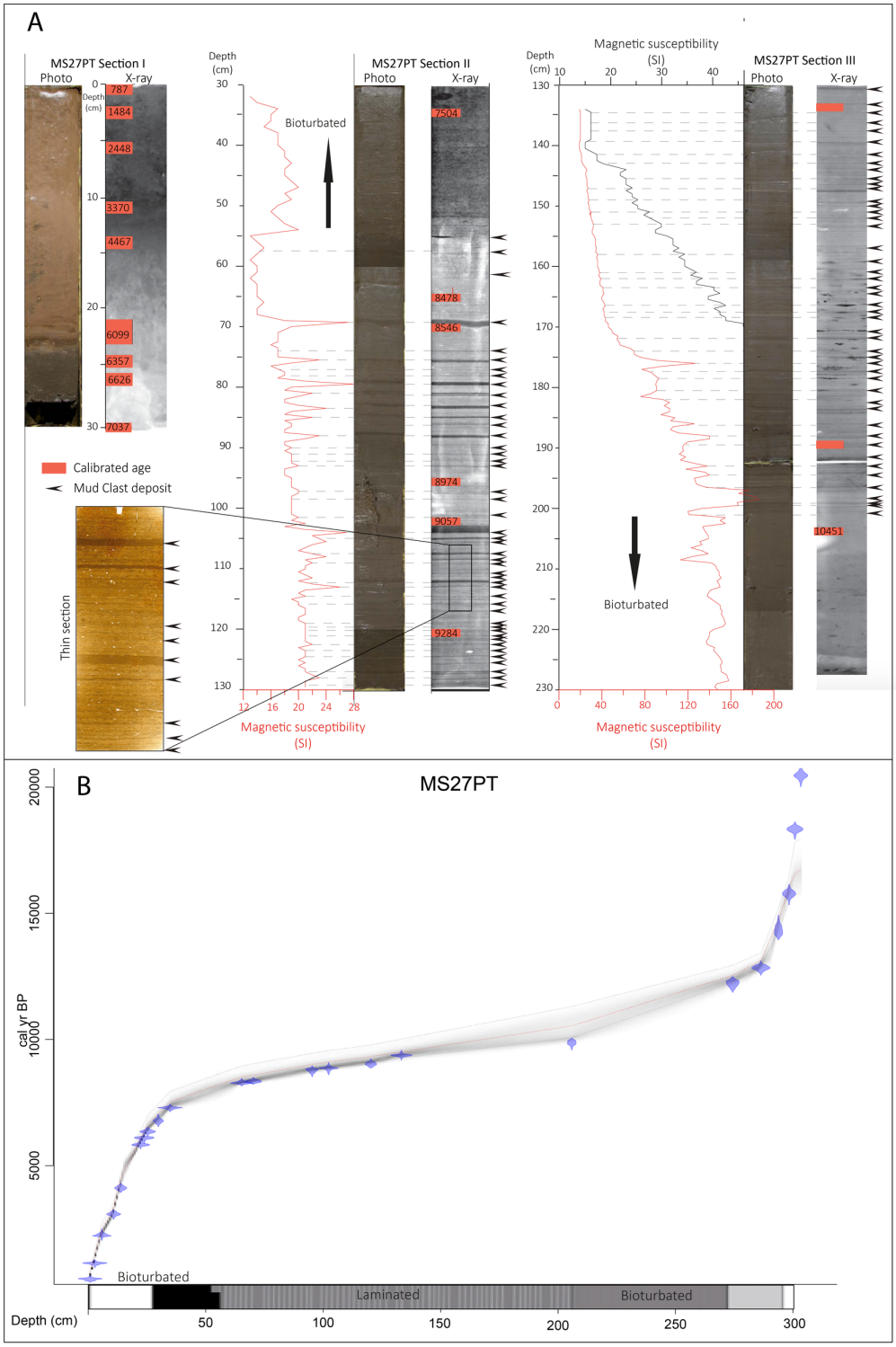

Figure BI.2: (continued)

Event layer type	Total depth (cm)	Age (yr cal. BP)	Thickness (cm)	Q90/Q50
T1α	156	7337	3.5	5,99799197
T1α	159	7346	2	6,89673551
T1α	181	7410	2.5	5,24381625
T1α	194	7452	3	10,7729885
T1α	218	7573	2.5	9,80263158
T1α	221	7588	3.5	10,2992701
T1α	246	7690	1.5	12,2478485
T1α	252	7713	2	5,47855228
T1α	285	7832	2	3,79764706
T1α	327	7983	0.5	6,35176991
T1α	347	8056	2	12,4965229
T1α	353	8078	0.5	5,41881919
T1α	354	8081	1	5,56812339
T1α	378	8187	2	6,15849057
T1α	389	8246	1.5	6,9877551
T1α	393	8268	2	5,67836676
T1α	398	8294	2.2	9,87432868
T1α	406	8337	2.2	5,62331839
T1α	418	8400	2.5	8,70998415
T1α	430	8411	2.5	7,54265403
T1α	443	8463	2	8,74351978
T1α	449	8532	3	7,06008584
T1α	451,5	8564	2	5,31273644
T1α	462	8577	1	5,12676056
T1α	469	8633	1.5	5,73061224
T1α	474,8	8670	2.5	6,36024423
T1α	505,5	8701	2	4,86445013
T1α	507	8844	0.7	4,17018284
T1α	511	8851	2.5	4,94906621
T1α	520	8870	4	10,137577
T1α	526,5	8911	3	6,40885417
T1α	541	8942	2	4,18550725
T1α	543	9010	1.5	5,19251337
T1α	546	9020	1.5	6,61469265
T1α	549	9034	1.5	4,76447625
T1α	553	9049	2	5,45931759
T1α	557	9070	2.3	4,52331606
T1α	560	9096	2	5,79697987
T1α	570	9116	2	6,67220903
T1α	572	9183	0.4	6,80763116
T1α	576	9197	1	5,55950266
T1α	578	9223	1	6,39450355
T1α	581	9237	1	5,22222222
T1α	595,5	9257	1	7,51265823
T1α	607	9353	1	6,99491094
T1α	611	9430	1	4,03819174
T1α	642,5	9457	1.2	6,69899666
T1α	649,2	9668	0.8	5,2406639
T1α	654	9712	0.8	4,32824427

Table BI.1: Total depth (cm), age (yr cal. BP), thickness (cm) and Q90/Q50 of events-layers (T1α, T1β) counted on MD04-2726 piston core.

Event layer type	Total depth (cm)	Age (yr cal. BP)	Thickness (cm)	Q90/Q50
T2	150	7324	1.5	9,705685619
T2	168	7376	1.5	3,07526638
T2	185	7426	0.3	11,2385159
T2	192	7447	3	7,294420601
T2	259	7742	2	4,87698987
T2	263	7757	2	6,631799163
T2	279	7815	1	12,6958457
T2	304	7905	2.5	4,893884892
T2	308	7919	1.5	10,95126354
T2	313	7938	1	3,980662983
T2	426	8446	2	5,338827839
T2	477	8717	0.3	11,03811659
T2	481	8736	0.5	10,87206266
T2	487	8764	0.3	5,182952183
T2	490	8777	0.3	4,908433735
T2	532	8973	0.3	10,34259259
T2	620,5	9280	0.2	5,731443995

Table BI.2: Total depth (cm), age (yr cal. BP), thickness (cm) and Q90/Q50 of events-layers (T2) counted on MD04-2726 piston core.

Sediment Type	Depth (cm)	Age (yr cal. BP)	Incertitude (± yr)	Nd^{143}/Nd^{144}	Nd (<63 µm)
Hemipelagic	24,5	7324	7324	0,512330	-6,01
Hemipelagic	37	7376	7376	0,512328	-6,05
Hemipelagic	56	7426	7426	0,512374	-5,15
Hemipelagic	75	7447	7447	0,512421	-4,23
Hemipelagic	76,1	7742	7742	0,512403	-4,58
Hemipelagic	83	7757	7757	0,512482	-3,04
Hemipelagic	91	7815	7815	0,512406	-4,53
Hemipelagic	103	7905	7905	0,512407	-4,51
Hemipelagic	115	7919	7919	0,512450	-3,67
Hemipelagic	123	7938	7938	0,512416	-4,33
Hemipelagic	142	8446	8446	0,512421	-4,23
Hemipelagic	177	8717	8717	0,512402	-4,60
Hemipelagic	262	8736	8736	0,512396	-4,72
Hemipelagic	499	8764	8764	0,512478	-3,12
Hemipelagic	508	8777	8777	0,512441	-3,84
Hemipelagic	569	8973	8973	0,512461	-3,45
Hemipelagic	694	9280	9280	0,512480	-3,08
T1 event-layer	167	7365	102	0,512461	-3,45
T1 event-layer	222	7602	91	0,51243577	-3,94
T1 event-layer	328,5	8032	111	0,512429	-4,08
T1 event-layer	430,5	8617	197	0,512471	-3,26
T1 event-layer	633,6	9566	195	0,512509	-2,52
T1 event-layer	636,1	9632	191	0,512489	-2,91

Table BI.3: Total depth (cm), age (yr cal. BP), $^{143}Nd/^{144}Nd$ ratio and ϵNd values on <63 µm fraction of hemipelagic and T1 event-layers sedimentary facies type on MD04-2726 core.

Sediment Type	Depth (cm)	Age (yr cal. BP)	Nd (<63 µm)
Hemipelagic	1	953	-9,69495043
Hemipelagic	6	2536	-10,0070615
Hemipelagic	9	3037	-10,533749
Hemipelagic	10	3205	-10,7873392
Hemipelagic	13	4251	-7,54918676
Hemipelagic	16	5116	-7,45
Hemipelagic	25	6604	-5,41
Hemipelagic	29	6992	-5,55947862
Hemipelagic	32	7270	-6,00579281
Hemipelagic	33	7360	-5,96287229
Hemipelagic	34	7442	-4,8
Hemipelagic	34,5	7500	-6,28544176
Hemipelagic	36,5	7596	-5,84862684
Hemipelagic	38,9	7667	-6,48393624
Hemipelagic	40,5	7717	-6,17802863
Hemipelagic	41,5	7749	-6,17617475
Hemipelagic	42	7764	-7,19806179
Hemipelagic	43,5	7814	-6,12623064
Hemipelagic	45,5	7874	-6,20524514
Hemipelagic	47,5	7941	-5,63849673
Hemipelagic	49,5	8010	-5,67061752
Hemipelagic	50	8045	-3,41371494
Hemipelagic	51,5	8070	-6,46524308
Hemipelagic	53,5	8135	-5,63989402
Hemipelagic	55,5	8202	-5,47718414
Hemipelagic	57,5	8264	-5,3496133
Hemipelagic	59,5	8332	-5,19158809
Hemipelagic	65,5	8475	-5,13293649
Hemipelagic	67,5	8502	-4,88711871
Hemipelagic	70,5	8525	-4,68980951
Hemipelagic	69	8549	-6,08616607
Hemipelagic	95,5	8967	-4,46798897
Hemipelagic	103	9053	-4,46708984
Hemipelagic	108,5	9115	-4,50163616
Hemipelagic	111,5	9147	-4,32248789
Hemipelagic	113,5	9169	-5,4200635
Hemipelagic	117,5	9213	-4,89384893
Hemipelagic	120,5	9247	-4,67281317
Hemipelagic	123,5	9287	-4,94328432
Hemipelagic	126,5	9325	-4,61670855
Hemipelagic	136	9440	-5,03
Hemipelagic	141	9498	-4,77
Hemipelagic	146	9558	-4,65
Hemipelagic	156	9679	-4,67
Hemipelagic	163	9762	-4,64
Hemipelagic	200	10159	-4,79870786
Hemipelagic	205	10211	-4,64265232
Mud Clast	69	8517	-3,98
Mud Clast	80	8712	-4,64265232
Mud Clast	84	8779	-7,88080478
Mud Clast	89	8862	-4,50610372
Mud Clast	103	9045	-3,41
Mud Clast	105,5	9075	-3,377718
Mud Clast	112	9144	-4,36955512
Mud Clast	151	9608	-4,23
Mud Clast	171	9838	-3,87
Mud Clast	177	9903	-4,58413149
Mud Clast	193	10075	-3,87

Table BI.4: Total depth (cm), age (yr cal. BP) and ϵNd values on <63 µm fraction of hemipelagic Mud Clasts sedimentary facies type on MS27PT core.

Figure BI.2: A) Orthophoto and X-ray images of sections I-II-III of the core MS27PT, with the magnetic susceptibility values mesured with a Bartington MS2E each 5mm (red and black lines) against depth; the localisation of Mud Clast beds (black arrows) presented in the paper (Fig 8d); the depth of radiocarbone ages (G. ruber alba, red squares, yr cal. BP) already published in Menot et al., 2020 and recalculated in this paper using the Bacon so□ware (Blaauw and Christen, 2011) to homogenize the age model of the three cores compared; and the scan of one thin section with some Mud Clast beds indicated with black arrows. B) Age-model of the core MS27PT obtained by a Bayesian approach that was realized (as well as the plot) using the Bacon software (Blaauw and Christen, 2011), with at the bottom the schematic lithostratigraphy of the core MS27PT.

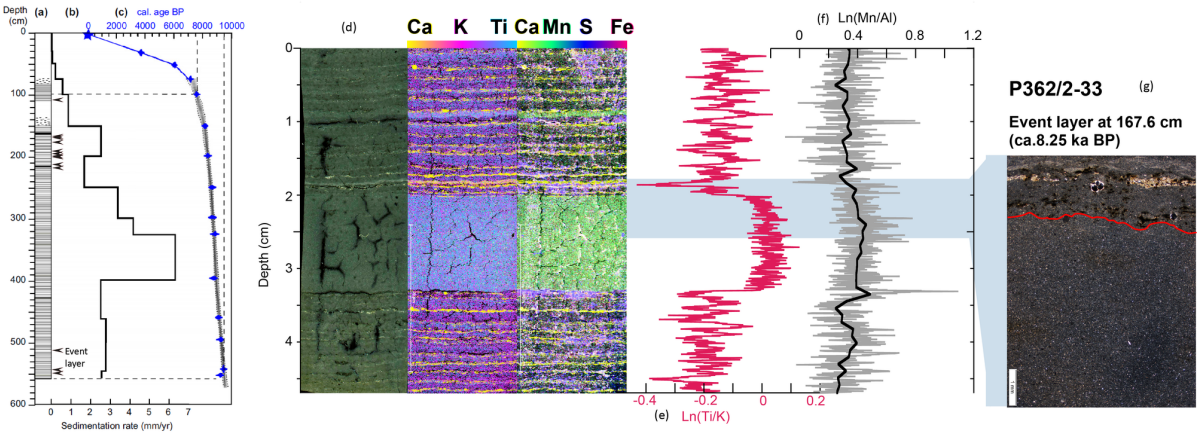

Figure BI.3: Lithology and age model for core P362/2-33. (a) Log of lithologic changes against depth, with black arrows representing the event-layers (Mud Clasts; Table.S4) presented in the peaper. (b) Changes in sedimentation rates along depth. (c) Violin plot of the calibrated 14C ages,which gives an estimation of the statistical density of the age-depth relationship for eachage. The gray shading represents the age-model obtained by a Bayesian approach that was realized (as well as the plot) using the Bacon software (Blaauw and Christen, 2011). The star at the top of the core represents the estimated age of remnants teamboat cinders. (d) Thin section scan and XRF high resolution scan of the event-layer (Mud Clast at 167.6 cm depth), with Ca (yellow), K (pink), Ti (light blue), Mn (green), S (blue) and Fe (red) values intensities represented. (e) Ti/K ratio of the event-layer (Mud Clast at 167.6 cm depth). (f) Mn/Al ratio of the event-layer (Mud Clast at 167.6 cm depth). (g) Thin section scan showing the transition between the event-layer (Mud Clast at 167.6 cm depth) and the upper hemipelagic sediment.

Sediment type	Depth (cm)	Age (ka cal. BP)	Thickness (mm)
Mud Clast bed	549,5	9,60	6,4
Mud Clast bed	542,2	9,58	2,5
Mud Clast bed	511,4	9,46	3,5
Mud Clast bed	329,6	8,86	8
Mud Clast bed	218,8	8,48	2,4
Mud Clast bed	211,8	8,45	0,9
Mud Clast bed	199,2	8,40	1,1
Mud Clast bed	198,2	8,40	0,6
Mud Clast bed	193,8	8,38	0,5
Mud Clast bed	190,2	8,36	0,9
Mud Clast bed	176,9	8,29	0,9
Mud Clast bed	167,6	8,25	14,5
Mud Clast bed	166,2	8,24	0,7
Mud Clast bed	107,2	7,89	0,7

Table BI.5: Depth (cm), Age (ka cal. BP) and thickness (mm) of Mud Clast beds counted on P362/2-33 core.

BI.2 Chapter-V Supplementary Materials

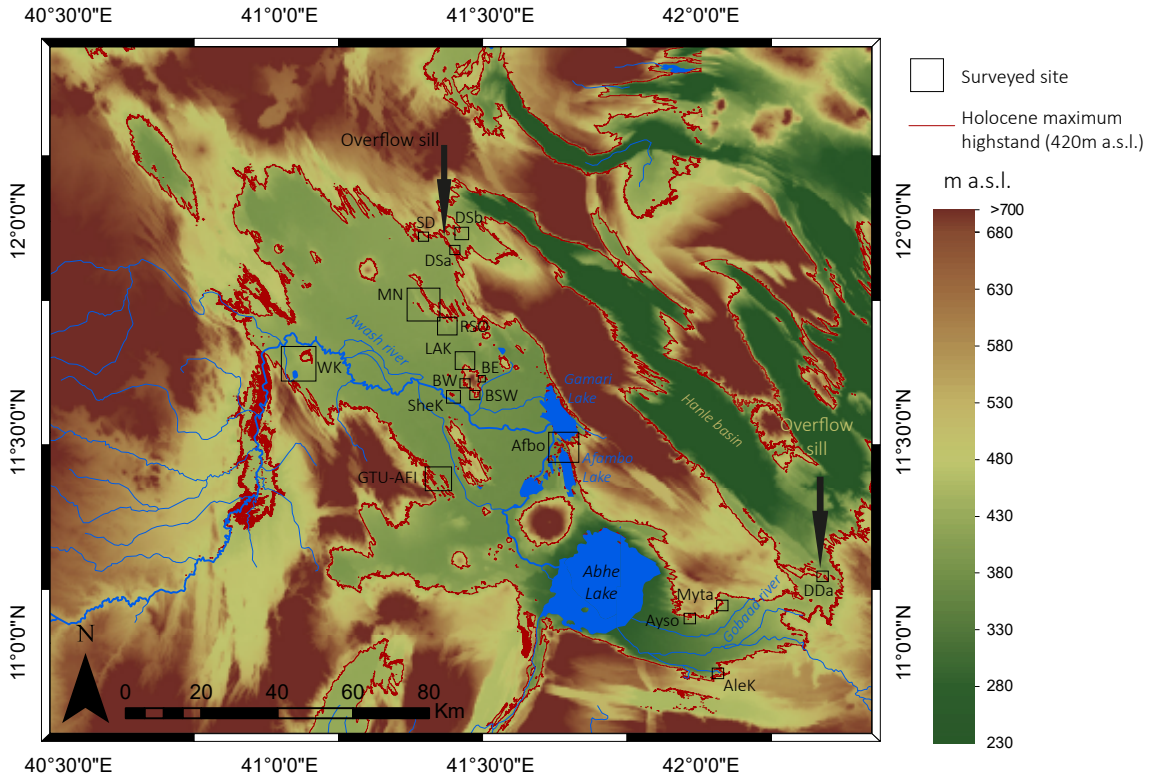

Figure BI.4: Localisation map of surveyed sites across the Lake Abhe basin (black line squares) with the Maximal Holocene Highstand Shoreline (MHHS; red line), the location of the ancient overflow sills (black arrows) and the Hanle basin.

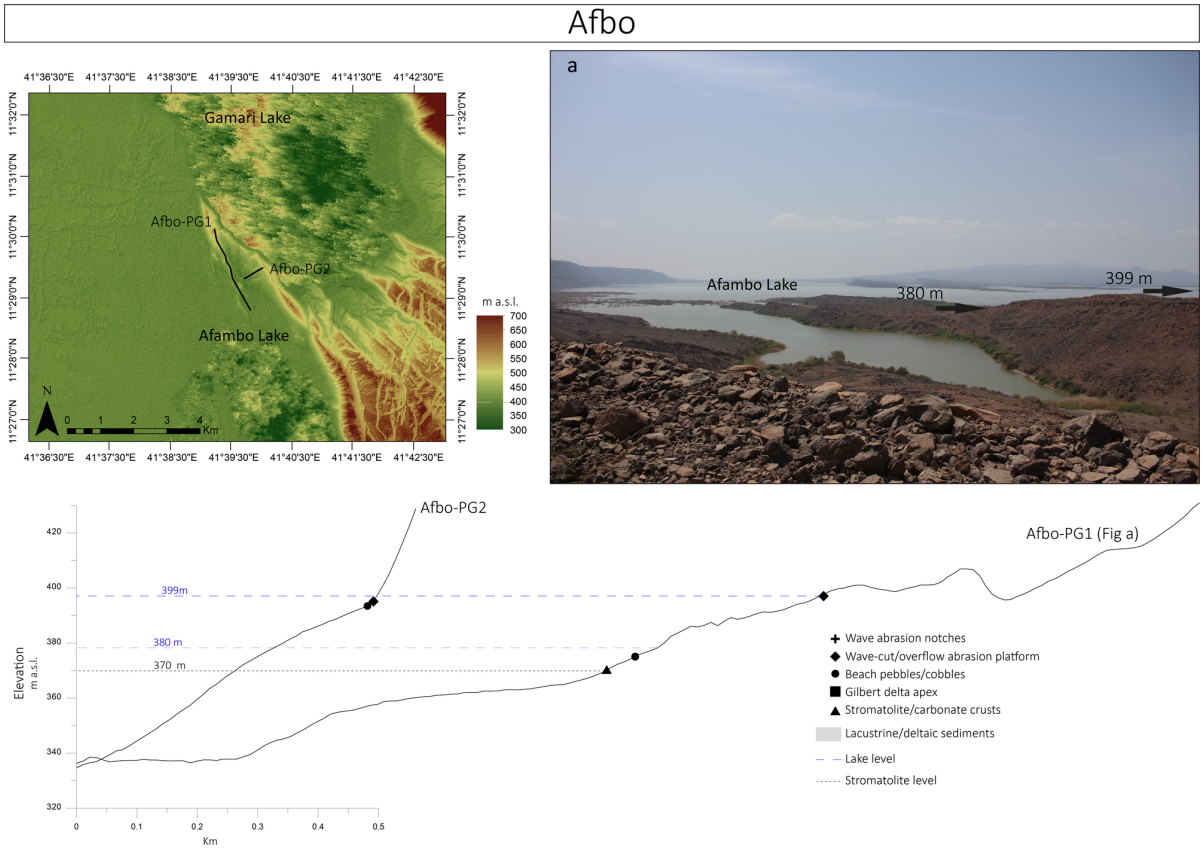

Figure BI.5: Site Afbo ('Afambo') is a thin ridge located on the foot wall of the stratoid series which separate the Gamari and Afambo Lake waterbodies BI.4. Survey profiles were carried out on the S-W flank of the hill and on a headland crest plunging to Afambo Lake. Two well pronounced sub-horizontal abrasion platforms at 399 and 380 m a.s.l were recognized (a), and are associated with beach pebbles concentrations. A stromatolitic cover was observed at 370 m a.s.l.

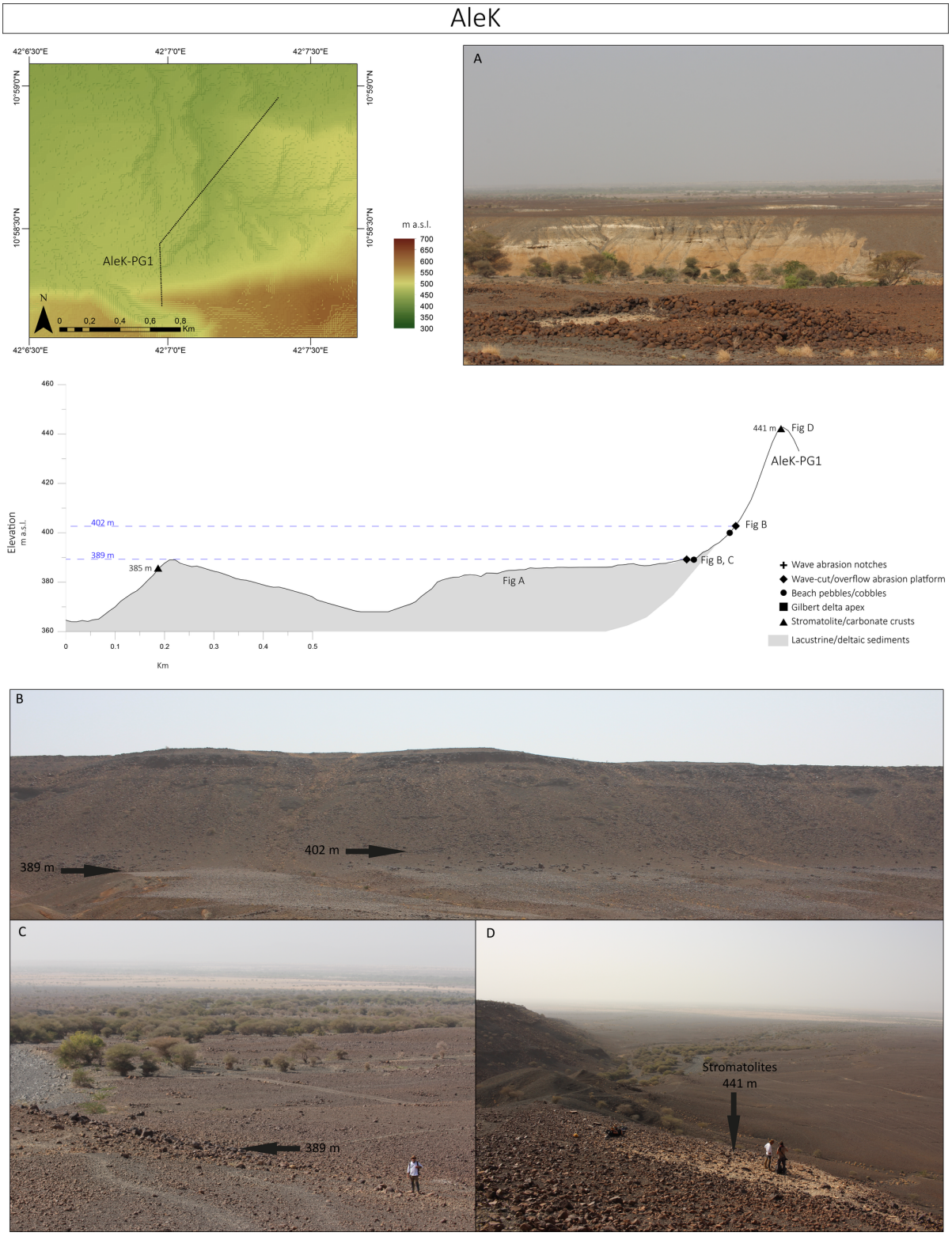

Figure BI.6: Site AleK ('Ara le Koma') is located on a fault scarp on the south ridge of the Gobaad valley (Djibouti) BI.4. Two paleo-shoreline levels were recognised: the upper one (402 m a.s.l.) is characterized by a sorted line of beach clastic material (cobbles), which likely forms a beach ridge (b); the lower (389 m a.s.l.) is clear marked by a well-developed abrasion platform on lacustrine deposits (a), and by a beach ridge feature composed of cobbles and sub-rounded blocks (b,c). Additionally, one stromatolitic level documented at 441 m a.s.l. is associated with a well-developed horizontal abrasion terrace (d), and a second stromatolitic cover at 385 m a.s.l.

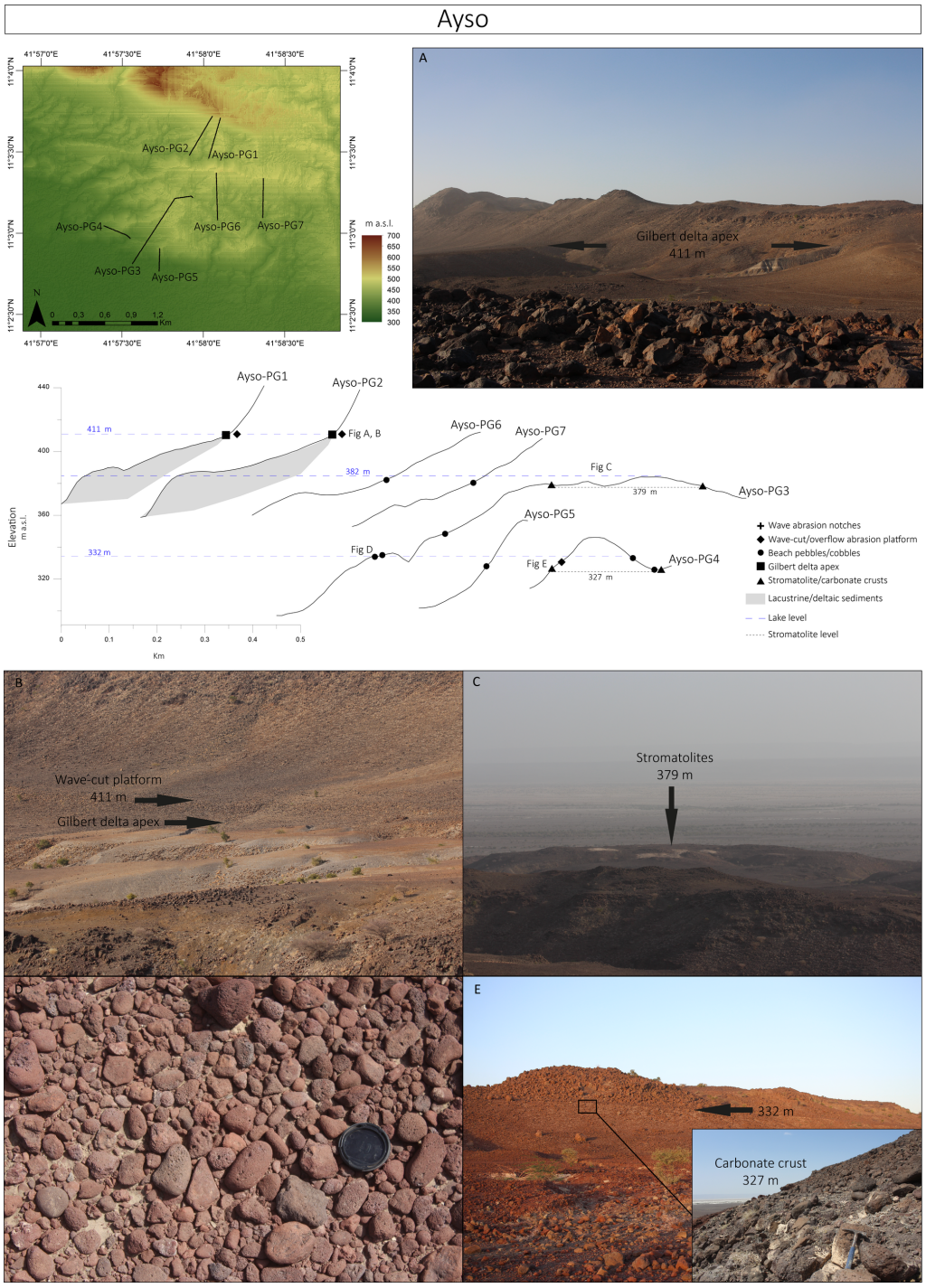

Figure BI.7: Site Ayso ('Aysilo') is located on the northern flank of the Gobaad valley (Djibouti) as a foot wall plateau mainly composed of acid volcanism products (rhyolitic flows and ejecta) which are intercalated in the stratoid series BI.4. Three main paleo-shorelines were recognised. The upper level, at 411 m a.s.l., is materialised by a gilbert-delta apex deposit associated with an overlying sub-horizontal and well-developed wave-cut platform (a,b). The median level is void of any clear upper foreshore geomorphic markers (wave-cut features), however a beach pebbles concentration band at 382 m a.s.l. indicates a paleo-shoreline level overlying this elevation. A thick and large stromatolite cover combined with reworked littoral lacustrine material (379 m a.s.l.; c) is probably associated with the medial paleo-shoreline level. The lower paleo-shoreline level is characterized by a wave-cut abrasion terrace (e) and by abundant beach pebble/cobble concentration lines at 332 m a.s.l. (d). A thin littoral carbonate crust line (microbialite) at 327 m a.s.l. (e insert) is clearly associated with the lower paleo-shoreline of Ayso site.

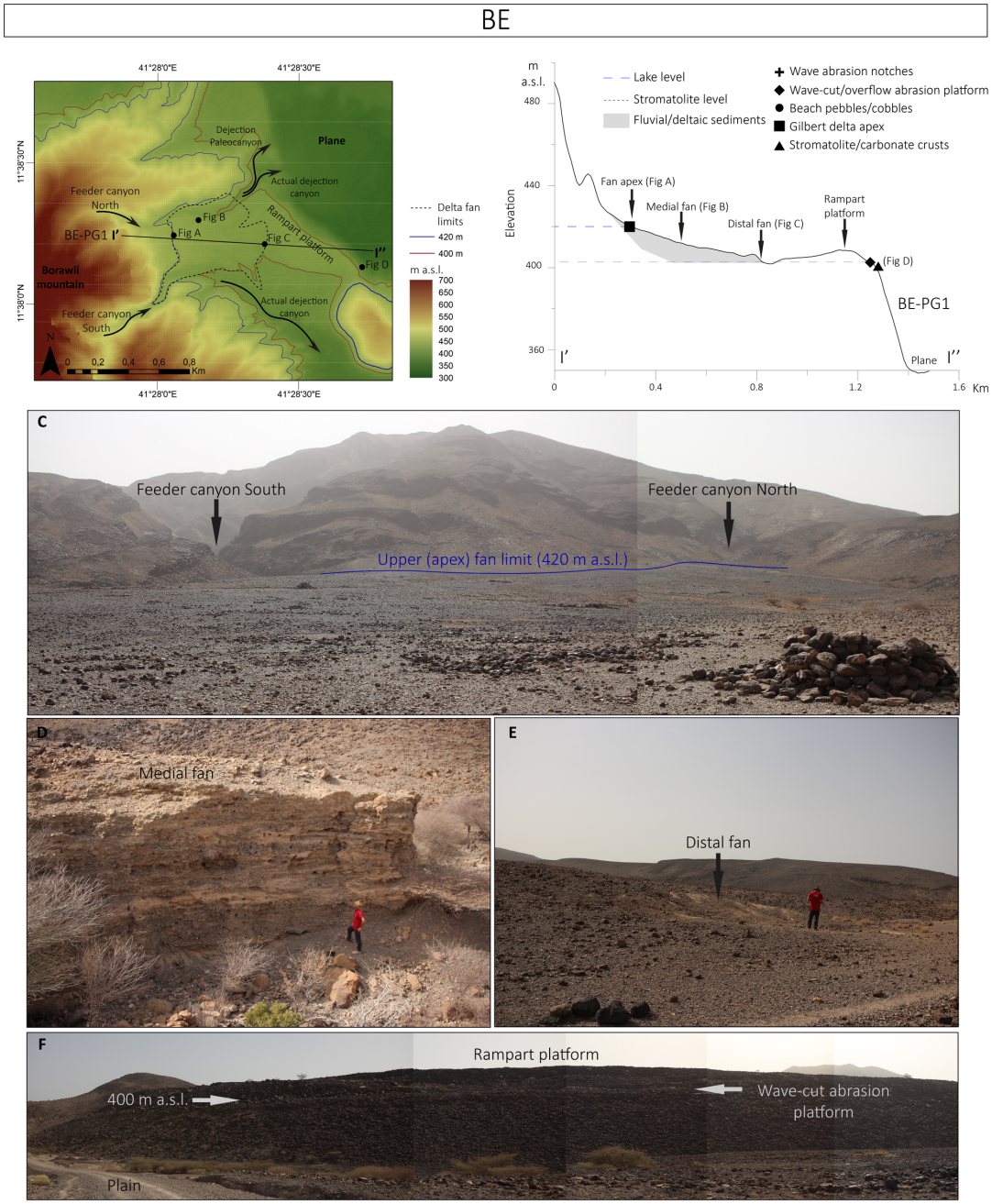

Figure BI.8: Site BE ('Borawli East') is situated on the East flank of the Borawli rhyolitic volcanoBI.4. Because very few faults cut the current topographic surface, the Borawli mountain represents a good landscape feature to localise paleo-shoreline morphologic features. The BE surveyed profile crosses the limit between the rhyolitic flows and the stratoid series, in which an elevated sedimentary flat-fan deposit was formed (materialised as a plateau; c). It is delimited by the rhyolitic slopes to the West, North and South, and by a basaltic rampart to the East. The basin is supplied the mountain detrital load by two feeder canyons and is drained by two dejection channels towards the plain (a, c). The sub-horizontal shape of the fan against the steep mountain slopes suggests a Gilbert-type delta morphology. This hypothesis is confirmed by the horizontal topset layers observed at the medial-proximal part of the fan and by the horizontal shape of the fan apex (d). Thus, we consider the proximal-apex part of the deltaic fan as a marker of an ancient foreshore-line localised at 420 m a.s.l. In addition, delta sediments are heavily incised by the current lateral streams which permit us to easily observe the sequence and to suggest a post-lacustrine torrential erosive transport regime, indicating the drop of the water-level from the top to the base of the basin, thus confirming our interpretations. Finally, at BE site, a wave-cut abrasion terrace is documented at 402 m a.s.l. on the stratoid eastern fault scarp, which is clearly associated with a stromatolitic cover-line at 400 m a.s.l (f).

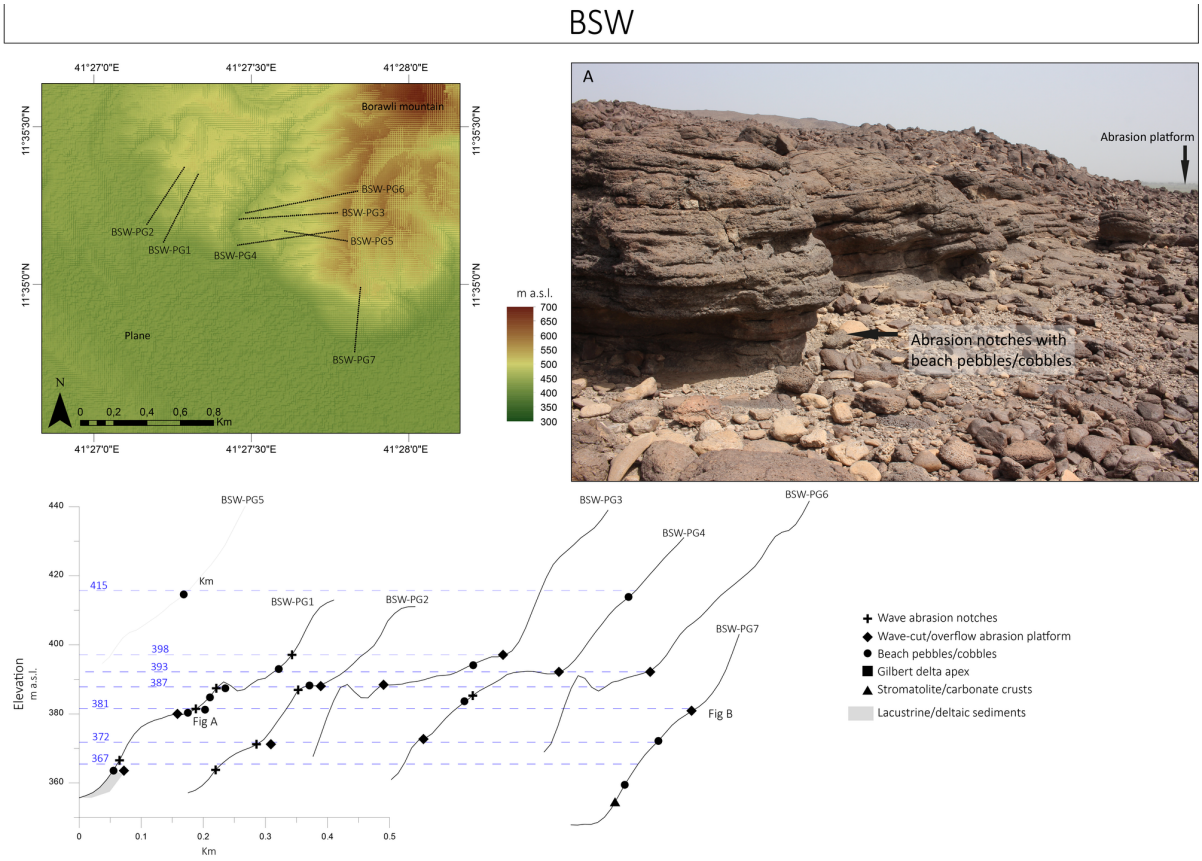

Figure BI.9: Site BSW ('Borawli South-West'), like the BE site, benefits from reduced structural faults, which favored the detection of morphologic features BI.4. Additionally, the rhyolitic and ignimbritic outcrops of the South-West flank of Borawli mountain provide more pronounced wave erosion features. For this reason, we counted several well-developed paleo-shorelines. At 415 m a.s.l. some beach cobbles were observed without any clear upper-shore morphologic marker. At 398 m a.s.l. a well-developed wave-cut notches and abrasion platforms indicate an ancient shoreline at this elevation (a). A few meters below (393 m a.s.l.) a concentration-line of beach cobbles associated with an abrasion platform could belong to the low foreshore zone of the overlying paleo-shoreline or indicate an additional paleolake-level. Downward, several wave-cut notches associated with abundant beach pebbles/cobbles and with large and well-developed abrasion platforms indicate a series of paleo-shorelines at 387, 381, 372 and 367 m a.s.l. Only one stromatolite level is documented at 354 m a.s.l.

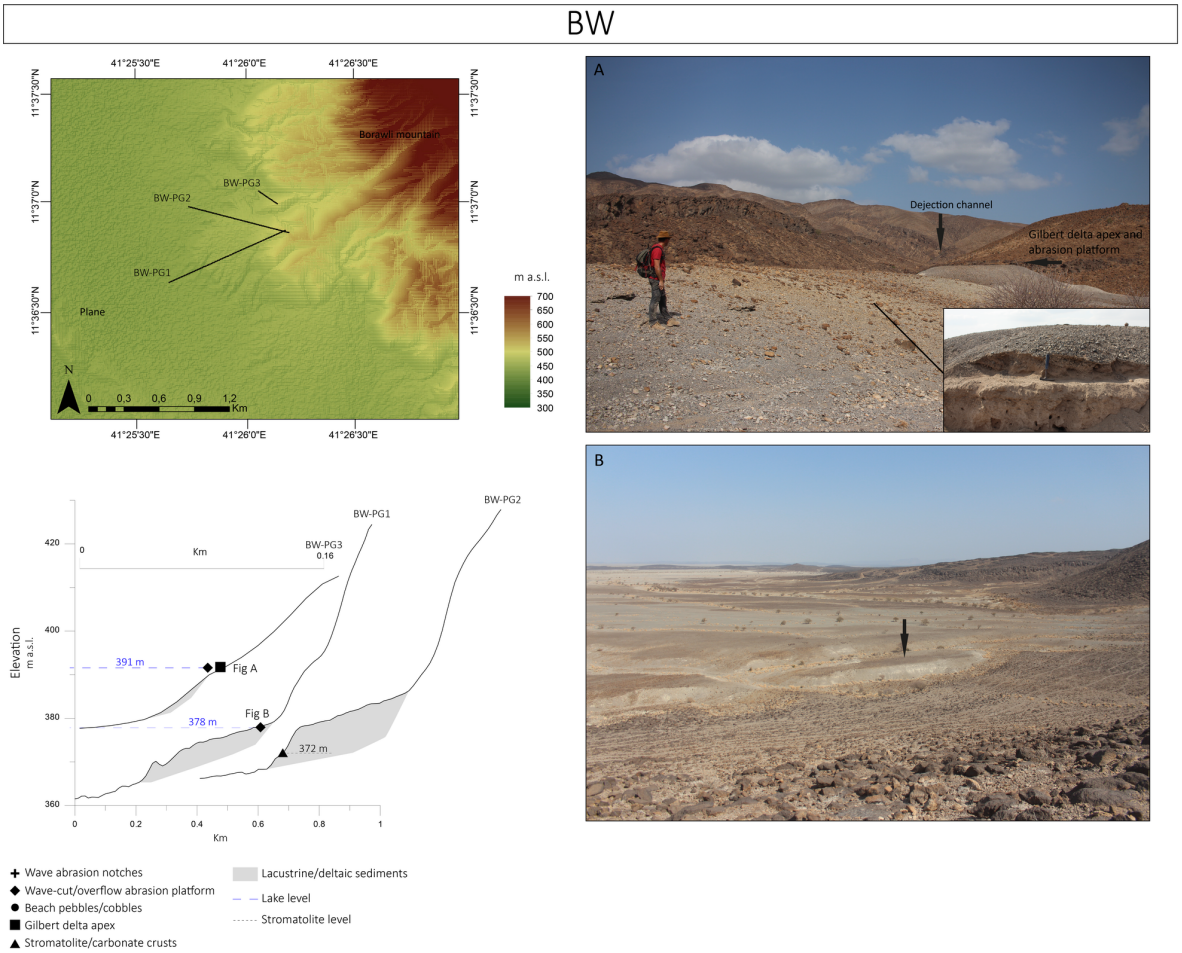

Figure BI.10: Site BW ('Borawli West') is characterized by well-preserved Gilbert-type delta deposits posed on the West flank of Borawli mountain BI.4(a). At 391 m a.s.l. a sub-horizontal delta apex, associated with an abrasion terrace feature, indicates a paleo-shoreline at this level. On the delta section the offshore-transition is clearly observable from fine lacustrine deposit, through the bottomset layers to the foreset progradation (a), suggesting that these deposits and the related paleo-shoreline were probably developed following a regression from previous higher lake level. A lower level was also localised at 379 m a.s.l., materialised in a well-developed wave-cut abrasion platform on nearshore sediments (b).

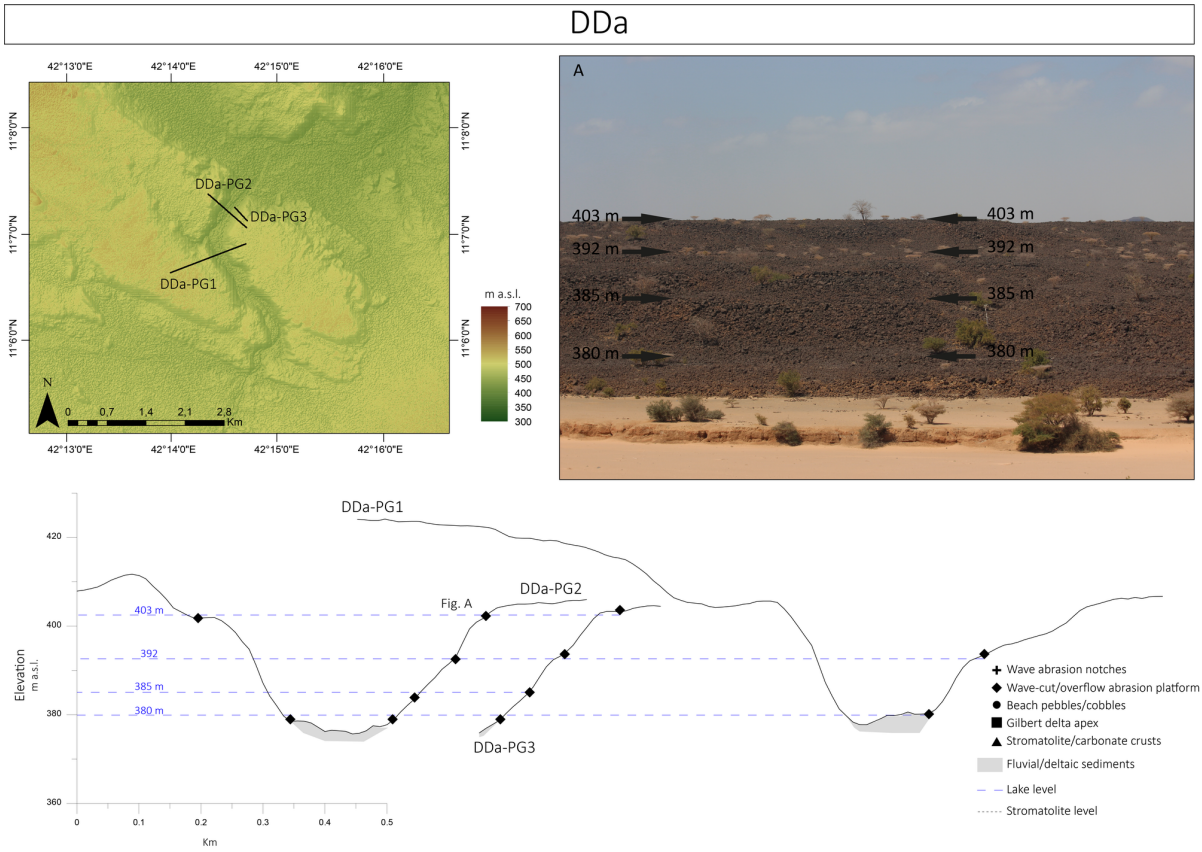

Figure BI.11: Site DDa ('Deversoir Djibouti A') is located along the first part of the southern overflow sill channel of the Abhe basin, which drained the lake water towards the Hanle basin BI.4. Along the sill, only abrasion platform features were documented, probably due to the high energy of the drainage that occurred through the sill channel. This is confirmed by the thick fan deposit composed of coarse sediments localised at the mouth of the sill channel. On the sill flanks, 4 overflow abrasion terraces were detected at 403, 392, 385, 380 m a.s.l. (a).

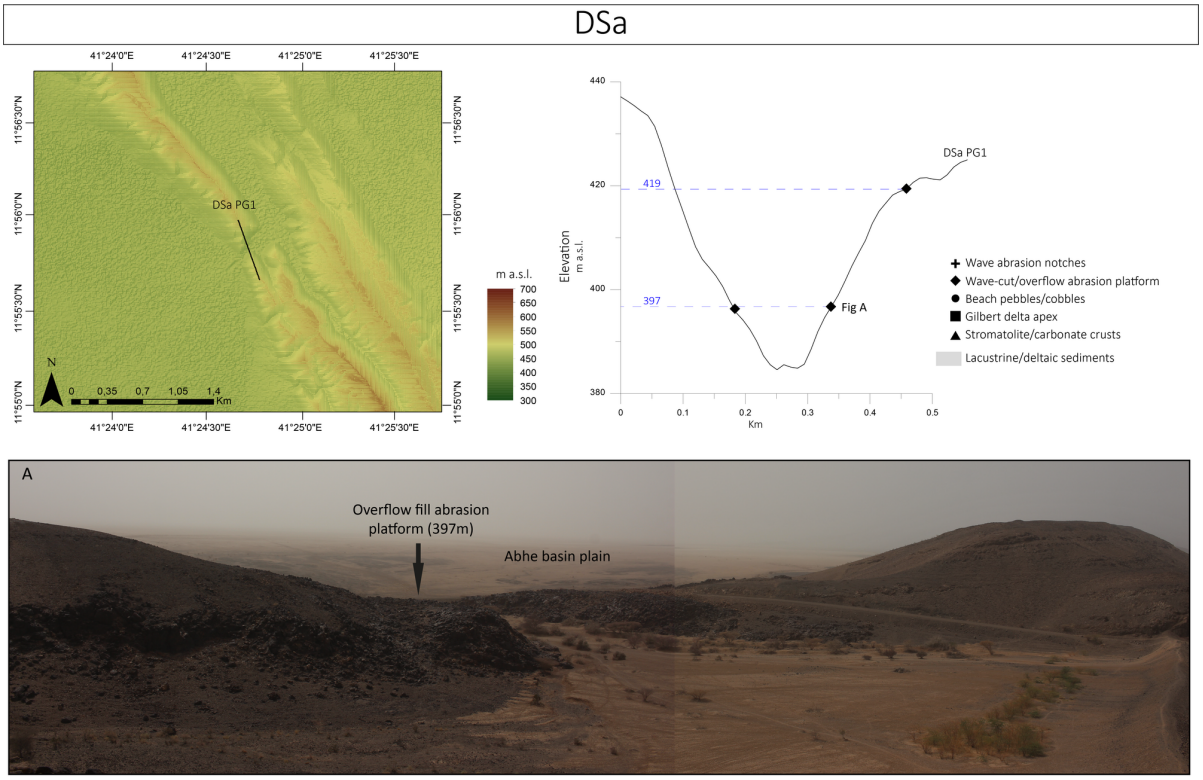

Figure BI.12: Site DSa ('Deversoir Serdo A') corresponds to the proximal part of the northern overflow sill of the Abhe basin, which drained the lake water towards the Hanle basin BI.4. The first and the second part of the sill is intercalated by a small alluvial plane. This sill is higher in elevation then DDa sill, thus it potentially records only the more ancient and higher drainage phases of the paleo-lake highstands. Our results confirm this hypothesis with the recognition of two overflow abrasion platforms at 419 and 397 m a.s.l. (a).

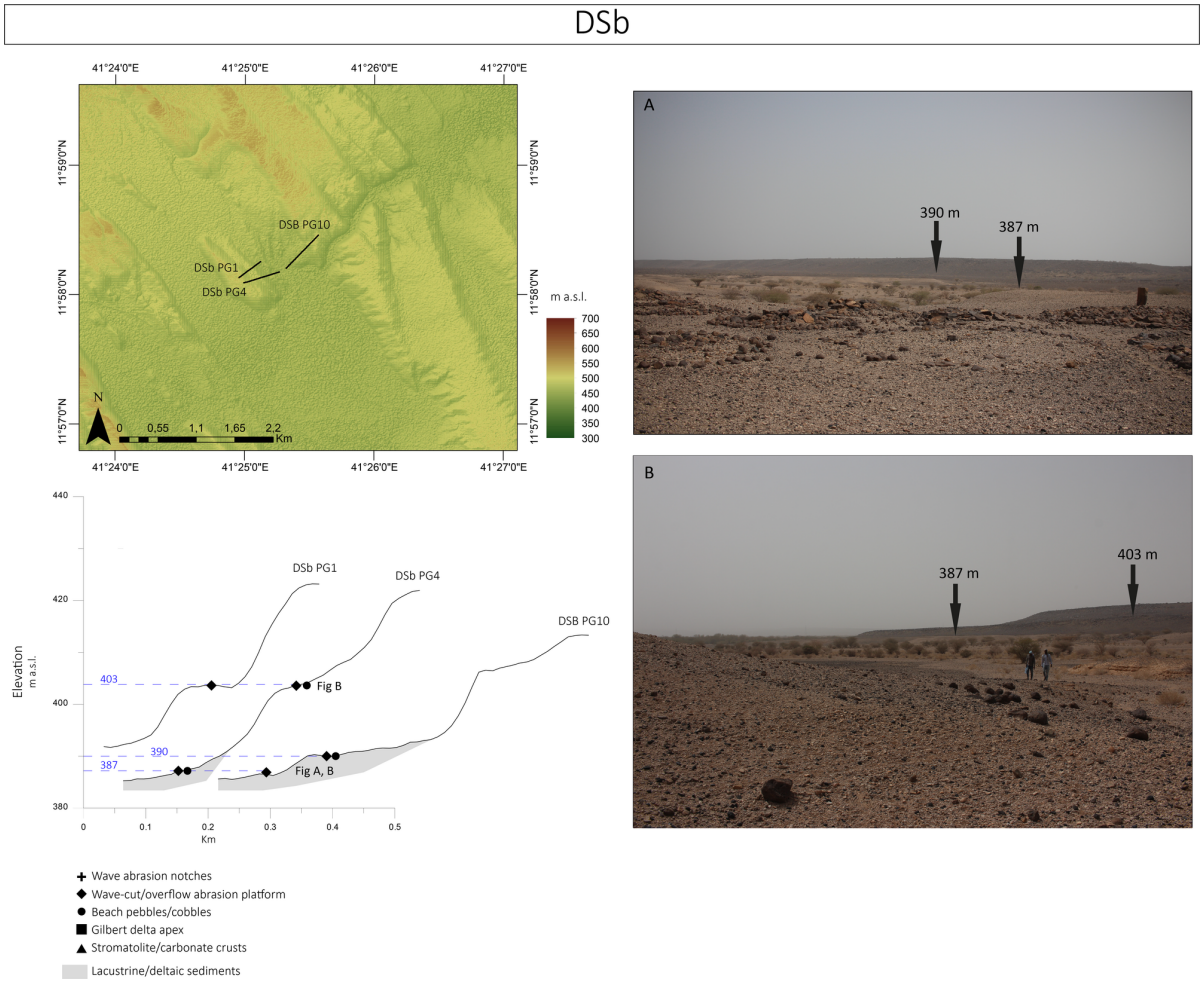

Figure BI.13: Site DSb ('Deversoir Serdo B') is located at the beginning of the distal part of the northern overflow sill of the Abhe Lake basin BI.4. The overflow channel is not exploitable for paleo-shoreline reconstruction because of the crossing of several faults. However, at the canyon entrance, three paleo-shorelines were documented: the first (403 m a.s.l.) is characterized by a well-developed abrasion platform on the stratoid outcrops and associated with abundant beach cobbles/pebbles, and the lower two (390, 387 m a.s.l.) are characterized by a well-developed abrasion platform on previous lacustrine sediments associated with beach cobbles/pebbles (a, b).

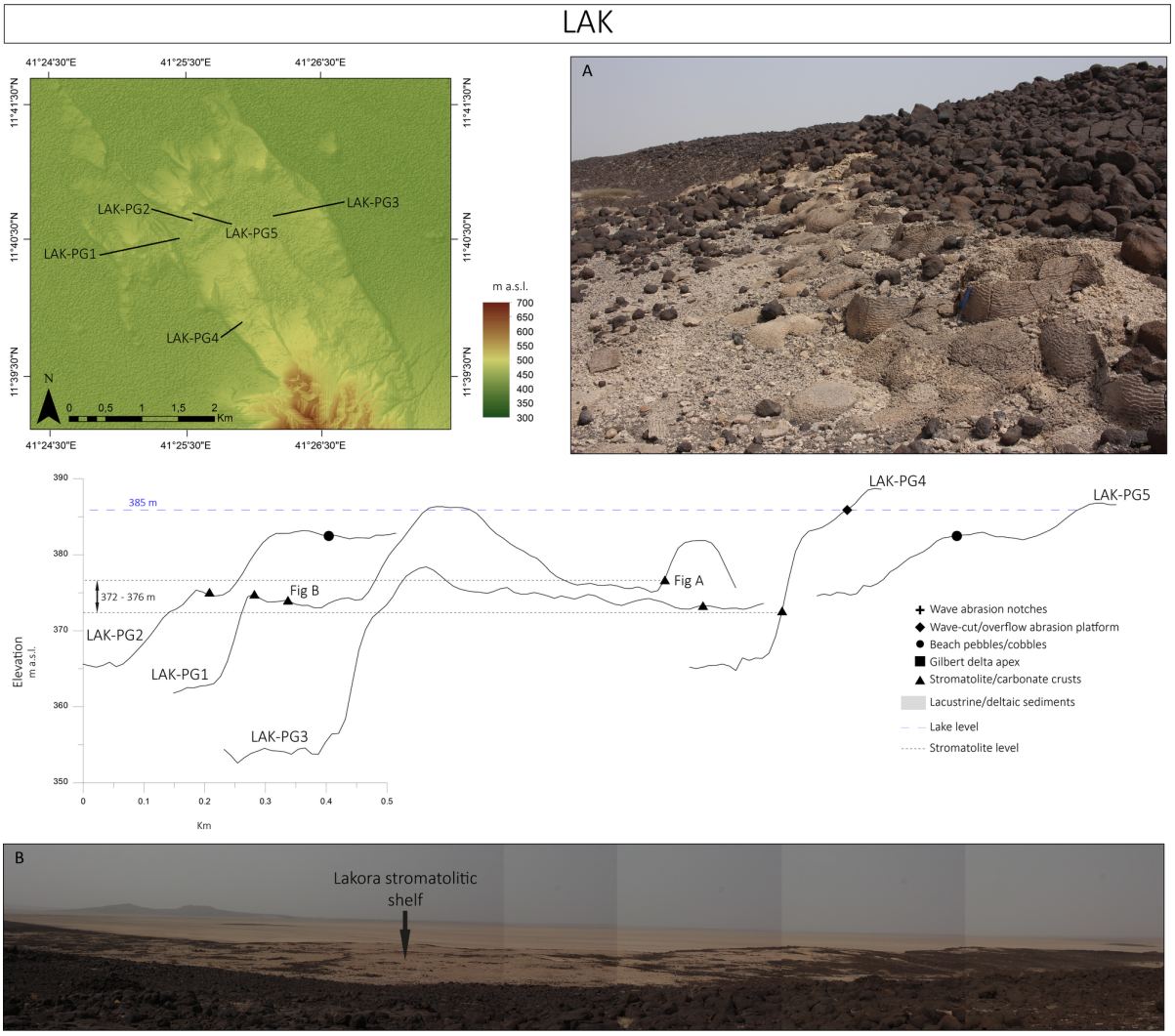

Figure BI.14: Site LAK ('Lakora') corresponds to the Northern extension of the Borawli massif BI.4: a large plateau composed of basaltic Stratoid series and crossed by few North-West/South-East faults. One paleo-shoreline level was detected at 385 m a.s.l. from an abrasion platform underlined by a beach pebbles concentration (383 m a.s.l.). The particularity of this site its large stromatolitic shelf posed on the Lakora plateau and ranging between 372 and 376 m a.s.l. (a, b).

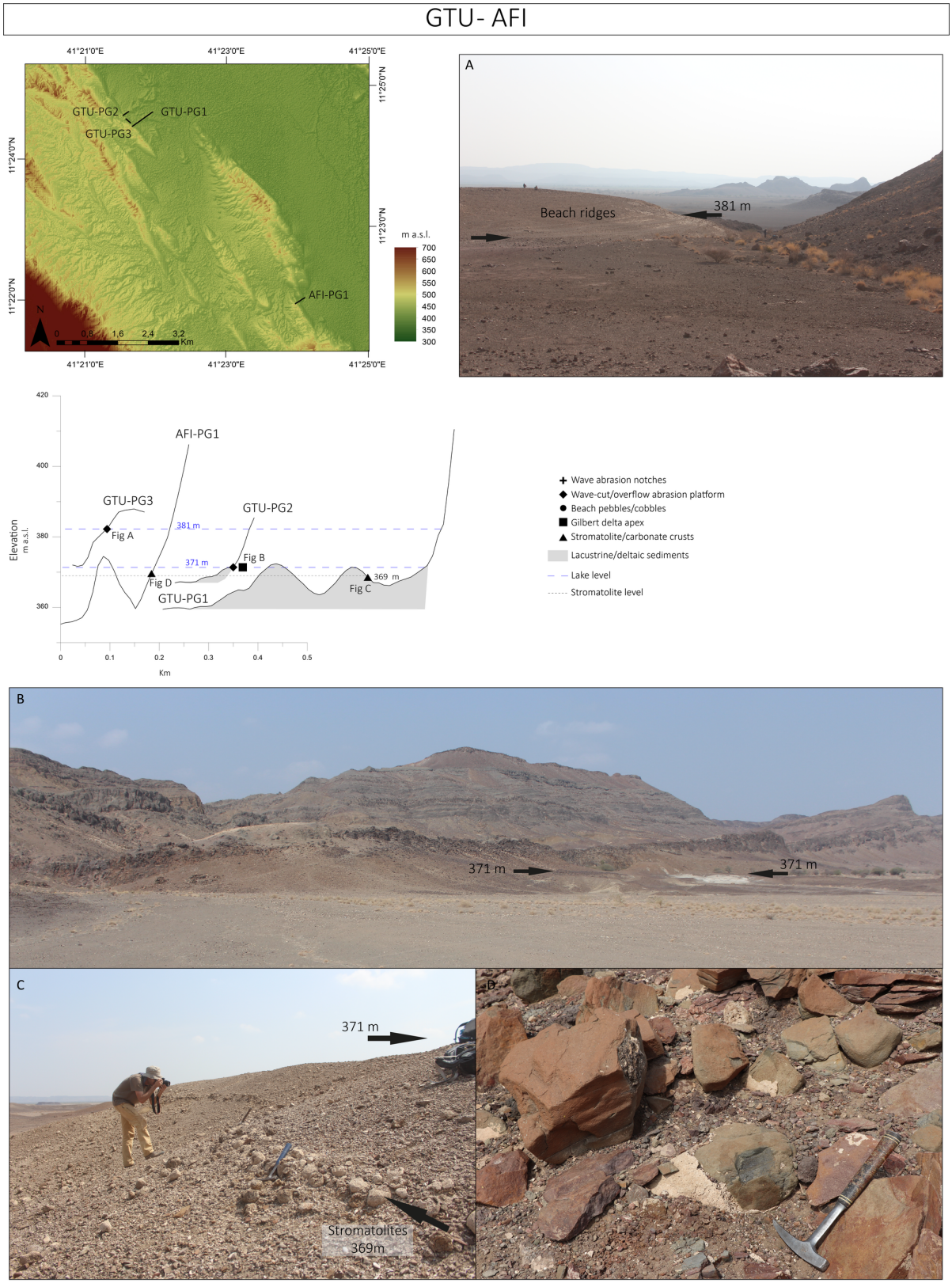

Figure BI.15: Site GTU-AFI ("Goma'tu-Afa'si") is the only site surveyed on the Western scarp of the Tendaho-Gobaad graben which provided some geomorphic paleo-shorelines information BI.4. The limited data is a result of the difficulty of access to the Magenta zone. Nevertheless, two paleo-shorelines were documented. The upper one, materialised at 381 m a.s.l. by some beach ridges (a) and the lower, localised at 371 m a.s.l. and characterized by a large wave-cut abrasion platform on lacustrine sediments (d). One oncolite level is observed at 369 m a.s.l (d).

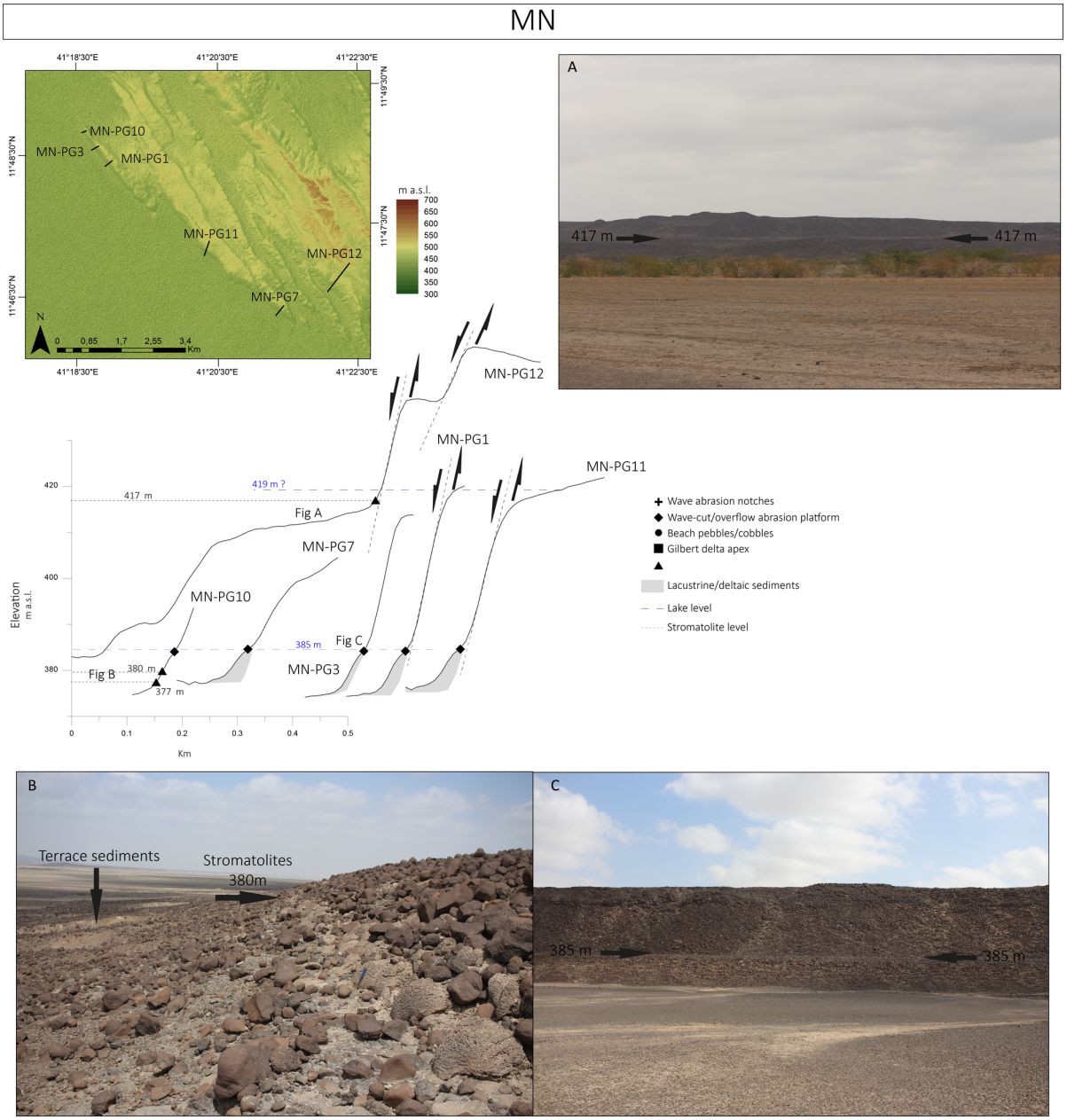

Figure BI.16: Site MN ('Manda North') is located on the East fault scarps of the Abhe basin BI.4, on well-defined North-West/South-East faults. The particularity of this site is the continuity of a well-developed wave-cut abrasion platform located at 385 m a.s.l. that extends over more than 10 km (c). This shoreline platform is clearly discernable from the faults because it is incised on previous sedimentary deposits posed on the scarp margin. A stromatolitic dome level ranging between 380 and 377 m a.s.l. is likely associated with this highstand level (b), while a thin and sporadic littoral carbonate crust (microbialite) was detected at 417 m a.s.l. (a).

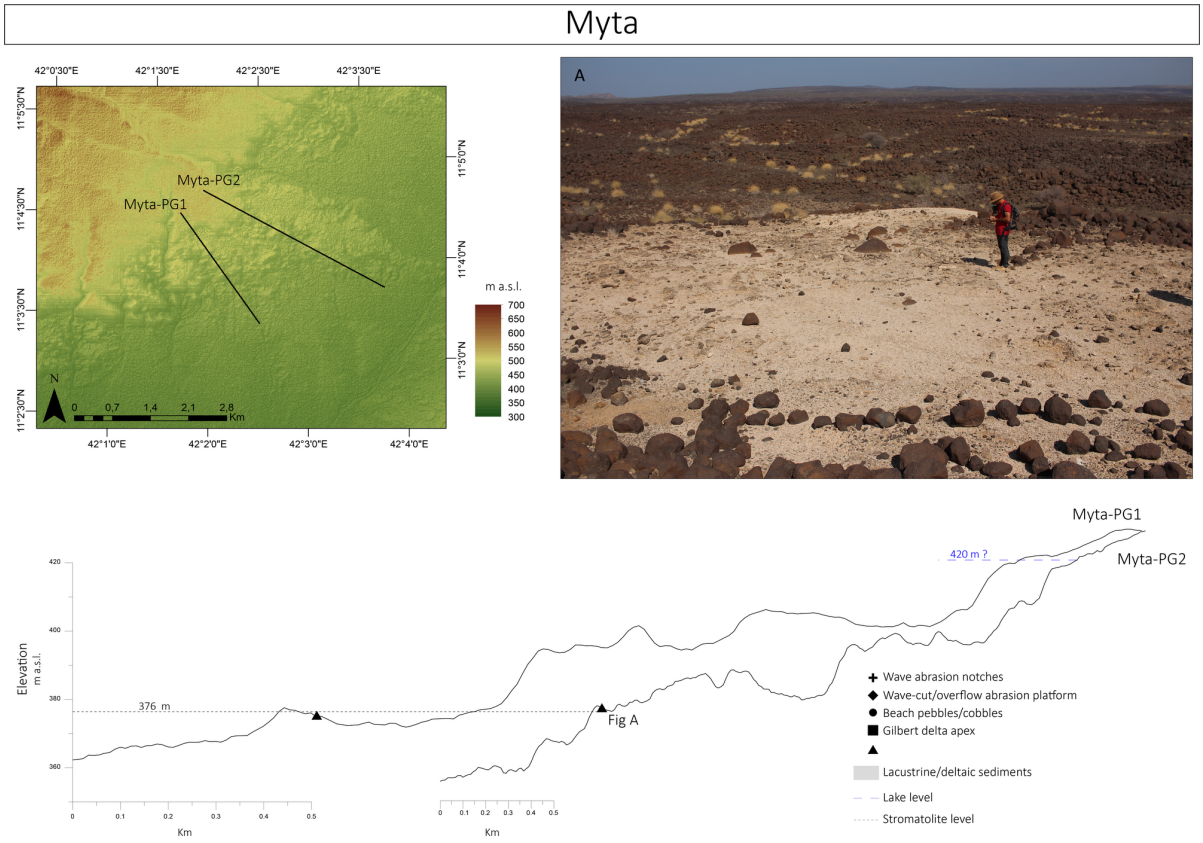

Figure BI.17: Site Myta ('Mokoyta'), located on the northern side of the Gobaad valley (Djibouti; BI.4), is characterized by a stromatolitic cover level at 376 m a.s.l. (a), while no clear paleo-shoreline has been detected. A continuous platform surface is localised on topographic profiles around 420 m a.s.l., but no other littoral markers were observed.

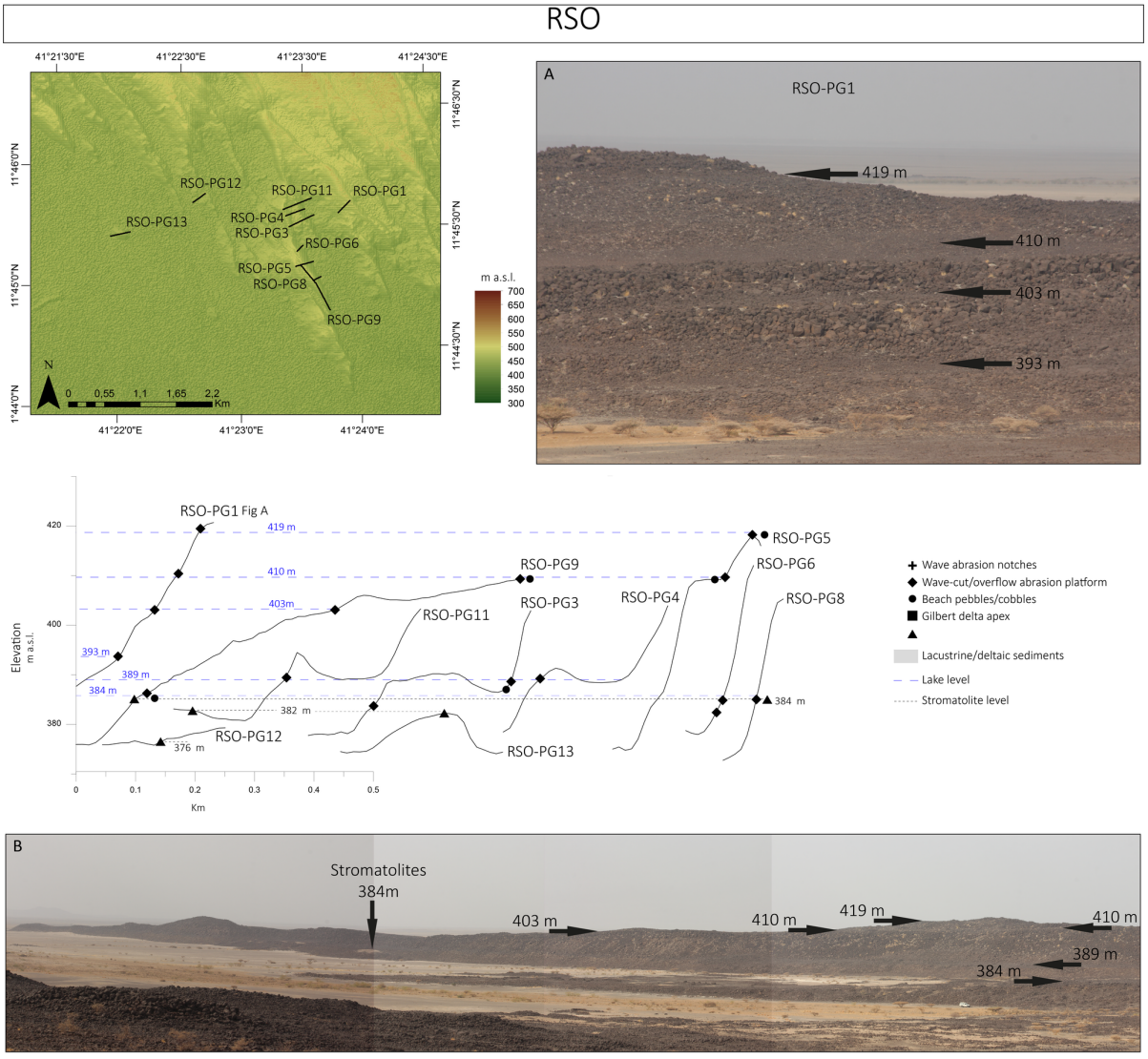

Figure BI.18: Site RSO ('Raso') corresponds to a semi-enclosed basin delimited by North-West/South-East oriented foot-wall basaltic outcrops, located at the Eastern margin of the Awash plain BI.4. The particularity of this site is it the gulf or semi-enclosed bay paleo-morphology, where onshore winds would have maintained stable high-water levels that produced well-developed littoral geomorphic markers (Bird, 2008). These favorable morphological factors, coupled with an intensive fieldwork survey, allow us to recognise multiple ancient paleolake levels. Well-defined wave-cut abrasion platforms combined with beach pebble assemblages observed both on the East and West margins of the semi-enclosed bay indicate paleo-shorelines at 419, 410, 403, 393, 389, 384 m a.s.l. (a, b) The lower level is associated with a thin stromatolitic line located at the same elevation, while two other stromatolitic levels were detected Westward at 382 and 376 m a.s.l. (b).

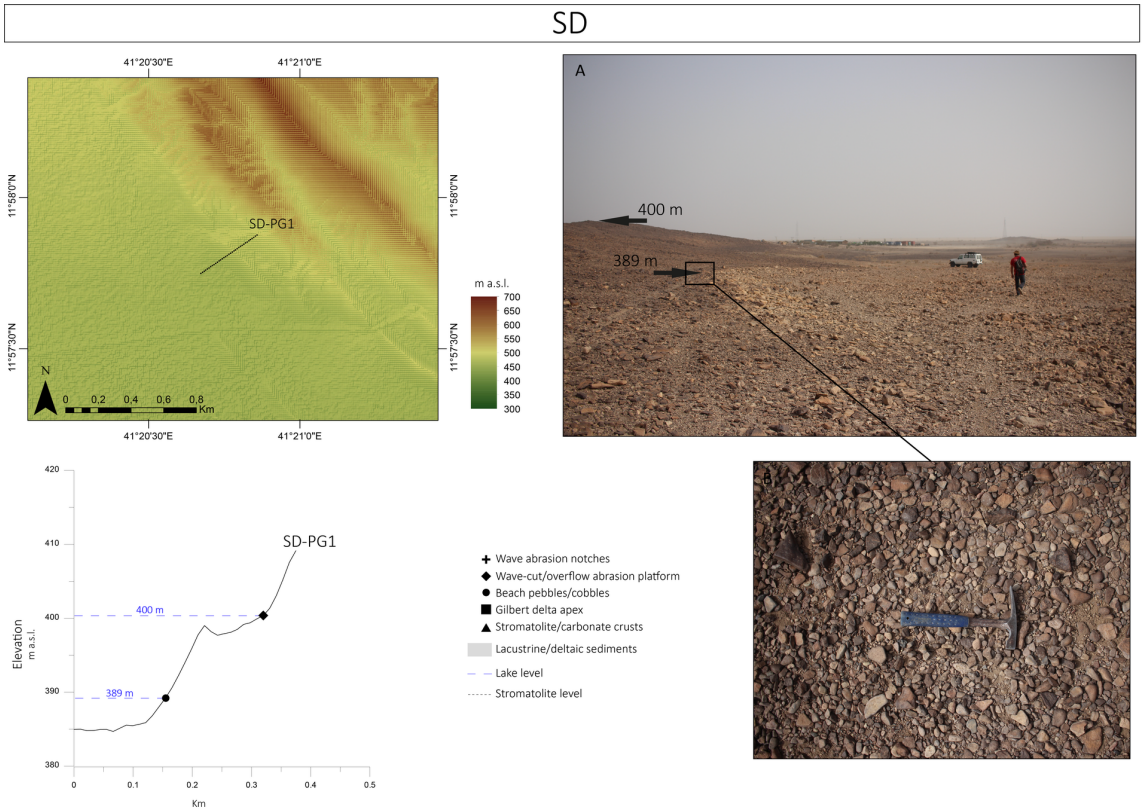

Figure BI.19: Site SD ('Serdo') is the northernmost surveyed area which provided some littoral geomorphic markers BI.4. The extended plain areas in the north of the basin, ranging between 370 and 380 m a.s.l., would have produced a large foreshore and shorelines geomorphic markers making recognition of paleo-shore limits more difficult. However, in the Serdo area, in the North-Eastern part of the basin, a continuous abrasion platform and a beach pebble ridge permitted us to define two paleo-shorelines at 400 and 389 m a.s.l. (a).

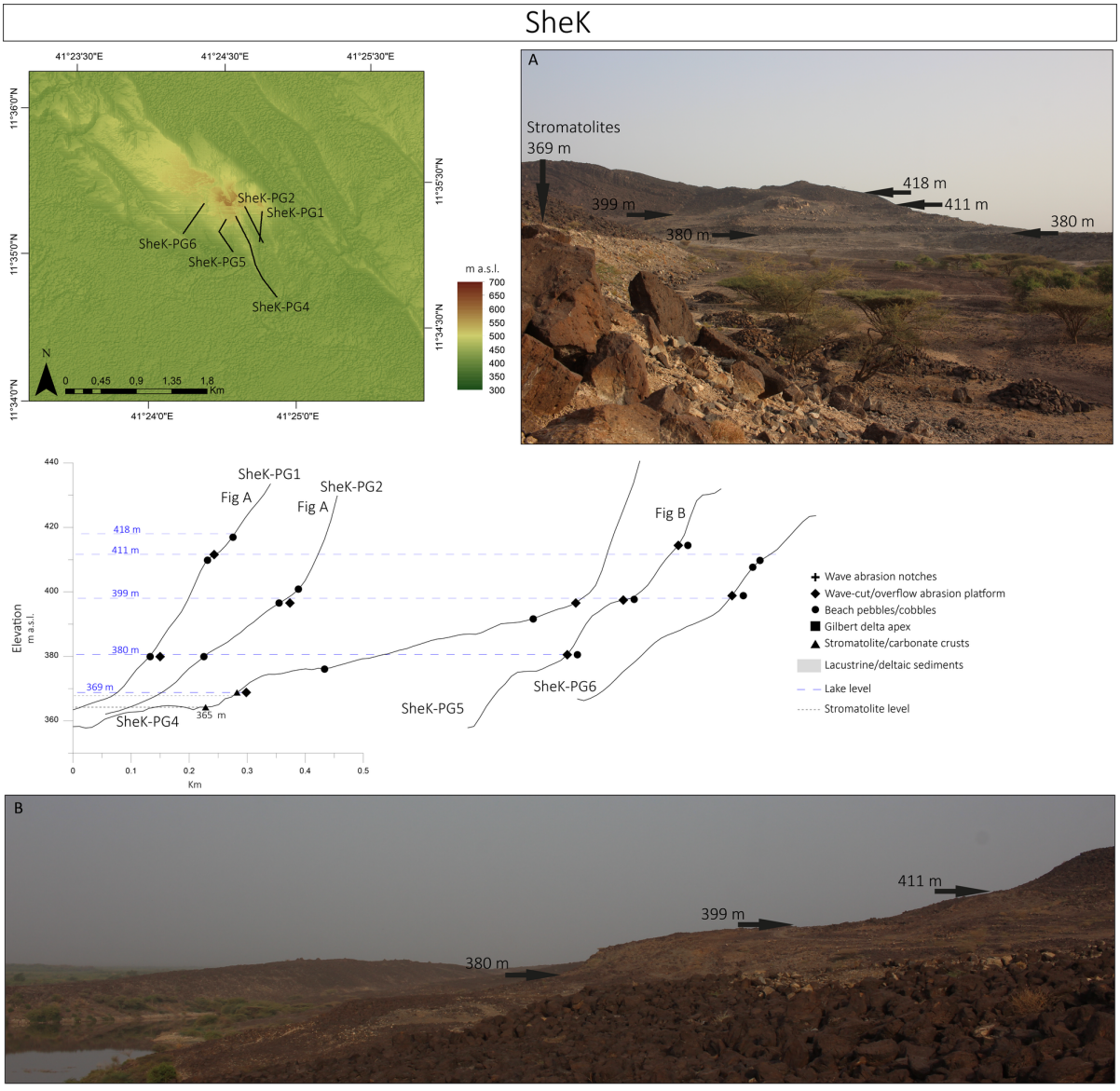

Figure BI.20: Site SheK ('Shekaito Koma') is located on a small stratoid basaltic outcrop at the center of the Abhe basin BI.4. The surveyed site where several paleo-shorelines were documented offered the same semi-enclosed basin morphological advantages described for the RSO site. The highest level at 418 m a.s.l. is marked by abundant beach pebble/cobble concentrations belonging to the paleo-shore/foreshore zone. The underlying levels were detected thanks to abundant beach clastic components and well-developed abrasion platforms at 411, 399, 380 ad 369 m a.s.l. The platform at 380 m is incised in foreshore deposits. One stromatolitic line was observed between 369 and 365 m a.s.l.

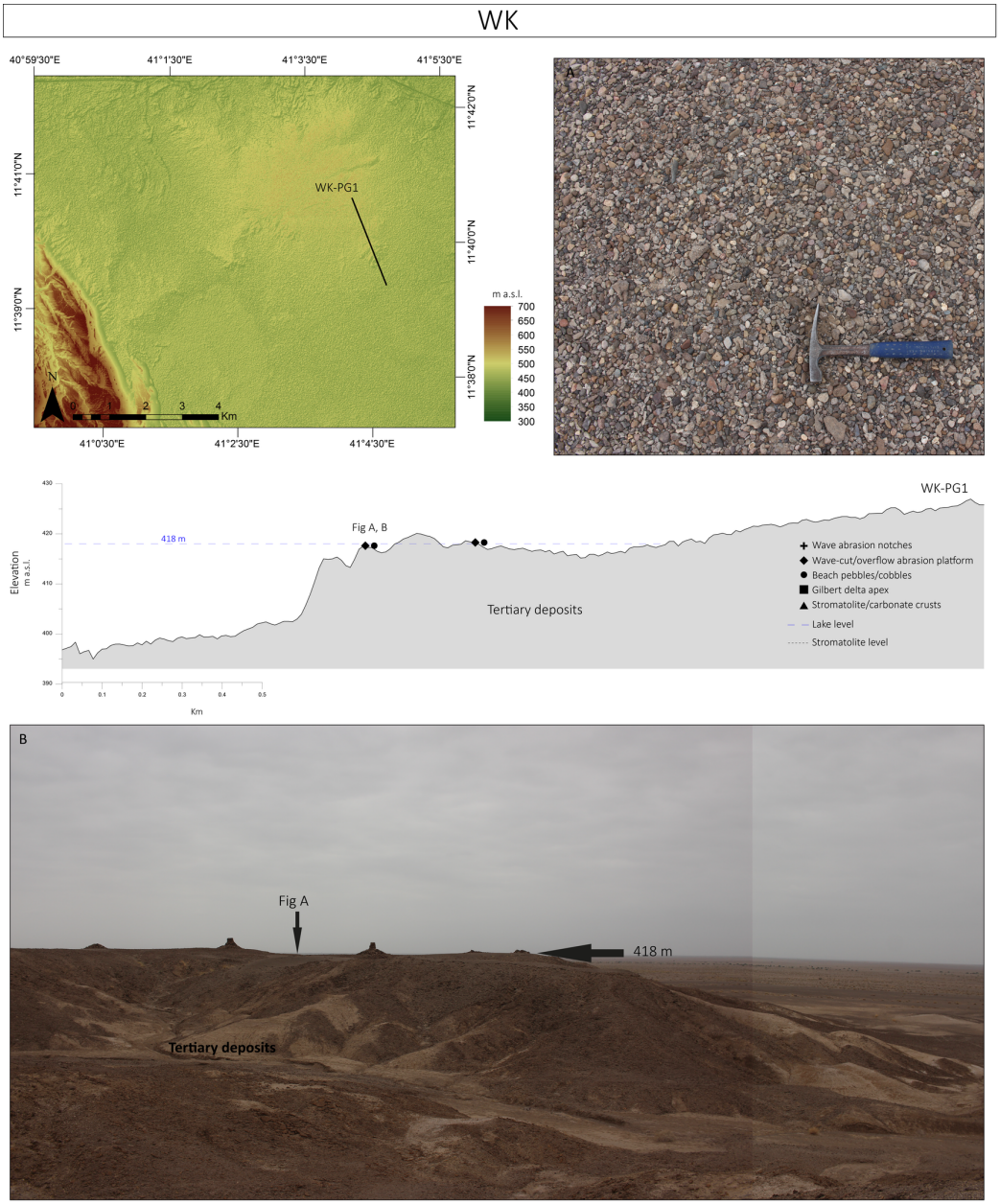

Figure BI.21: Site WK ('Wedelli Koma'), is located in the Det-Bahari plain, on the right bank of the Awash River BI.4. Is represented by a hill composed of Tertiary deposits. Wave-cut abrasion platform at 418 m a.s.l. is well developed on these deposits and is associated with a large amount of pebbles which present an allochthonous origin (a, b). The allochtonous mineralogical assemblage could be part of an ancient (Plio-Pleistocene) delta of the Awash River that developed at the entrance of the Abhe basin, not far from WK.

FID	Lat	Long	Name	Elevation (m) TanDEMx
1	11,635491	41,479091	Stromatolite 1 Sup	370,354706
2	11,757237	41,367070	Stromatolite 2	382,012115
3	11,757237	41,367070	Stromato Colline	382,012115
4	11,644480	41,428930	Stromatolite 4	378,751007
5	11,649400	41,432330	Stromatolite 5	378,406494
6	11,649400	41,432330	Stromatolite 6	378,406494
7	11,663550	41,430580	Stromatolite 7	371,532013
8	11,672526	41,416390	Stromatolite 8	374,993378
9	11,673369	41,416020	Stromatolite 9B	374,563385
10	11,673369	41,416020	Stromatolite 9A	374,563385
11	11,673500	41,415580	Stromatolite 10A	376,800568
12	11,673500	41,415580	Stromatolite 10B	376,800568
13	11,737810	41,431650	Stromatolite 11	381,883759
14	11,407931	41,362540	Stromatolite 13	369,001953
15	11,365398	41,400310	Stromatolite 14	367,795593
16	11,855210	41,238360	Stromato 16 sup	376,238892
17	11,855210	41,238360	Stromato 16 inf	376,238892
18	11,678130	41,422720	Stromato 17 A	375,396912
19	11,678130	41,422720	Stromato 17 B	375,396912
20	11,678130	41,422720	Lakora3 US3 stromato18	375,396912
21	11,673520	41,415570	Stromato 19	376,800568
22	11,900340	41,065600	Stromato 20 US1	369,008331
23	11,780470	41,371360	Stromato 32	416,604279
24	11,852740	41,256320	Stromato 31 (base stromatolis)	381,70163
25	11,852730	41,316230	Stromato 39A	380,142212
26	11,852760	41,256460	Stromatolis US1	381,671051
27	11,762010	41,377410	Raso2 Sondage2 US2 strom	376,039734
28	10,98131	42,12173	Ara le Koma_Stromato 1	384
29	10,97078	42,11616	Ara le Koma_Stromato 2	442
30	11,04993	41,95876	Aysilo_encroutement calcaire 1	325,350525
31	11,05187	41,96243	Aysilo_stromatolite 1	378,656128
32	11,05389	41,96472	Aysilo 5	377,92569
33	11,06555	42,05611	Mokoyta Stromato 1	376,565704
34	11,06028	42,03889	Mokoyta Stromato 2	375,544403
35	11,06194	42,0425	Mokoyta Stromato 3	376,652893
36	11,814438	41,30987	Strom 40	383,251923
37	11,814251	41,30984	Strom 41	380,910767
38	11,814206	41,309783	Strom 42	378,370453
39	11,761961	41,392663	Strom 43	383,200256
40	11,493965	41,654478	Strom 44	369,794983
41	11,615211	41,430543	Strom 45	374,425079
42	11,858006	41,249501	Strom 46 1ere gen	380,230774
43	11,858006	41,249398	Strom 46 2nd gen	379,420929
44	11,580406	41,463785	Strom 47	353,669861
45	11,58238	41,412343	Strom 48	363,4104
46	11,674548	41,422373	Strom 49	377,634583
47	11,751006	41,393756	Strom 50	384,095032
48	11,677836	41,436884	Strom 51	373,399078

Table BI.6: Coordinates, Elevation (TanDEMx, m) and ID name of stromatolite samples collected on the field.

ID/type	X_utm37N	Y_utm37N	ID_Point DGPS	TanDEMx (m)	ALOS12.5 (m)	SRTM30 (m)	GPS Geo7X (m)
galet lit12inf	768701,940	1281302,89	29	350	348	358,659	349,106
galet lit8 inf	767877,170	1281767,59	19	355	349	356,838	353,231
galet lit12sup	768718,235	1281333,45	27	356	351	361,856	357,950
galet lit inf1	767599,573	1281921,20	1	359	349	358,338	357,977
galet lit12	768718,463	1281333,54	26	356	351	361,856	358,047
galet lit8 sup	767891,064	1281788,39	20	359	351	362,726	358,775
galet lit1sup	767593,318	1281946,07	2	363	352	361,968	363,043
encoche lit	767510,248	1282029,88	18	365	356	365,087	365,649
encoche lit	767599,195	1281958,09	3	366	356	369,262	367,147
encoche lit	767529,442	1282083,63	17	369	360	371,812	368,653
galet lit 17inf	763054,406	1281852,28	33	371	363	374,188	370,459
stromato48 linge rivage	763058,182	1281482,48	54	370	360	369,267	370,921
galet lit13	768727,739	1281398,53	28	373	362	373,357	372,430
galet lit23	763041,881	1281518,63	55	376	362	372,680	376,232
galet lit2inf	767621,317	1282012,68	4	378	371	379,46	376,268
galet lit7	767620,982	1282105,61	16	380	375	382,615	378,137
encoche lit	767622,043	1282109,35	15	380	375	386,432	378,606
encoche litoral	767663,960	1282068,31	6	382	373	381,701	379,323
galet lit2 sup	767663,860	1282068,32	5	382	373	381,701	379,412
galet lit17sup	763049,950	1281902,86	32	379	372	381,670	380,270
galet lit5	767648,536	1282120,21	12	385	377	386,716	383,015
encoche lit	767650,080	1282122,20	11	385	377	386,716	383,582
galet lit9	768143,074	1281895,97	21	385	376	382,867	383,673
encoche lit	768147,094	1281896,23	22	385	376	382,867	384,463
galet lit4	767678,690	1282102,88	10	387	376	384,574	385,733
encoche lit	767571,252	1282161,10	14	385	376	383,599	385,800
galet lit6	767596,955	1282176,09	13	388	378	387,719	386,139
replat d abrasion	760889,083	1300132,21	53	385	381	396,493	386,185
stromato50	760889,381	1300131,90	52	385	381	396,493	386,205
replat d abrasion	760624,510	1300584,85	45	384	377	387,194	386,519
galet lit20	760648,164	1300556,43	47	386	378	394,228	387,273
galet lit19	760600,121	1300613,89	44	385	378	388,598	387,328
replat d abrasion	760596,002	1300614,07	43	385	378	388,598	387,683
encoche lit	767676,725	1282109,53	9	387	376	387,439	387,889
galet lit18	760531,259	1300865,39	42	387	384	391,346	389,722
replat d abrasion	760720,564	1301041,95	39	384	376	385,087	390,356
replat d abrasion	760634,854	1301164,98	40	388	379	389,201	391,846
galet lit 3	767799,436	1282113,21	8	394	384	395,529	392,208
replat d abrasion	760496,204	1300934,77	41	390	385	396,212	392,277
galet lit10	768291,814	1282050,57	23	394	386	397,176	393,946
encoche lit	767789,055	1282124,25	7	395	385	394,245	394,060
replat d abrasion	761251,147	1301195,58	35	394	387	398,226	396,153
galet lit15	762939,631	1282072,80	30	401	395	403,062	399,853
replat d abrasion	760636,458	1300592,43	46	382	374	384,220	403,322
replat d abrasion	761293,428	1301241,89	36	402	396	404,294	405,456
galet lit21	760642,551	1300335,75	49	409	401	411,172	412,279
replat d abrasion	760643,557	1300340,47	48	409	400	411,172	412,490
galet lit11	768426,154	1281937,53	24	414	404	415,816	413,024
replat d abrasion	761331,662	1301272,92	37	411	402	410,767	413,306
galet lit16rare	763086,148	1282064,00	31	416	407	417,844	418,105
galet lit11sup	768457,295	1281935,59	25	420	408	420,517	419,401
replat d abrasion	760589,800	1300322,61	50	417	406	415,185	419,782
galet lit22	760584,361	1300318,69	51	417	406	415,185	420,687
replat d abrasion	761377,802	1301292,76	38	419	406	415,132	421,689

Table BI.7: Lacustrine littoral geomorphic features elevation measured with DGPS Geo7X and compared with ALOS, SRTM and TanDEMx Digital Elevation Models

FID	Coordonnées				Type		
	Lat	Long	SRTM (m)	TanDEMx (m)	Pebbles	Abrasion surface	Proximal Gilbert delta
1	11.673255	41.048611	416,911987	417,263824	oui	oui	non
2	11.663071	41.076011	416	417,5625	oui	oui	non
3	11.804931	41.315503	378,050995	374,477905	non	oui	non
4	11.495485	41.653088	377,225006	374,197632	non	oui	non
5	11.765900	41.388303	389,903992	384,740021	non	oui	non
6	11.766915	41.394390	411,352997	413,867828	non	oui	non
7	11.765426	41.395116	422,131989	416,14151	non	oui	non
8	11.613000	41.433145	379,828003	377,950592	oui	oui	non
9	11.491840	41.664640	396,131012	392,756256	oui	oui	non
10	11.616920	41.435086	391,13501	391,292816	oui	oui	oui
11	11.857400	41.249778	387,320007	384,039032	non	oui	non
12	11.968845	41.420298	385,911011	387,828583	oui	oui	non
13	11.972843	41.425523	408,153015	409,329041	non	oui	non
14	11.966293	41.420558	393,881012	395,581787	non	oui	non
15	11.929611	41.412333	394,704987	397,922302	non	oui	non
16	11.963298	41.345705	388,459991	389,009094	oui	non	non
17	11.586011	41.460315	397,160004	393,860199	oui	oui	non
18	11.635466	41.478713	383,108002	383,88501	oui	oui	non
19	11.635465	41.477846	403,550995	406,894501	non	oui	non
20	11.638235	41.469066	411,127014	410,260498	oui	non	oui
21	11.582431	41.412338	369,266998	363,40152	oui	oui	non
22	11.58263	41.412236	366,789001	366,907745	oui	oui	non
23	11.586640	41.408086	412,985992	414,074707	oui	oui	non
24	11.585898	41.407803	399,863007	397,775879	oui	oui	non
25	11.585865	41.407695	399,785004	397,547913	oui	non	non
26	11.585100	41.408351	385,497009	380,370087	oui	oui	non
27	11.588301	41.405425	407,222992	409,415558	oui	non	non
28	11.588255	41.405331	407,222992	407,253784	oui	non	non
29	11.587256	41.412876	411,640991	408,395752	oui	non	non
30	11.587460	41.411345	403,561005	397,063202	oui	oui	non
31	11.587516	41.410988	404,756012	399,583496	oui	oui	non
32	11.677221	41.424543	383,596985	382,199554	oui	non	non
33	10.964000	42.098889	398,829987	396	oui	non	autre
34	11.047639	41.961944	327,359009	323,387787	oui	non	non
35	11.054194	41.972778	384,424988	379,773529	oui	non	non
36	11.054250	41.968056	383,752014	382,260406	oui	non	non
37	11.047833	41.961389	326,671997	316,809021	non	oui	non
38	10.97191	42.11645	400,709015	398	oui	oui	non
39	11.04884	41.96053	338,053986	334,493225	oui	non	non
40	11.04993	41.95876	336,529999	325,350525	oui	oui	non
41	11.057472	41.966667	375,815002	374,073151	non	oui	non
42	11.050528	41.957222	336,041992	333,150757	oui	non	non
43	11.050750	41.956667	332,39801	325,830505	oui	oui	non
44	11.049972	41.961389	353,707001	350,091522	oui	non	non
45	11.049917	41.958611	338,640015	327,830566	non	oui	non
46	11.048778	41.960556	332,324005	334,03949	oui	non	non
47	10.970806	42.116389	442,416992	449	non	oui	non
48	10.975389	42.118611	380,03299	382	non	oui	non
49	10.971722	42.116389	406,091003	404	oui	non	non
50	11.047611	41.962222	331,43399	324,65564	oui	non	non
51	11.806631	41.315625	388,113007	383,874786	non	oui	non
52	11.806676	41.315695	388,113007	383,874786	non	oui	non

Table BI.8: Lacustrine littoral geomorphic features measured with GPS. Elevations extracted from TanDEMx treatment.

Soil Type	Sample ID	Log(Si/Al)	Log(K/Al)	Log(Ti/Al)	LOI (%)	Log(Q10)	Log(Q90)
Soil Type-1	KUR-07_US29	0,55715469	-0,63371318	-0,82976419	4,80648621	0,11058971	2,02110657
	KUR-07_US26	0,5618606	-0,65523743	-0,81254782	4,12194565	0,09691001	2,02702325
	GB_paleosol-moy	0,54865972	-0,70315309	-0,7391469		0,15228834	2,11942086
	GB_paleosol-inf	0,54371822	-0,68230334	-0,8892375	4,24923391	0,09342169	2,01063912
	GB_paleosol-sup	0,54739252	-0,69625382	-0,89506338	5,35455861	0,41161971	1,98824672
	TwD_US5-02-2	0,74680713	-0,57999695	-1,00198975	1,42608696	0,9459607	
Soil Type 2	GB_ST1_US5-02	0,55260547	-0,69026028	-0,79383303	3,86257764	0,17897695	1,67182056
	Stromatolis_US4	0,62708865	-0,64001288	-0,75218042	3,57701329	0,21484385	2,62647382
	MS2_US4	0,5683749	-0,6946346	-0,76936389		0,42160393	2,01038477
	Raso2_US6sup	0,59112943	-0,71917398	-0,81561145	5,21317829	0,55990663	2,29859111
	MS2_US3	0,55937385	-0,71685459	-0,74438363		0,06069784	2,07110842
	GB_ST1_US5-01	0,54496644	-0,70412486	-0,7397894		0,11058971	1,55822842
	Raso2_US8	0,60230136	-0,58089379	-0,97165275	5,66373296	1,07077646	2,40942587
	Det-Bahari	0,53585438	-0,67766534	-0,97015489	9,41605183	0,02938378	1,45939249
	KUR-01_S5_US9	0,54984959	-0,71210088	-0,78647941		0,28555731	1,8049568
	KUR-01_S5_US7	0,55521612	-0,71655655	-0,68190881		0,22010809	1,91839734
	Raso2_US7	0,58806855	-0,64926216	-0,93116674	6,75506953	0,04532298	1,67577834
	Strom20_US7	0,5612657	-0,58820326	-0,98145085	8,80642866	0,05690485	1,37125263
	KUR-07_US18	0,56341297	-0,63970442	-0,7878246	5,16399163	0,06069784	1,91671708
	GB_ST1_US5-02	0,55058897	-0,70153735	-0,72626367	3,86257764	0,161368	
	HD1_US5	0,58006435	-0,70654057	-1,03454617	8,12547885	0,90308999	2,51113439
	Raso2_US1b	0,54393216	-0,6827523	-0,94582331	6,38528139	0,10037055	1,34927753
	Raso2_US6	0,58384671	-0,6830102	-0,79887901	6,37970941	0,462398	2,10499895
	GB_ST1_US5-03	0,54684421	-0,66919562	-0,91121613	4,89327631	0,08990511	1,94418646
	HD1_US3	0,54656128	-0,69596057	-1,02964978	4,86728401	0,30535137	2,03173154
	Manda_sol-1	0,5575452	-0,62559917	-0,92002935	6,84702464	0,16435286	1,91492465
	MS1_US1	0,55917875	-0,7331887	-0,71538463		0,15836249	1,75350646
	Kur-07_ST1_US1	0,56345767	-0,65339216	-0,77654222		0,15836249	2,16467994
	HD1-US2	0,55947765	-0,67016046	-0,79316167	4,08517558	0,12385164	1,94086498
Soil Type-3	Aysilo5	0,52078383	-1,3177305	-0,32305025	3,09630787	1,00560945	3,07296639
	Masghidlou_US2	0,40317129	-1,10264311	-0,75848622	6,94169065	0,04921802	1,89658133
	Raso2_US5c	0,54362962	-0,91018434	-0,54477784		0,5797836	2,54846313
	SP1_US2inf	0,48324593	-0,75757121	-0,77896075	6,24336544	-0,02227639	1,64256344
	KUR-05_S3_US4	0,52261475	-0,72088251	-0,96104485			
	Raso2_US5d	0,56065739	-0,77506307	-0,68155611	4,6788376	0,02530587	1,41246055
Actual Soil Type-3	DD_paleosol_Hol	0,46727245	-0,9476508	-0,83010722	6,95821927	0,15533604	2,34717384
	GaliKoma_S1_US4	0,46564387	-0,98139831	-0,82361577	5,95269909	0,05690485	1,78632543
	DD_ST1_US3-01	0,51509825	-0,87408215	-0,88244105	6,61643314	0,06445799	1,92438268

Table BI.9: SI/Al, K/Al and Ti/Al elemental ratios, LOI (%), Q10 and Q90 measure results of soil samples, with Sample IDs and respective soil Type

BI.3 Chapter-VI Supplementary Materials

N° (Gasse 1975)	Sample name (Gasse 1975)	Conventional age yr BP	Longitude	Latitude	Selection and rejection criteria	Calibrated ages yr BP (range 95.4 %)	Calibrated ages yr BP (median)	Recalculated elevations (DEM ± 12 m)
Gasse_1	B88	98.8 ± 1.2	41°48'	11°59'		255 – 31	121 ± 78	240
Gasse_2		100.6 ± 0.9	41°52'	11°09'		255 – 31	122 ± 78	231.7
Gasse_6	M 245	110 ± 50	41°50'	11°15'		276 – 9	124 ± 81	256.4
Gasse_7	M 108	1030 ± 100	41°41'	11°29'		1178 – 738	984 ± 115	256.4
Gasse_8	M 104	1300 ± 100	11°37'	11°09'	Gamari residual lake	\	\	\
Gasse_9		1570 ± 60	41°52'	11°09'		1597 – 1337	1464 ± 63	314
Gasse_11		2360 ± 80	41°52'	11°09'		2715 – 2160	2429 ± 140	295
Gasse_13		2720 ± 120	41°52'	11°09'		3172 – 2490	2850 ± 55	285
Gasse_14	M 284	3290 ± 160	41°26'	11°39'	Residual lake	\	\	\
Gasse_16	A 646	4120 ± 110	42°08'27	11°00'34''		4874 – 4297	4643 ± 144	346.8
Gasse_18		4740 ± 150	42°08'27	11°00'34''		5881 – 4983	5455 ± 93	354.9
Gasse_19		4750 ± 230	42°08'	11°05'	Pedological deposit (Fontes et al. 1973)	\	\	\
Gasse_22	M 277	5080 ± 480			Incomplete coordinates	\	\	\
Gasse_29		5775 ± 115			Incomplete coordinates of pedological deposit (Semmel 1971)	\	\	\
Gasse_30	B 38	5830 ± 140	42°09'	11°00'		6972 – 6316	6647 ± 167	355.6
Gasse_33	A 648	5930 ± 130	42°09'	11°00'		7156 – 6468	6769 ± 167	355.6
Gasse_34	A 32	6020 ± 160	41°24'	11°21'		7256 – 6501	6884 ± 196	349.6
Gasse_35		6130 ± 250	41°51'	11°15'		7498 – 6448	7002 ± 271	327
Gasse_38		6290 ± 100	41°52'	11°09'	Lack of interpretation of formation processes (Fontes & Pouchan 1975)	\	\	\
Gasse_39		6335 ± 110			Incomplete coordinates of pedological deposit (Semmel 1971)	\	\	\
Gasse_40		6350 ± 105			Incomplete coordinates of pedological deposit (Semmel 1971)	\	\	\
Gasse_41	M 109	6360 ± 260	41°40'	11°36'	Gamari residual lake	\	\	\
Gasse_43		6610 ± 100			Incomplete coordinates of pedological deposit (Semmel 1971)	\	\	\
Gasse_44	M 105	6630 ± 220	41°41'	11°34'	Gamari residual lake	\	\	\

Table BI.10: (continued)

Gasse_47	M 105	6690 ± 160	41°41'	11°34'	Gamari residual lake	\	\	\
Gasse_49	B 459	6835 ± 160	42°08'	11°05'		7965 – 7432	7697 ± 142	371.3
Gasse_50	S 94	6910 ± 180	40°51'	11°47'	Incoherent age	\	\	\
Gasse_53	C7	7000 ± 140	41°53'	11°08'	Deepwater lacustrine deposit	\	\	\
Gasse_54	B 87	7150 ± 320	41°49'	10°59'	Reworked sediment	\	\	\
Gasse_56	B 126	7190 ± 220	41°42	11°29'	Gamari residual lake	\	\	\
Gasse_57	M 238	7250 ± 150	41°49'35	11°15'02		8375 – 7795	8082 ± 148	239.7
Gasse_58		7265 ± 60	42°08'	11°15'	Inverted age with M 238	\	\	\
Gasse_62	B 428	7450 ± 100	42°04'	11°06'		8416 – 8037	8263 ± 99	363.7
Gasse_63	A 30	7460 ± 180	41°22'	11°24'		8630 – 7934	8268 ± 181	362.2
Gasse_64	A 645	7610 ± 140	42°08'27	11°00'34"		8770 – 8054	8420 ± 158	346.8
Gasse_74	A 100	8000 ± 170	41°29'	11°39'	Residual lake	\	\	\
Gasse_76	M 185	8340 ± 180	41°26'	11°27'		9704 – 8770	9302 ± 219	391.8
Gasse_77		8380 ± 100			Incomplete coordinates	\	\	\
Gasse_79	A11	8450 ± 190	41°?	11°32'	Incomplete coordinates	\	\	\
Gasse_80	A 26	8450 ± 190	41°22'	11°24'		10129 – 8996	9434 ± 255	362.2
Gasse_82	A 6	8530 ± 190	41°04'	11°44'		10154 – 9090	9545 ± 263	369.6
Gasse_84	M 282	8580 ± 160	41°26'	11°34'	Deepwater lacustrine deposit	\	\	\
Gasse_85	M79	8600 ± 140	41°26'	11°38'		10151 – 9305	9633 ± 194	366.5
Gasse_86	M2 246	8620 ± 75	41°45'	11°18'	Deepwater lacustrine deposit	\	\	\
Gasse_87	A 25	8650 ± 160			Incomplete coordinates	\	\	\
Gasse_88		8715 ± 120	41°20'	11°40°	Lack of interpretation and contextualization of formation processes interpretation and contextualisation (Taieb 1971)	\	\	\
Gasse_90	A 22	8770 ± 190	41°19'	11°26'		10273 – 9436	9848 ± 230	432.4
Gasse_93		9180 ± 220	41°51'	11°?	Incomplete coordinates	\	\	\
Gasse_94	S 119	9230 ± 180	40°54'	11°48'		11084 – 9917	10444 ± 260	408.2
Gasse_96	M 135	9380 ± 130	41°27'	11°35'		11086 – 10253	10623 ± 216	342.1
Gasse_100	M 101	10760 ± 220	41°42'	11°28'	Gamari residual lake	\	\	\
Gasse_103	M 161	13170 ± 170	41°53'	11°08'	Residual groundwater carbonates	\	\	\

Table BI.10: Selected and calibrated ages of Holocene Abhe Lake from Gasse (1975) and recalculated elevations.

Chapter BII

Field reports

BII.1 VAPOR-Afar 2018 Field Season - Geomorphological and Geoarchaeological Survey Report

VAPOR-Afar 2018 Field Season

Geomorphological and Geoarchaeological Survey Report

By Carlo Mologni
PhD Student, University Cote d'Azur
GEOAZUR-UMR7329/CEPAM-UMR7264

Introduction	*Geomorphological approach as a tool for understand the Human-Paleoenvironment relationship at the Abhe Lake paleobasin*

In this report we present and summarize the geomorphological and geoarchaeological work conducted over the 2018 field season for the *Volcanological and Archaeological Program for Obsidian Research (VAPOR)-Afar.* One of the principal goals of the VAPOR-Afar program is to reconstruct the human-environment paleo-milieu and to refine the Later Stone Age (LSA)/ Neolithic chrono-cultural sequence in the Central Afar region (Ethiopia). In particular, this work is focused on the Abhe Lake paleobasin, which represents a geographic, geologic and hydrologic entity at the centre of the Afar triangle (Figure 1).
In this region, the geomorphological knowledge of sedimentary archives is limited to the works of F. Gasse, conducted in 70s, when she reconstructed the Abhe lake fluctuations between arid and humid periods during the Pleistocene and Holocene transition on the basis of the diatom flora of lacustrine sediments [1,2]. These studies on the Abhe Paleolake can give important information about East-African climate change and the activity of the African paleomonsoon in this region. However, much fieldwork remains to be done before we can understand the precise duration and the installation modalities of the arid-humid periods, and many questions remain unanswered: What was the real impact of the climatic change on the landscapes evolution and on the hydrological balance of the Lower Awash Valley and Abhe Lake basin? What kind of sedimentary environments and landscapes were connected to, and formed around, the Lake Abhe during the humid and arid periods? Can these environments host and preserve the remains of LSA or Neolithic occupations? Is there a relationship between the type of deposits and archaeological chronology? What is the impact of the climate and environmental change on prehistoric human occupation around the Abhe Lake between 15 000 and 3 000 years BP?
The new archaeological data collected during the 4 VAPOR-Afar field seasons (2014 to 2018) have become increasingly rich and the new ^{14}C AMS (accelerator mass spectrometry) ages show a longer period of human prehistoric occupation in the central Afar region. The study of the sedimentary environments connected to the remains of these human occupations is necessary to understand the relationship between the human landscape exploitation, and the landscape and climate evolution in the central Afar region. For this reason, during the 2018 field season of VAPOR-Afar program, we have focused our work on the sedimentary archives for the geomorphological and geoarchaeological surveys in the Lower Awash Valley.

Context	*Geological, Hydrological and Paleoclimatological settings of the Lower Awash Valley*

The Abhe Lake Basin is located along the axis of the Tendaho-Gobaad graben (NE-SW), a basaltic floor made on faulted basalts from the stratoid series (4.4-2.5 Ma). More recent quaternary volcanic basaltic lava partially covers the stratoid series and represents the base for the Pleistocene-Holocene lacustrine and pedological deposits presented in this work. The Abhe Lake receives its water catchment from the Awash river which is sourced from the Addis-Abeba region. Descending the Ethiopian Plateau (or Ethiopian Highlands) the Awash river receives many affluent rivers until it meets the Lower Awash Plain (4000 Km^2), where it continues without freshwater supplies until the Abhe Lake. This last and arid part of the Awash river course (200mm/yr precipitation, with an evaporation of 3500mm/yr; [3]) coincides with the VAPOR-Afar 2018 field area. This plain, including Tendaho (400 m) and Gamari Lake (339 m) and limited by the Gamari Cliff to the East (1300 m) and Magenta Cliff to the West (400 m; Figure 1), is inclined to the East as a consequence of the Holocene tectonic activity.
The eastern sector of the Lower Awash plain (Gamari and Afambo faults lakes) was tectonically active during the Middle and Upper Holocene (7000-6000 yr BP). The Lower Awash Plain has been tectonically tilted toward the eastern faults

of the graben with a 30 m split over a length of 30 km. This tectonic activity, coupled with some volcanic phenomena localised to the East of the ryolithic Borawli Mountain, probably caused the deviation of the Awash river (around Ayssaita) and the formations of Gamari and Afambo lakes. Consequently, the final hydrological tracing of the Awash River (and the associated lakes) would be the consequence of the recent tectonic movement post 7000-6000 yr BP [1]. A similar phenomenon (6000 yr BP) was also detected almost 80 km away from the Lower Awash Valley, at the Asal Lake (Afar, Djibouti), with a 70 m tectonic subsidence of the axial valley [4].

During the Pleistocene and Holocene humid periods, the Lower Awash alluvial plain was filled by a Hyper- (29-17,000 BP and 10-8,000 BP), Mega- (7,500-4,500 BP) or Macro- (0-2,500 BP) Lake, with the maximum extent estimated to be around 6000 km^2 (4000 km^2 on the Lower Awash Valley and 2000 km^2 on the Gobaad sector at Djibouti;[1,2]). The paleo-shorelines of Abhe Lake can represent, for archaeological research, the ideal areas for identifying the sedimentary formations containing the remains of prehistoric human occupations. For this reason, and because of the complex geological (lacustrine, tectonic, volcanic) history of the Abhe Lake paleobasin, a geomorphological approach is needed to better understand the human-paleoenvironment co-evolution.

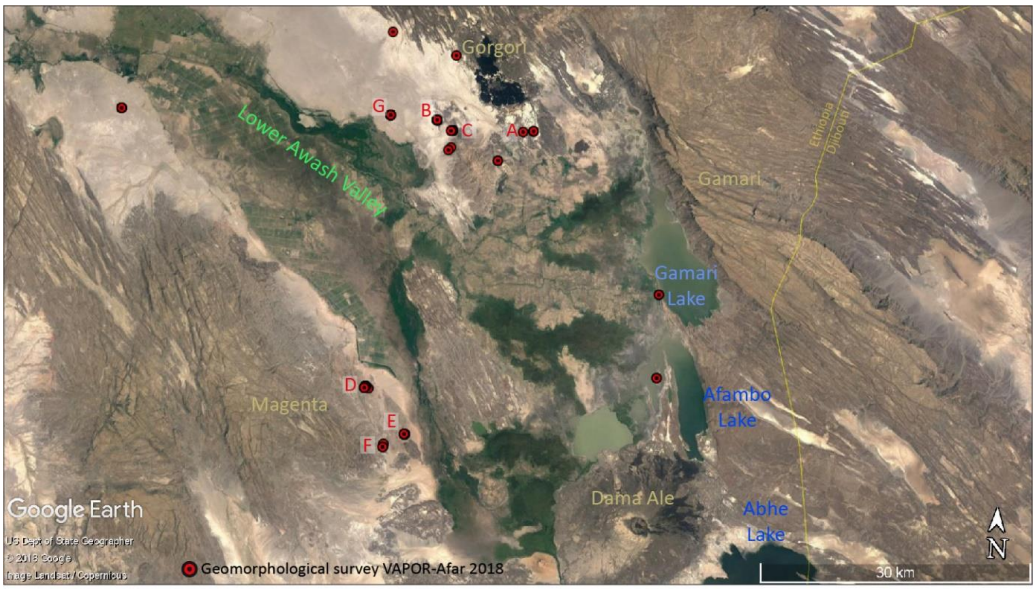

***Figure 1**: Lower Awash Plain map with relative lakes (blue), principal reliefs (pale yellow) and geomorphological 2018 VAPOR-Afar survey points (red circles). **A)** Pleistocene-Holocene diatomitic sequence at Gorgori sector, Fig.3; **B)** Kulsi Koma Hill and relative lacustrine and pedological/archeological sequences, Fig.2, 4, 6, 8; **C)** Litoral facies carbonate conglomerate at Borawli Mountain, Fig.5; **D)** Goma'tu lacustrine limestone and volcanic-lacustrine sequences, Fig.7, 9; **E)** Af'asi Volcanic-lacustrine sequence, Fig.7; **F)** Gali Koma sequence, Fig.10; **G)** 'Mine de Sable' pedological/archeological sequence at Kurub plain, Fig.8.*

Field Methods	*Goals and methods of geomorphological and geoarchaeological VAPOR-Afar 2018 survey*

We have conducted the 2018 geomorphological survey in the Lower Awash valley with the aim to document and sample sedimentary formations from the Pleistocene and Holocene until today. This work seeks to provide the data for the landscape reconstruction of the Lower Awash Valley and to lay the foundations to revisit and ameliorate the paleocliamtological theories proposed by F. Gasse in 70s. The geomorphological work is coupled with archaeological research, which is the essential element of the VAPOR-Afar program. The 2018 geomorphological and geoarchaeological survey was based on the exploration of the field areas not previously studied. The potential survey areas and sedimentary archives were estimated from the known geological data [5], literature from the 70s focused on this area, DEM (Digital Elevation Model) analyses, thematic maps, and from the information collected through the 2014-2017 VAPOR-Afar missions. Over the 2018 survey we have documented more than 10 sedimentary formations, with the objective to date them and will return on forthcoming field trips to conduct more extensive analyses. The field work included the description of sedimentary formations and their sampling using a selective sampling methodology.

Results	*The variability and significance of sedimentary archives at the Abhe Lake Paleobasin*

In this section we present the results and observations obtained from the VAPOR-Afar 2018 geomorphological and geoarchaeological survey, starting with the presentation of the Holocene formations and following with the other Plio-Pleistocene formations detected in the field.

Holocene Deposits

1) Lacustrine deposits and their significance

During the fieldwork we recognised different types of lacustrine deposits, each with a precise significance. The variability of these lacustrine deposits depends from their spatial distribution and principally from their niche-environment formation. The niche-environment formation depends on the water column depth where sediments form. Consequently, each type of lacustrine deposit immediately gives us the information about their water depth provenance and the relative significance of the paleoenvironment. We present these formations following their spatial sedimentary genesis from the bottom waters to the upper water levels of the Abhe paleolake. Four types of lacustrine sediments are recognised: the diatomite bottom sediments, the *Melanoides tuberculata* shell sediments, the stromatolite formations and the wave abrasion surfaces and related formations.

A) The Lake Bottom (diatomite formations)

Diatomite is present across the entire Abhe Paleolake basin: at the centre of the Awash plain and on the slope margins of the basin. The preservation of diatomite is directly correlated with the erosion rate and thus represents a non-continuous sedimentary archive. Diatomites are generally formed at the bottom of the lake, following the substrate morphology, and consequently they do not represent a water level indicator. They are composed principally of diatoms and detrital/authigenic material (clays, silts, authigenic carbonates). The study of diatom flora can give qualitatively rich information about the salinity, the pH, the trophism characteristics of water and their biotope (planktonic, littoral, aerophyte, etc.;[1,6]). During the 2018 fieldwork we recognised and documented some diatomite at the edge of the Abhe paleolake basin (Figure 2).

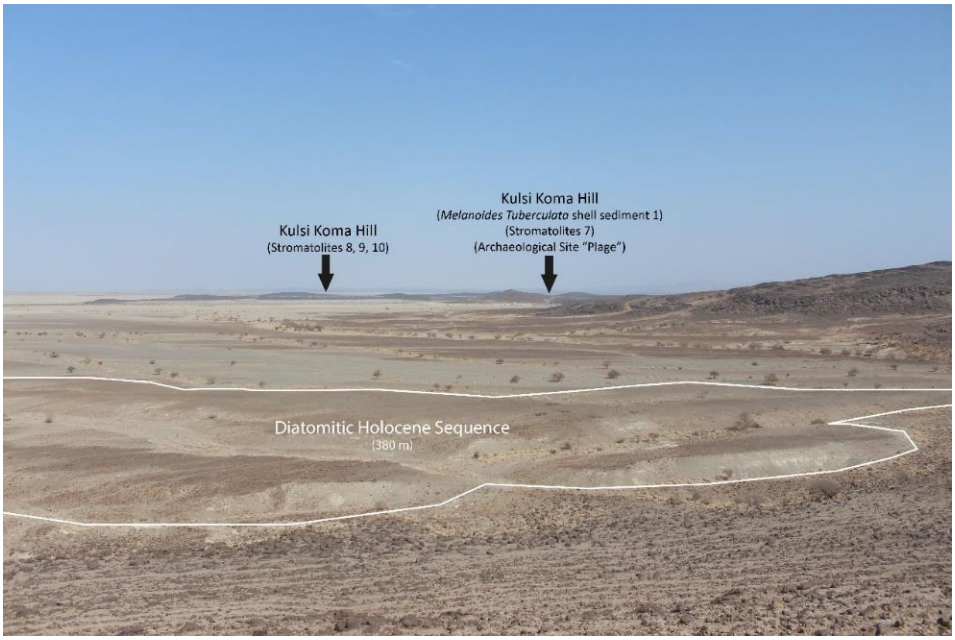

***Figure 2**: View of Kulsi Koma Hill (point B, Fig.1) and the DIatomitic Holocene sequence at Kurub Plain from western slopes of Borawli (point C Fig.1).*

The most complete diatomitic sequence documented during the 2018 VAPOR-Afar field season was identified at the Gorgori sector, to the East of Borawli Mountain (point A, Figure **1**). This diatomitic formation was reposed on irregular recent quaternary volcanic formations [7]. One layer of white diatomite, probably Holocene (Figure 3), was reposed on the foothills of this basaltic formation. At the top of the basaltic hills another diatomitic formation was found. From the bottom to the top it was composed of: A) gray clay-diatomitic sediment with rare *Melanoides tuberculata* shells; B) pale-brownish clay-diatomitic sediment with rare *Melanoides tuberculata*; C) one carbonate thin layer; and D) alluvial and colluvium deposits (Figure 3). This second upper diatomite formation probably had a Pleistocene origin (as it was more elevated then the Holocene formations; sediment similar to the Pleistocene facies documented by Gasse[1]). Therefore, some *Melanoides* was sampled for dating analysis and to confirm this hypothesis. The carbonate layer may indicate a regression lacustrine phase, while the alluvial and colluvium deposit reflects the activation of the hydrologic peripheral system of the Abhe Lake basin subsequent to the lake regression.

Table 1

Diatomite deposit samples				
Sample Name	**East**	**North**	**UTM**	**Elevation (m)**
Diatomite Pleis 1	41,51283572214420	11,667379	37P 0773957 ; 1290989	
Diatomite Hol 1	41,43143781278560	11,647098	37P 0765097 ; 1288667	381,00
Diatomites Pleis 2, Niveau 1	41,51301476170290	11,667919	37P 0773976 ; 1291049	
Diatomites Pleis 2, Niveau 3	41,51301476170290	11,667919	37P 0773976 ; 1291049	
Gada 'Ale Diatomite	41,38055134240640	11,354841	37P 0759814 ; 1256278	373,00

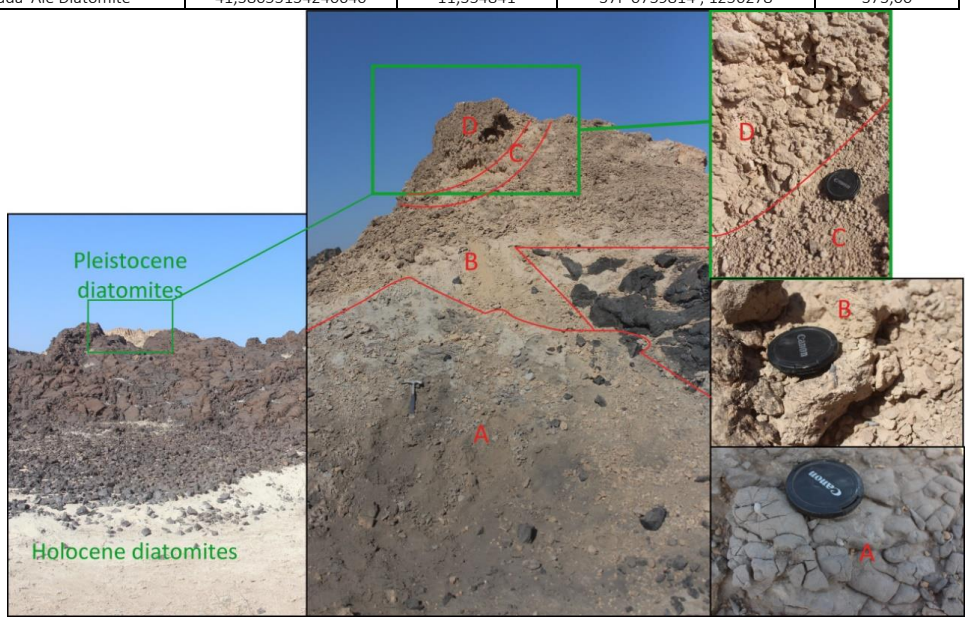

***Figure 3**: Pleistocene-Holocene diatomitic sequence at the Gorgori sector (point A, Fig.1): : **A)** gray clay-diatomitic sediment with rare Melanoides tuberculata shells; **B)** pale-brownish clay-diatomitic sediment with rare Melanoides tuberculata; **C)** carbonate thin layer; **D)** alluvial and colluvium deposits.*

B) **Upper Level Waters** *(Melanoides tuberculata* shell deposits)

A typical lacustrine sediment founded in the Abhe paleolake basin is the *Melanoides tuberculata* shell deposits. It is a deposit that is composed by one part of detrital material (silts and sands), authigenic carbonate and several quantities of freshwater gastropods (*Melanoides tuberculata* or red-rimmed melania). These gastropods can be found in a substratum consisting of soft mud, sand or occasionally rock between 1 and 3 m of water depth [8]. *Melanoides* are frequently associated with bivalve shells. We found this type of deposit at the Kulsi Koma Hill sequence (point B, Figure 1; Figure 7) and at the Af'asi sector (point E, Figure 1; Figure 4).

***Figure 4**: Melanoides tuberculata shell deposit covered by a volcanic pyroclastic layer at the Af'asi sector (point E, Fig.1).*

Melanoides tuberculata shell deposit samples				
Sample Name	East	North	UTM	Elevation (m)
Niv Coquilles 1	41,43046000000000	11,663480	37P 0764975 ; 1290478	381,00
Niv Coquilles 2	41,35991000000000	11,409820		369,00
Niv Coquilles 3	41,40132000000000	11,365370		

Table 2

Shallow Level Waters (stromatolite formations)

Stromatolites are lacustrine layered accretionary fossil sediments built by cyanobacterial activity. Stromatolitic sequences are formed in the shallow water of evaporitic lakes, therefore they represent a precise indicator of the paleo-shoreline, and relate to the lake high water-levels [9–11]. We have documented 12 stromatolitic formations on the slopes of the Abhe paleolake basin. They represent the principal tool for the reconstruction of the paleo-shorelines of the Pleistocene and Holocene lakes. In particular, at Kulsi Koma Hill (371 m; Figure 2, point B Figure 1) we documented the biggest stromatolitic formation ever observed in the Abhe paleolake basin, with 50-60 cm thick stromatolitic domes (Figure 5). Stromatolites are indicators of the climatic stability of the littoral lake environments. The dating of these littoral lacustrine biogenic rocks can provide the precise age of the lake high water level relative to the humid climatic periods.

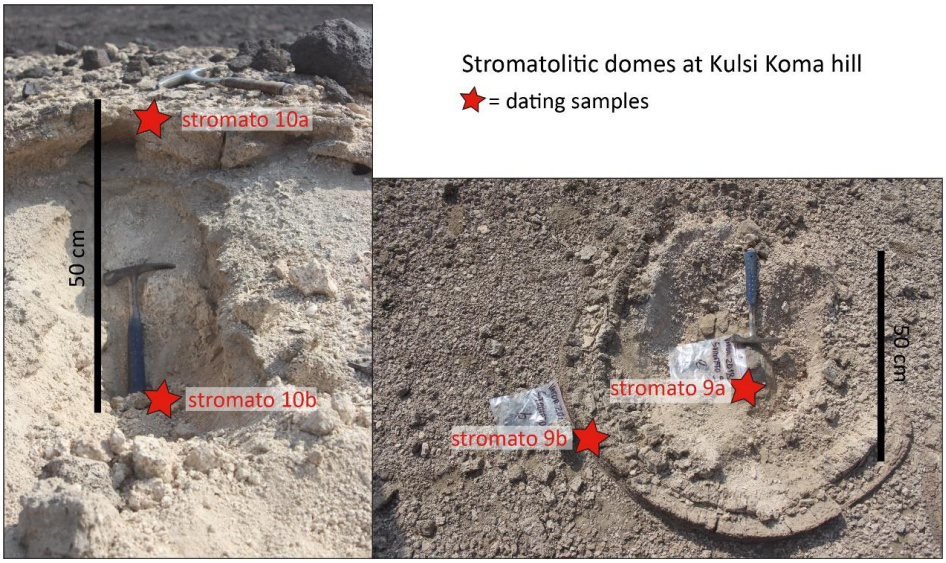

***Figure 5**: Stromatolitic domes at Kulsi Kome Hill (point B, Fig.1) and relative dating sample locations.*

Stromatolite samples				
Sample Name	East	North	UTM	Elevation (m)
Stromatolite 1 Sup	41,47885706923230	11,6367810	37P 0770280 ; 1287570	387,00
Stromatolite 1 Inf	41,47885706923230	11,6367810	37P 0770280 ; 1287570	375,00
Stromato Colline	41,36706895170450	11,7572370	37P 0757973 ; 1300796	389,00
Stromatolite 4	41,42893087501330	11,6444800	37P 0764826 ; 1288375	374,00
Stromatolite 5	41,43233	11,6494		
Stromatolite 6	41,43233	11,6494		
Stromatolite 7	41,43058	11,66355		
Stromatolite 8	41,41639503038760	11,672526	37P 0763432 ; 1291467	368,00
Stromatolite 9B	41,41601729197720	11,673369	37P 0763390 ; 1291560	371,00
Stromatolite 9A	41,41601729197720	11,673369	37P 0763390 ; 1291560	371,00
Stromatolite 10A	41,41558	11,6735		
Stromatolite 10B	41,41558	11,6735		
Stromatolite 11	41,43165	11,73781	37P 0765020 ; 1298701	384,00
Stromatolite 13	41,36254581661970	11,407931	37P 0757800 ; 1262137	381,00
Stromatolite 14	41,40031012595420	11,365398	37P 0761962 ; 1257464	372,00

Table 3

C) **Lacustrine Littoral Morphologies** (wave abrasion surfaces and carbonated conglomerates)

The lacustrine littoral activity is observed on the slopes thanks to the abrasion surfaces generated by the wave action (Figure 7). We also documented some carbonate conglomerates produced by the surface lithological remains of a lake paleo-beach (Figure 6).

***Figure 6**: Carbonate conglomerate produced by the surface lithological remains of a lake paleo-beach on the western side of Borawli Mountain (point C, Fig.1).*

On Kulsi Koma Hill we found a semi-complete lacustrine sequence, which probably correlated with a paleosoil development and human occupation (Figure 7) discussed in the paragraph 3 (page 8).

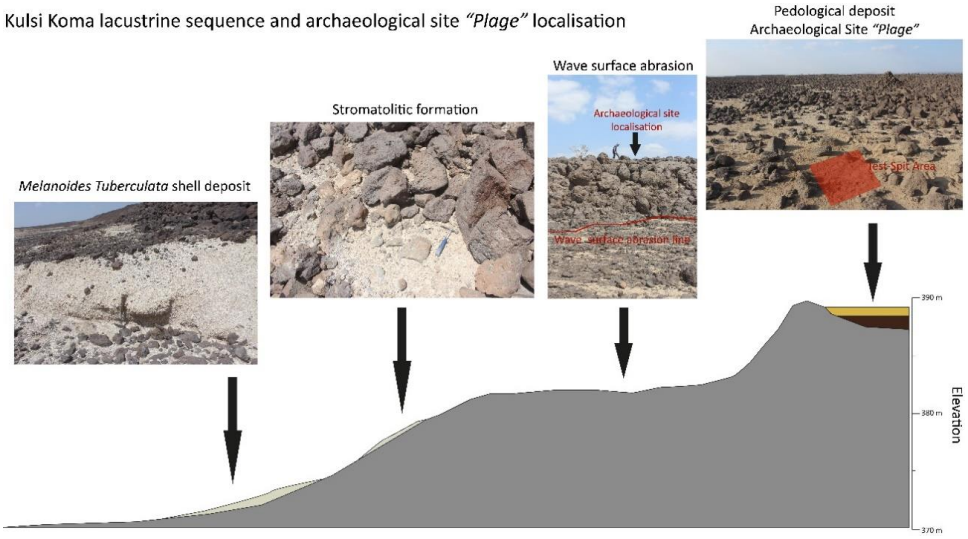

Figure 7: *Illustration of the Kulsi Koma Hill lacustrine sequence (point B, Fig.1) and archaeological site "Plage" location (Fig.9).*

2) Volcanic-Lacustrine Deposits

The central Afar region is known to include the most volcanic areas of the Eastern Africa. In the Lower Awash Plain some volcanos were active during the Holocene and the Pleistocene periods. However, the precise Pleistocene-Holocene volcanic history of the Central Afar is still unknown. The first attempt at tephrochronology of the Afar was only recently achieved [12].

During our field campaign, we recognised and documented different volcanic deposits intercalated, or included in lacustrine sequences. At Af'asi (point E, Figure 1) we observed pyroclastic products associated with bivalve or gastropod remains or *in situ* layers (Figure 8), while at Goma'tu we found around 7 meters of lacustrine and palustrine sedimentary sequences affected by burnt sediments and volcanic *facies* (Figure 8).

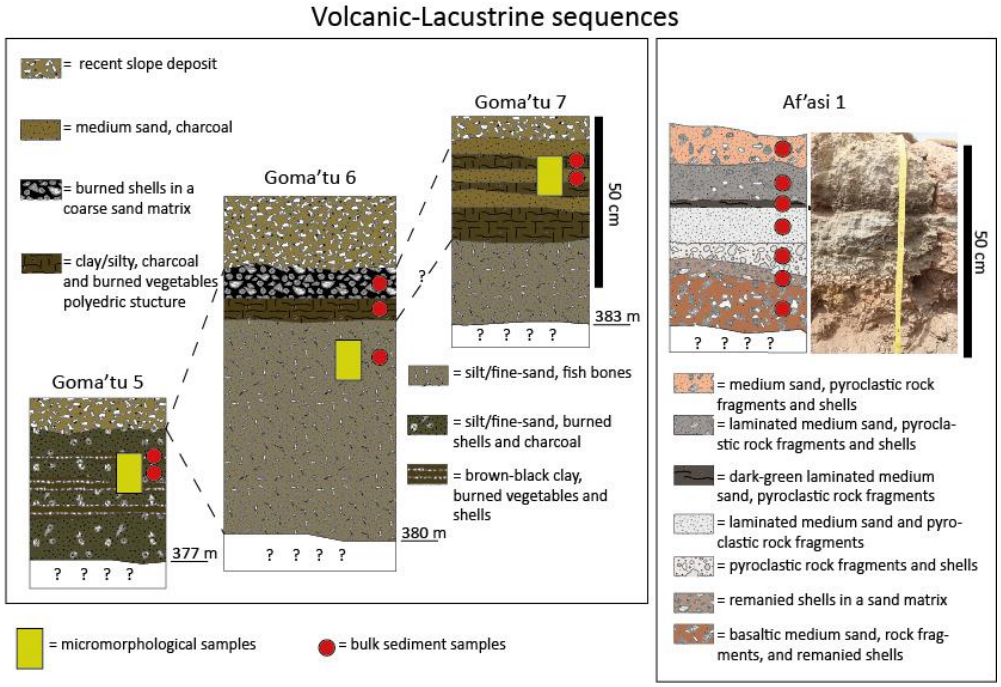

Figure 8*: Goma'tu (point D, Fig.1) and Af'asi (point E, Fig.1) volcanic-lacustrine sequences*

Volcanic-lacustrine sediment samples				
Sample Name	East	North	UTM	Elevation (m)
Goma'tu 5	41,35952046016450	11,409817	37P 0757468 ; 1262343	377,00
Goma'tu 6, US 3	41,35940131968210	11,409809	37P 0757455 ; 1262342	380,00
Goma'tu 6, US 2	41,35940131968210	11,409809	37P 0757455 ; 1262342	380,00
Goma'tu 6, US 1	41,35940131968210	11,409809	37P 0757455 ; 1262342	380,00
Goma'tu 7 Litage argile	41,35943840325530	11,409863	37P 0757459 ; 1262348	383,00
Goma'tu 7 Litage sable	41,35943840325530	11,409863	37P 0757459 ; 1262348	383,00
Af'asi 1, US 1	41,40077457150990	11,365087	37P 0762013 ; 1257430	367,00
Af'asi 1, US 2	41,40077457150990	11,365087	37P 0762013 ; 1257430	367,00
Af'asi 1, US 3	41,40077457150990	11,365087	37P 0762013 ; 1257430	367,00
Af'asi 1, US 4	41,40077457150990	11,365087	37P 0762013 ; 1257430	367,00
Af'asi 1, US 6	41,40077457150990	11,365087	37P 0762013 ; 1257430	367,00
Af'asi 1, US 7	41,40077457150990	11,365087	37P 0762013 ; 1257430	367,00

Table 4

3) Archaeological evidence in the Paleosoils/Paleodunes sequences of the Lower Awash Plain

One of the purposes of the 2018 campaign was to try to better understand the sedimentary context and the formation processes of the archaeological sites discovered and excavated during the 2014-2017 VAPOR-Afar field seasons (Det-Bahari, Kurub-07). These sites are based on paleosoil formations and are covered by fixed or mobile dunes. In the Lower Awash Plain, the origin and the environmental significance of these paleosoils is still unknown today. We started the 2018 VAPOR-Afar campaign with the documentation and the study of pedological sequences with the ambition to develop a paleosoil typology of the Lower Awash Valley. We recognised and documented 3 paleosoil sequences:
A) The first sequence ("Mine de Sable" 1 and 2, Figure 9), in the Kurub-Bahari area (point G, Figure 1) contains 10 paleosoils only 3 m in depth, intercalated with some aeolian deposits. In one of these paleosoils we found an obsidian knapped flake. The alternation between aeolian and pedological deposits throughout the same sequence might reflect the alternation between humid and arid periods in the past. B) One test-pit on Kusi Koma Hill (point B, Figure 1) has allowed us to find a 50 cm thick paleosoil containing some obsidian knapped flakes (Figure 9). This paleosoil is located on the Kulsi Koma slope, continuous with the *Melaonides* shell deposit, the stromatolite formation and the wave abrasion surface illustrated in Figure 7. The human occupation associated with the paleosoil probably occurred at the same time as the high water level evidenced by the closed lacustrine deposits. The dating of the lacustrine and pedological deposits could confirm this hypothesis. C) At Goma'tu 7 (point D, Figure 1, Figure 8) we localised one little sequence of thin paleosoils that were rich in charcoal and fish bones.

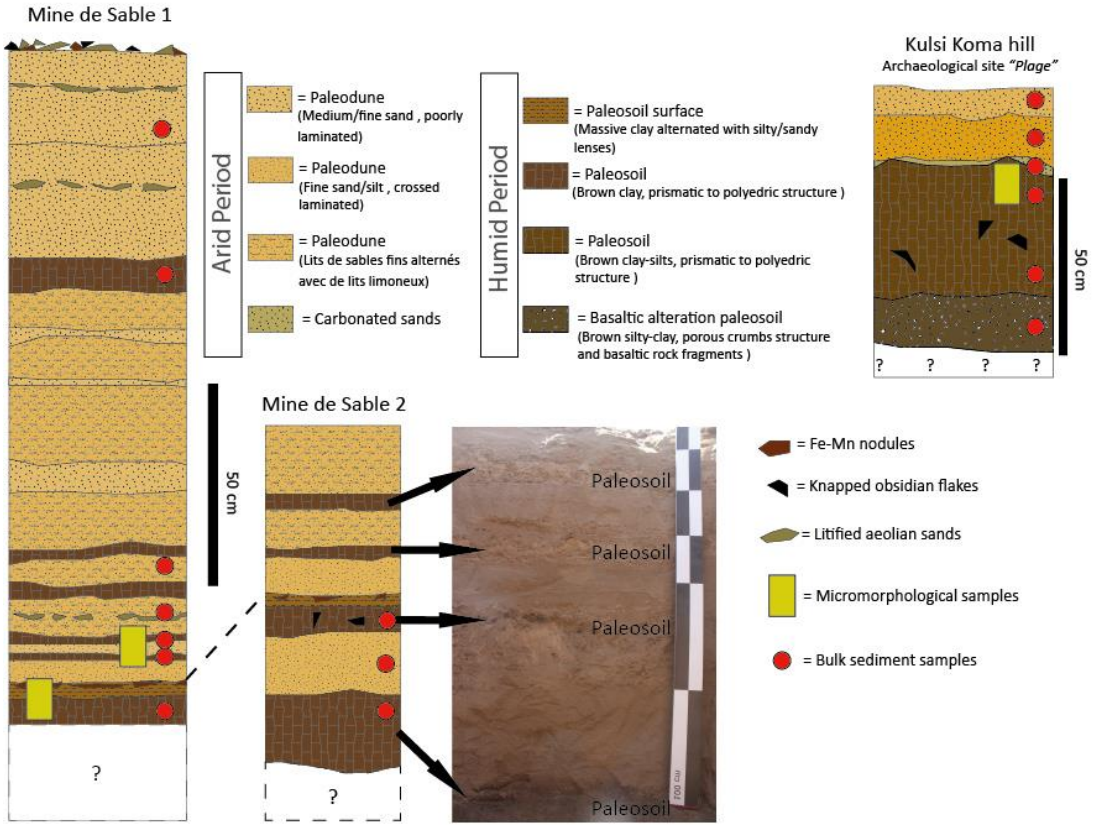

***Figure 9**: Pedological sequences and associated archaeological sites in the Lower Awash Valley.*

Pedological and dune/paleodune sediment samples				
Sample Name	East	North	UTM	Elevation (m)
Sables eoliennes 1	41,50256085072670	11,666502	37P 0772837 ; 1290882	363,00
Sables eoliennes Det Bahari	41,10280480723600	11,667148	37P 729234 ; 1290599	386,00
Det Bahari Site	41,10280480723600	11,667148	37P 729234 ; 1290599	386,00
Mine de Sable 2, US 2	41,36947266342840	11,675619	37P 0758311 ; 1291766	
Site Plage 1, Test Pit 1, US 3	41,43220764669640	11,663925	37P 0765165 ; 1290530	392,00
Mine de Sable 2, US 3	41,36947266342840	11,675619	37P 0758311 ; 1291766	
Mine de Sable 2, US 1	41,36947266342840	11,675619	37P 0758311 ; 1291766	
Site Plage 1, Test Pit 1, US 2, Sup	41,43220764669640	11,663925	37P 0765165 ; 1290530	392,00
Site Plage 1, Test Pit 1, US 2, Inf	41,43220764669640	11,663925	37P 0765165 ; 1290530	392,00
Mine de Sable 1, US 1	41,36939015620230	11,675619	37P 0758302 ; 1291766	
Site Plage 1, Test Pit 1, US 4	41,43220764669640	11,663925	37P 0765165 ; 1290530	392,00
Site Plage 1, Test Pit 1, US 5	41,43220764669640	11,663925	37P 0765165 ; 1290530	392,00
Mine Sable 1, US 3	41,36939015620230	11,675619	37P 0758302 ; 1291766	
Site Plage 1, Test Pit 1, US 1	41,43220764669640	11,663925	37P 0765165 ; 1290530	392,00
Mine de Sable 1, US 2	41,36939015620230	11,675619	37P 0758302 ; 1291766	
Mine Sable 1, US 12	41,36939015620230	11,675619	37P 0758302 ; 1291766	360,00
Mine Sable 1, US 14	41,36939015620230	11,675619	37P 0758302 ; 1291766	360,00
Mine Sable 1, US 9	41,36939015620230	11,675619	37P 0758302 ; 1291766	360,00
Mine Sable 1, US 7	41,36939015620230	11,675619	37P 0758302 ; 1291766	360,00
Mine Sable 1, US 4	41,36939015620230	11,675619	37P 0758302 ; 1291766	360,00

Table 5

Plio-Pleistocene Deposits

1) The Goma'tu lacustrine limestone and related volcanic activity

Around the Goma'tu area (point D, Figure 1), from 385 to 400 meters of elevation, we have documented and sampled a lacustrine limestone that is very different and not attributable to the Holocene diatomites observed in the rest of the Lower Awash Plain. Normally the Holocene diatomites and limestones are located between 250 and 380m. Furthermore, the Holocene shallow water deposits (shell deposits and stromatolites, page 5) reach a maximum of 390 meters. In addition, this deep-water limestone deposit presents some differences from the more recent diatomite facies: it is partially or completely diagenised and much more layered in comparison with the Holocene diatomitic formations.

From an elevation of 380 m, the Goma'tu limestone follows the slope inclination with a sub-horizontal layering and ends on the basalt substratum cliff at 400 m elevation. The contact with the substratum is highly irregular: the limestone is frequently crushed and covered by posterior basaltic subaqueous flows (C. Doubre personal communication) and then verticalised (inverse and vertical layering; Figure 10).

We predict that this Pleistocene (possibly 2nd lacustrine phase between 40 and 35 ka BP [1]) deep water sediment was deformed and partially covered by a basaltic flow descending from the slope into the lake waters.

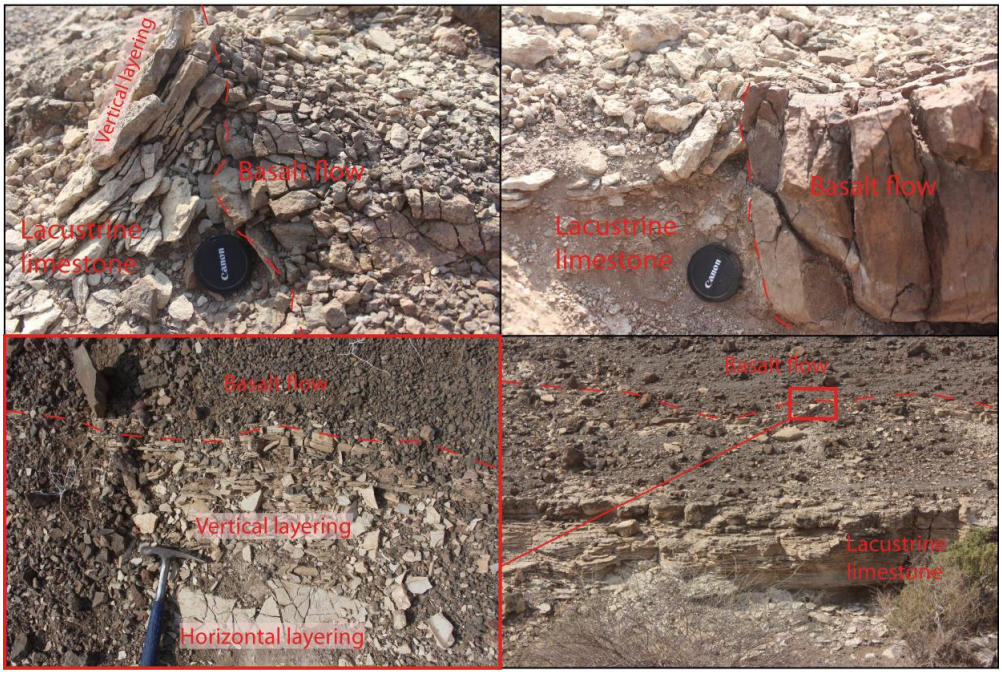

***Figure 10**: Goma'tu lacustrine limestone and related basaltic flow.*

2) The Gali Koma Sequence

In the middle of the Galedda'ar Plain (point F, Figure 1) the Gali Koma Mountain was attributed to the basaltic fissure flows from the upper part of stratoid series by Varet [5,7]. During the 2018 VAPOR-Afar field season we observed that the Gali Koma mountain is composed almost exclusively of lacustrine, fluvio-lacustrine and pedological sedimentary deposits. The Gali Koma sequence started from the Galedda'ar plain at 370 m and finished with a 2 meter layer of basaltic rock at an elevation of 460 m (Table 6, Figure 12). Sedimentary unit 6 contained a lot of mammal fossils (Figure 11, Table 6), unit 4 had some bivalve shells (g, Figure 12) and the unit 1 was composed principally of plant fossils (i, Figure 12). This sedimentary formation may represent the first complete Plio-Pleistocene sequence with the stratigraphic

documentation of mammal fossils in the Lower Awash Valley. The dating of the upper basaltic layer is planned to determine the first time-frame of the Gali Koma sequence.

***Figure 11**: Mammal fossils collected from US6 of the Gali Koma sequence.*

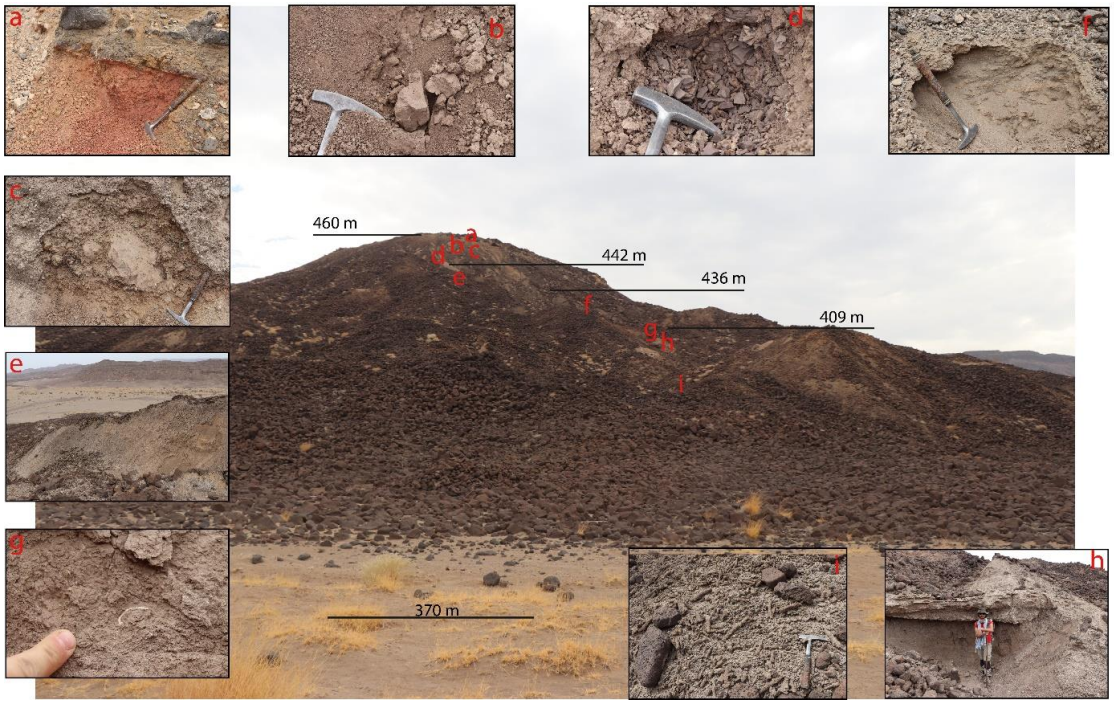

***Figure 12**: Gali Koma sequence (Tab.6) pictures: **a)** US14-13-12; **b)** US11 ; **c)** US10 ; **d)** US8 ; **e)** US7-6; **f)** US6 ; **g)** US4 ; **h)** US3-2 ; **i)** US1.*

Preliminary stratigraphic description of the "*Gali Koma*" sequence (Afar, Ethiopia)						
US	**Deposit Type**	**Stratigraphic Description**	**Coordinates**		**Elevation (m)**	**Location and pictures Fig. 12**
			Latitude	Longitude		
\	*Actual alluvial plain*	Actual alluvial plain: covers the lower part of Gali Koma slopes.			370	
1	*Plant fossil sands*	Coarse sand well selected, cross layered with plant fossils in sub-horizontal position				**i**
2	*Paleosoil*	Brownish clay-silts, oblique prismatic macrostructure (oblique elongate prisms 20x40 cm) and prismatic columnar to polyedric mesostructure (aggregates 2-4 cm), carbonate infillings along the macrostructure plane porosity.				**h**
3	*Coarse sandy conglomerate*	Coarse sand conglomerate, well selected and planar layering, erosive surface on the paleosoil (US2).				**h**
4	*Bivalve sands*	Medium layered sand, well selected with *in situ* bivalve shells.	11,35287	41,38054	409	**g**
5	*Lacustrine silts*	Brown-grey massive silt-clays.				
6	*Mammal sands*	Grey medium sands, crossed layering, well selected, alternated with a cemented layered sand level with mammalian fossils.	11,3522	41,38018	436	**e-f**
7	*Gipsy paleosoil*	Brownish clay-silts, prismatic to polyedric structure, gypsum and low developed porosity.				**e**
8	*Massive clays*	Dark brown massive clays slightly lithified, without inclusion and no developed porosity	11,35191	41,38026	442	**d**
9	*Lacustrine silts*	Brown-grey silt-fine sands, massive (lacustrine?).				
10	*Erosive conglomerate*	Poorly layered conglomerate, poorly selected with coarse sands, gravels and rounded rocks, and brown-grey silty-sandy relict sedimentary rounded blocs (sedimentary blocs similar to US9).				**c**
11	*Paleosoil*	Massive brown silty-clays with authigenic carbonates.				**b**
12	*Rubefied paleosoil*	Pale red silty-clays with polyedric sub-angular structure (aggregats 1-2cm)				**a**
13	*Altered basalts*	Altered basalt with fine sand inclusions in plane voids porosity.				**a**
14	*Basalts*	Basaltic fissure flows from the upper part of stratoid series? (Dating sample for age determination)	11,35169	41,37994	455	**a**
15	*Top/recent silt and clays*	On the basalt layer (US14) are based few anthropic circular stone structures and >40 cm of sandy-clay sedimentary deposit + obsidian knapped flakes.	11,35147	41,37964	460	

Table 6

Future Work	Toward the reconstruction of the Human-Environment coevolution in the Lower Awash Valley

The Age Model of the Abhe Lake Paleobasin Sedimentary Archives

To better understand the landscape evolution and the relative Pleistocene-Holocene prehistoric occupation of the Lake Abhe paleobasin, the construction of a new age model of the principal sedimentary archives is required. Until 1975, 73 ages were measured almost only on lacustrine sediments. It is only since 2014 that the VAPOR-Afar program started a new dating campaign with the age determination of 2 archaeological sites and one sedimentary sequence.
In this report we have shown the great variability in the sedimentary archive of the Lower Awash region, represented by pedological, aeolian, volcanic, lacustrine, palustrine and fluviatile deposits. The aim of this project is to document all sedimentary deposits that can give new paleoclimatologic, paleoenvironmental and archaeological information.
For this reason, before the next VAPOR-Afar field season (December 2018), we plan to date the paleosoil sequences and the stromatolitic formations documented during the last fieldwork expedition in the Afar region.

References	

1. Gasse, F. L'évolution des lacs de l'Afar Central (Ethiopie et T.F.A.I.) du Plio-Pléistocène à l'Actuel. Recostitution des paléomilieux lacustres à partir de l'étude des Diatomées. (Université de Paris VI, 1975).
2. Gasse, F. Evolution of Lake Abhe (T.F.A.I.), from 70,000 BP. *Nature* **265,** 42–45 (1977).
3. Rognon, P. & Gasse, F. Depots lacustres quaternaires de la basse vallée de l'Awash (Afar, Ethiopie): leurs rapports avec la techtonique et le volcanisme sous-aquatique. *Révue Gèographie Phys. Géologie Dyn.* **XV,** 295–316 (1973).
4. Ruegg, J.-F. & Briole, P. Mouvements du sol holocènes dans le rift d'Asal à Djibouti, Holocene crustal movements in the Asal Rift, Djibouti. *Comptes Rendus Académie Sci. Sér. 2 Mécanique Phys. Chim. Sci. Univers Sci. Terre* **310,** 1687–1694 (1990).
5. J. Varet. *Geology of Afar (East Africa)*. (2018).
6. Gasse, F., Barker, P., Gell, P. A., Fritz, S. C. & Chalié, F. Diatom-inferred salinity in palaeolakes: an indirect tracer of climate change. *Quat. Sci. Rev.* **16,** 547–563 (1997).
7. Varet, J. *Geology of Central and Southern Afar (Ethiopia and Djibouti Republic)*. (Editions du Centre National de la Recherche Scientifique, 1978).
8. Murray, H. D. Melanoides tuberculata (Müller), Las Morras Creek, Bracketville. *Bullettin Am. Malacol. Union* 43 (1975).
9. Krumbein, W. E. Stromatolites — the challenge of a term in space and time. *Precambrian Res.* **20,** 493–531 (1983).
10. Reid, R. P. Stromatolites. in *Encyclopedia of Modern Coral Reefs* (ed. Hopley, D.) 1045–1051 (Springer Netherlands, 2011). doi:10.1007/978-90-481-2639-2_152
11. Riding, R. The term stromatolite: towards an essential definition. *Lethaia* **32,** 321–330 (2007).
12. Martin-Jones, C. M. *et al.* Glass compositions and tempo of post-17 ka eruptions from the Afar Triangle recorded in sediments from lakes Ashenge and Hayk, Ethiopia. *Quat. Geochronol.* **37,** 15–31 (2017).

BII.2 VAPOR-Afar 2018-2019 Field Season - Lake Coring, Geomorphological and Geoarchaeological Report

VAPOR-Afar 2018-2019 Field Season

Lake Coring, Geomorphological and Geoarchaeological Report

C. Mologni, M. Revel, L. Khalidi, F. Arnaud, M. Mallet, E. Chaumillon, T. Coulombier, G. Davtian

Paleoclimate - Gamari & Afambo Lake soundings

I - Scientific context

During the Pleistocene, tropical Africa has been affected by climatic oscillations of humid and arid periods, which are driven by the variability of the African monsoon (controlled by the position of the Earth in relation to the sun, mainly the precession; Gasse, 2000). The African Humid Period (AHP) was the last period of heavier rainfall than today, dated between 14 and 6 ka cal BP (Shanahan et al., 2015; Tierney et al., 2011). In the Afar region, the succession of humid, arid periods and hyper-arid events over the past 20,000 years both provided favorable ecosystems that may have facilitated societal development, but also arid environments that may have restricted human exploitation of the landscape (Hoelzmann et al., 2001; Kuper and Kröpelin, 2006; Trauth et al., 2010). In Afar region, paleoclimate knowledge is mainly based on the work of F. Gasse, conducted in the 1970s. A 6 to 50 m deep continuous core borehole was drilled along the eastern shoreline of the current Lake Abhé shoreline in 1971 by BRGM (Demange et al., 1971). The dates of this survey revealed that the 50 m core covers ~70,000 years (Gasse, 1977, 1975; Gasse and Street, 1978). The study of sedimentation facies coupled with the recognition of the different species of diatoms has led to the reconstruction of fluctuations in arid phases (low lake levels) and wet phases (high lake level).
In the VAPOR-Afar project, we propose to reconstruct the paleo-hydrological regime of the Awash River from multi-proxy studies of sediments from Lakes Gamari and Afambo. These lakes, formed within the northernmost half-graben basin of the East African Rift System are chosen for their location in the eastern end of the Sahel zone (at 11°N) and for the presence of numerous archaeological sites. Thus, the sediments of these lakes, accumulated since ~4 MA, are valuable witnesses to major environmental and paleoclimate changes in tropical latitudes.
The coring operations was effectuated both on Gamari and Afambo lakes under the supervision of M. Revel (GEOAZUR-UMR7329) during December 2018 VAPOR-Afar mission.

II –Methodology

- Field methods

Seismic reflection method was employed on Gamari Lake with ECHOES 5000 sub-bottom profiler (SBP) system allowing high resolution surveys in various operating conditions (lake, shallow & deep waters; E. Chaumillon, T. Coulombier expertise, LIENSs-UMR7266). A GPS Topcon is used for the profiles and cores localisation. For coring operations on both Gamari and Afambo Lakes, the Uwitec Gravity Corer was used (F. Arnaud and M. Mallet expertise, EDYTEM-UMR5204).

- Laboratory and dating methods

Seismic XTF signal was converted in SEGY with the Delph Traitement package (L. Schenini expertise, GEOAZUR-UMR7329). Lacustrine cores were opened, lithostartigraphically described and photo-documented at EDYTEM-UMR5204 laboratory. Colour description of sediments is made in accord with Munsell Cholor Chart system, while the pictures of the cores was assembled with Agistoft Photoscan program, giving a high-resolution orthophotos data. XRF major element analysis was performed with Avaatech XRF Core Scanner technology at EDYTEM-UMR5204 laboratory.
The age model of lacustrine sequences is based on Accelerator Mass Spectrometry (AMS) ^{14}C measures obtained on vegetal macroremains and lacustrine shells. Where organic or biogenic carbonated macroremains were absent, ^{14}C dating was performed on sediment bulk organic carbon (OC > 1%). Conventional ages were calibrated with the Oxcal 4.3 program (Bronk Ramsey, 2001) and IntCal13 curve (Reimer et al., 2013). The ages were considered here using 95.4% ranges and are reported in cal. yr BP and in cal. ka BP. The median probability of age is based on weighted average, two sigma probability distributions. For GEM18-03/_04B sequence, an age-depth model was constructed based on a 0.4

span smooth spline interpolation using the programme CLAM (Blaauw, 2010). Grain-size and clay mineralogy analysis on lacustrine sediments are envisaged.

II – Preliminary results

- Seismic profiles and cores localisation

A total 12 seismic profiles were obtained in the southern side of Gamari Lake, which cover the total width of the actual basin (Figure 1). In this part of the Lake, the water-column depth ranges between 2 and 7 meters. No seismic reflection measures were performed on Afambo Lake because of the difficulty of access for ECHOES 5000 equipment.

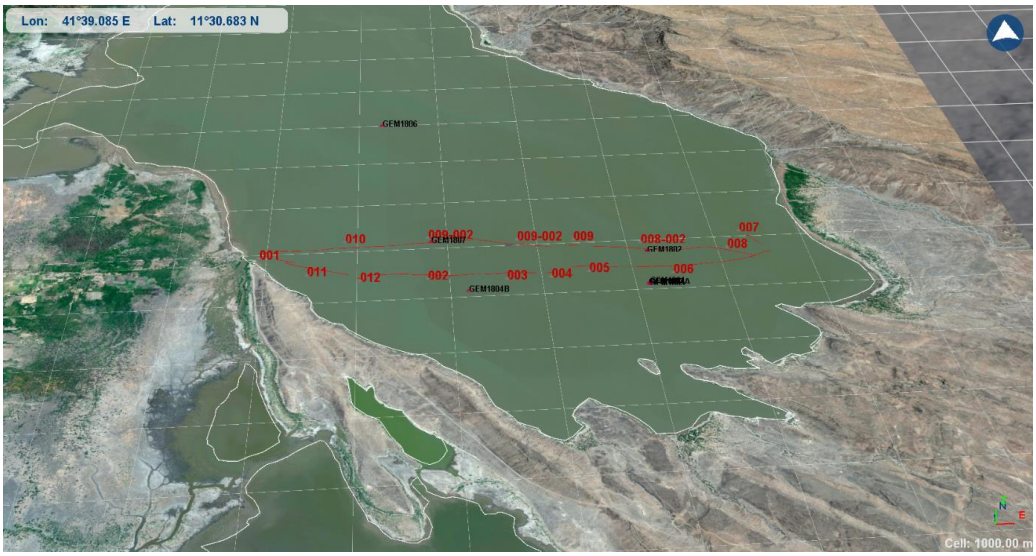

Figure 1 : Gamari Lake seismic profiles and coring points localisation (G. Davtian).

Seismic profiles which permitted the emplacement of coring points show a regular bottom sediment morphologies indicating a deltaic-type sedimentation modalities (Figure 2). No slump or fault morphologies are observed. Some channel-like morphologies at the bathymetric line and at the sub-bottom interface layers suggest that a period of dying waters occurs during which channels could be formed. Could infdicate deltaic progradation morphologies.

A total of 10 lacustrine sedimentary cores sections was retrieved from Gamari and Afambo Lakes (8 from Gamari and 2 from Afambo; Figure 3, Tab 1). At Gamari lake, coring operations was mainly performed in the southern part of the basin (Figure 3). While Afambo cores were retrieved in the deepest zone of the lake (~17m max water-column).

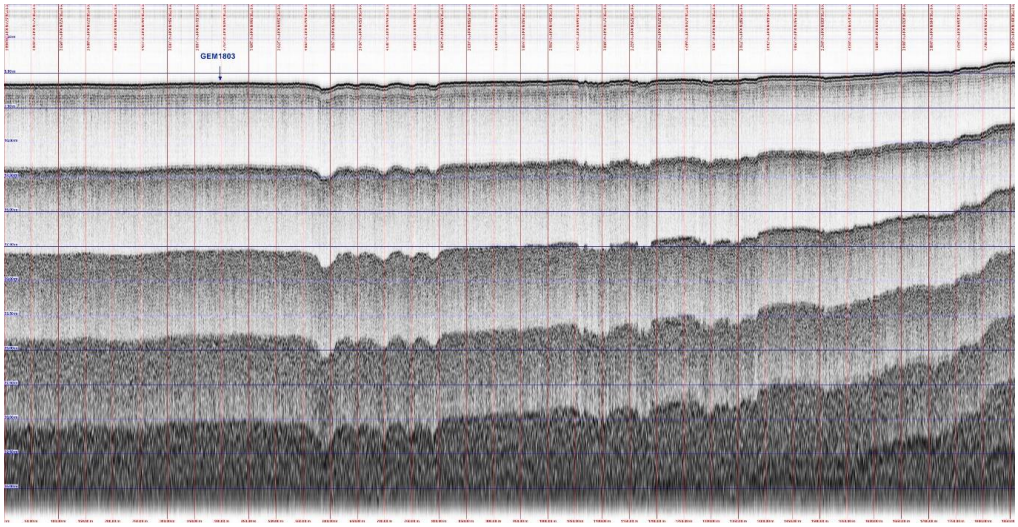

Figure 2 : Lake Gamari seismic profile N° 006 (Figure 1) and emplacement of GEM18-03 core (L. Schenini).

The south-eastern part of the Afambo lake was even chosen because of the strategical position: sheltered from high-energy riverine-induced current flows and from gravity dynamics localised along the eastern Afambo lake faults. The max core length from Gamari lake is 209 cm (GEM18-04A + GEM18-04B; Tab 1). However, GEM18-05 as a preserved bottom part of long core could belongs to a deeper level. AFA18-02 is the longest core obtained from Afambo lake sediments.

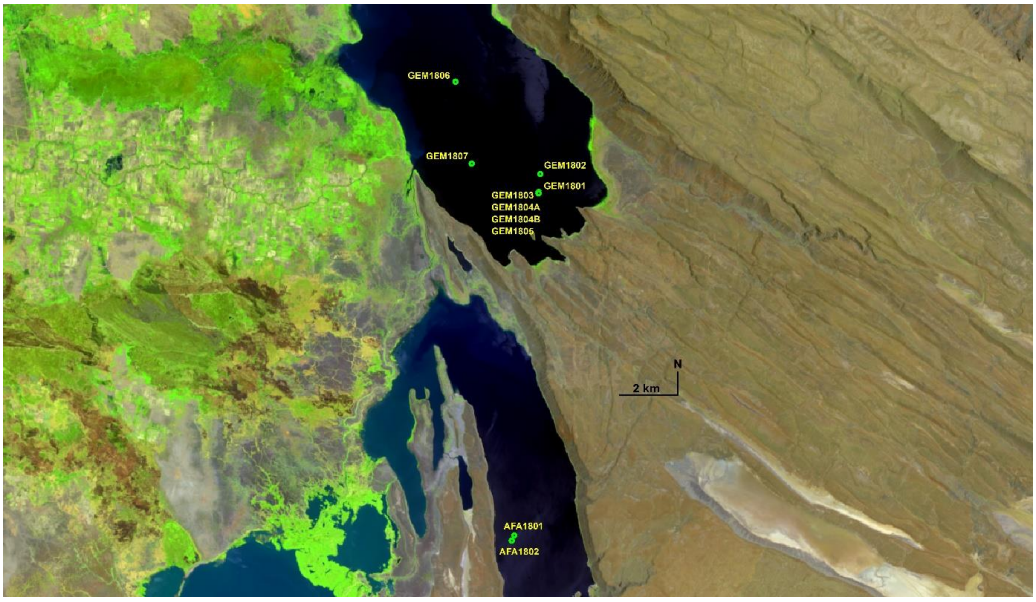

Figure 3 : Cores localisation on Gamari (GEM_) and Afambo (AFA_) lakes (G. Davtian).

Core	Length (cm)	Long	Lat	X UTM37N	Y UTM37N
GEM18-01	82	41,687099	11,506440	793136,108524	1273349,614560
GEM18-02	85	41,687630	11,512000	793188,310562	1273965,577340
GEM18-03	144	41,686939	11,506280	793118,808026	1273331,741120
GEM180-4A	100	41,686951	11,506290	793120,107636	1273332,860260
GEM180-4B	109	41,669510	11,506290	793120,107636	1273332,860260

GEM18-05	106	41,687000	11,506070	793125,684659	1273308,559200
GEM18-06	44	41,661350	11,540750	790289,998694	1277121,025440
GEM18-07	17	41,666199	11,515390	790845,386095	1274318,970800
AFA18-01	131	41,678429	11,400510	792298,577371	1261615,804640
AFA18-02	181	41,677631	11,398920	792213,059089	1261439,008840

Tab 1 : List of lacustrine cores (name, length, geographical and UTM coordinates) retrieved in Gamari and Afambo lakes during VAPOR-Afar December 2018 field season.

➢ Paleolimnology, geochemistry and age models

One lacustrine sequence core was preliminary investigated for each lake: GEM18-03 + GEM18-04B master-core from Gamari and AFA18-02 core from Afambo lake.

- *GEM18-03 + GEM18-04B master-core*

GEM18-03 + GEM18-04B master-core correlation was obtained on the basis of lithostratigraphical and XRF major elements data comparison.
From the top, the first 15 cm (2.5yr-5/2-4/2) are high liquefied, presenting a clayey texture with slight lamination. Between 15 and 34 cm (2.5yr-3/2) a granular to polyhedric structure suggests the development of a pedogenic event. Between 34 and 48 cm (2.5yr-4/2), the clay structure became more massive with a reduction of water content. From 48 cm to 80 cm (2.5yr-3/2) a slight lamination occurs with some shell fragment inclusions. From 85 to 147 cm. Along the sequence 4 shell layers (ostracods: *Melanoides tuberculata*) were observed: at 48.5, 84, 112, 167 cm.
The core sediment is mainly massive and highly compacted, suggesting the homopycnal character of sedimentation modalities. The homogeneity of fine sediment texture and the main massive structure could even indicate the filtering role of Lower Awash plain swamps.

Sample Name	Depth (cm)	Material	Lab Code	Conventional age	Median Cal. BP	σ
GEM18-03_14-15	14	organic sediment	SacA57090	175 ± 30	**179**	**88**
GEM18-03_48-49	48,5	organic sediment	SacA57091	170 ± 30	**178**	**87**
GEM18-03_48-49_malaco	48,5	shell (melania)	SacA57092	post 1950		
GEM18-03_113	113	organic sediment	SacA57093	1760 ± 30	**1664**	**46**
GEM18-03_84	84	organic sediment	SacA59132	1975 ± 30	**1906**	**44**
GEM18-03_84_malaco	84	shell (melania)	SacA59133	725 ± 30	670	28
GEM18-03_120	120	organic sediment	SacA57093	2465 ± 30	**2569**	**95**
GEM18-04B_10	124	organic sediment	SacA59134	2465 ± 30	**2569**	**95**
GEM18-04B_53	167	organic sediment	SacA59135	2845 ± 30	**2952**	**52**
GEM18-04B_53_malaco	167	shell (melania)	SacA59136	680 ± 30	647	40
GEM18-04B_100	214	organic sediment	SacA59137	2330 ± 30	**2346**	**43**
GEM18-04B_106	220	organic sediment	SacA57094	1785 ± 30	**1658**	**40**

Tab 2 : GEM18-03/-04B master-core samples for AMS ^{14}C measures.

A total of 7 layers sampled for AMS ^{14}C measures are in progress, while 4 preliminary dates are used for age model building (Tab 2; Figure 4). At 48, 84 and 167 cm depth, sampling for radiocarbon analysis was performed both on organic and on lacustrine biogenic carbonates with the aim to contain reservoir age effect on lacustrine carbonated products. Actually only one result at 48 cm shows a reservoir age effect >170 yr (Tab 2).
Preliminary age model shows that the GEM18-03/-04B master-core sediments cover the last ~2.3 ka cal. BP (Figure 4; Figure 5), with a sedimentation rate of 1,5 mm/yr between ~2.3 - ~1.6 ka cal. BP and 0,6 mm/yr between ~1.6 – ~0.2 ka cal. BP. At ~180 yr cal. BP two overlapped ages does not permit any sedimentation rate data. However, the synchronicity of these ages is probably caused by the pedogenic processes which affected this layer.

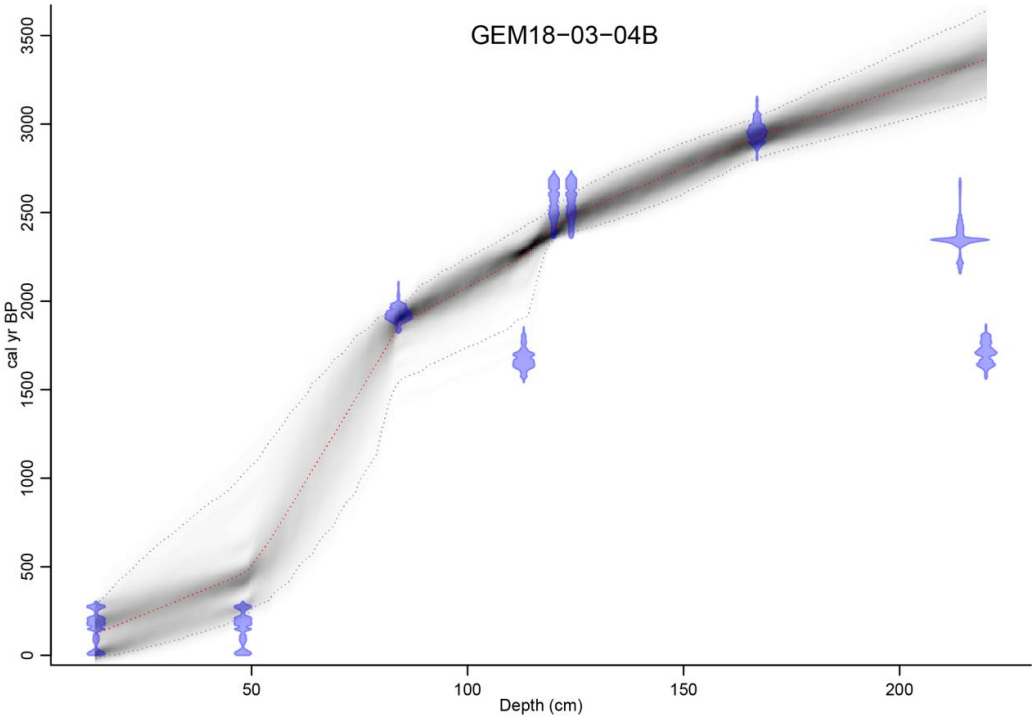

Figure 4 : Preliminary age model of GEM18-03/-04B master-core built on radiocarbon ages on organic sediment.

On GEM18-03/-04B master-core XRF major elements data was obtained with a 5mm resolution. Three geochemical elemental ratios are here presented and discussed.

The Fe/Mg ratio represents the marker of the main mineralogical source (Ethiopian trap basalts or stratoid series basalts; Fe and Mg major content). This ratio is quiet constant all over the sequence, suggesting the continuity of sources provenance and thus suggesting the basin geomorphological stability of the Awash river over the las ~2.3 ka cal. BP (Figure 5). Only at ~180 yr cal. BP, when a pedological event occurs (polyhedric clay structure, see lithostratigraphic description), an abrupt variation of Fe/Mg is detected, probably caused by the Fe and Mn oxide-reduction linked to the pedogenic processes.

Fe/K ratio is used as a primary-mineral/clay-mineral proxy (Croudace and Rothwell, 2015). Between ~2.3 and ~1.6 ka cal. BP, when highest sedimentation rate occurs, 6 peaks of primary-mineral inputs (maybe coarser) were recoded. These terrigenous inputs could correspond to the punctual activity of river floods. This depositional operating mode ends at 1.6 ka cal. BP, and Fe/K decrease gradually until the lake drying episode. The abrupt Fe increase around ~180 yr cal. BP is probably caused by the enrichment of Fe and Mn pedogenic oxides during the paleosoil development. After the pedogenic event Fe/K return to low values the until today, indicating the rise of water table.

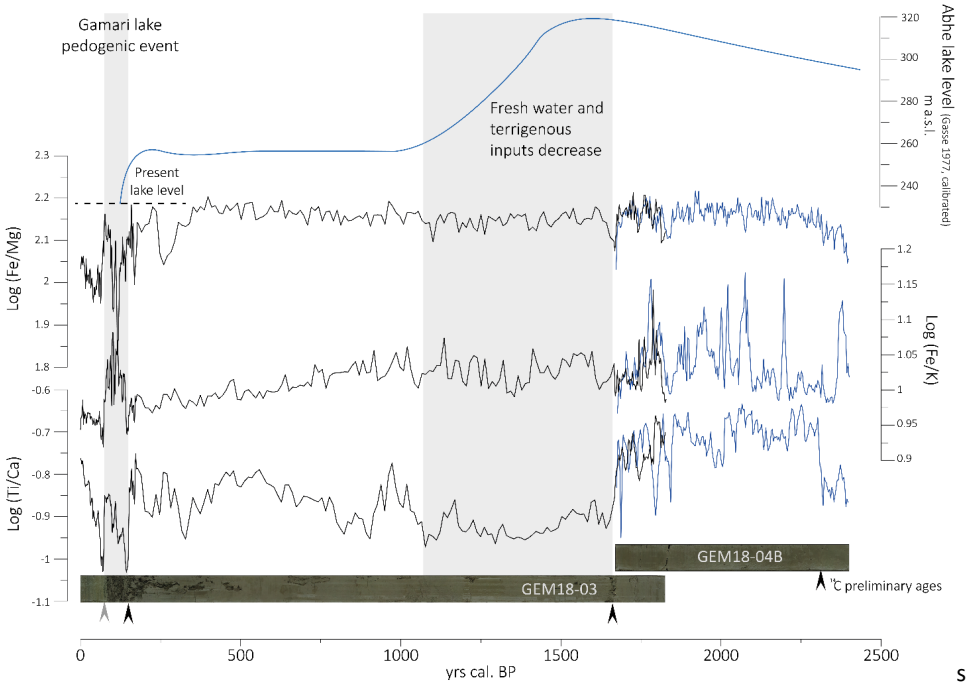

Figure 5 : GEM18-03/-04B master-core XRF major elements ratios

Finally, Ti/Ca ratio is used as a terrigenous-inputs/lacustrine-productivity proxy (Croudace and Rothwell, 2015). High Ti/Ca values are recorded between 2.3 and 1.6 ka cal. BP, while from 1.6 ka cal. BP the decrease of Ca suggests the fall-down of lacustrine productivity and then a probably lake regression phase. Around ~180 yr cal. BP the abrupt decrease of Ca followed by its gradual grow-up value could be interpretated as a drying lake episode followed by the precipitation of authigenic calcite which is commonly formed during the aridisoil development cycle.
Lithostratigraphic and major elements results/interpretations are in accord with the Abhe lake level calibrated curve from Gasse (1977) which shows a lacustrine regression after ~1.6 ka cal. BP and an abrupt regression episode (drying lake episode?) around ~180 yr cal. BP.

- *AFA18-02 core*

AFA18-02 core is 181 cm long, composed by high variable sedimentary facies which allow us to clearly differentiate this sequence from Gamari lake sediments (Figure 6). The first 130 cm are mainly clayey and high liquefy massive to slight laminated sediment. While the lower part of the sequence (130 to 168 cm) presents a clear lamination facies with a clay-silty texture. A convulsion sedimentary facies is observed at 158 cm, while from 168 to the core bottom a massive structure facies take place. Concerning secondary authigenic processes, several oxide layers were observed all along the sequence sometimes associated with carbonated beds (evaporites?). The high variability of sedimentary facies suggests and confirm the the to records.

Sample Name	Total Depth (cm)	Material	Lab Code	Status	Conventional age	Median Cal. BP	σ
AFA18-02A_10.5-11	10.5-11	bulk organic sediment	SacA57084	dated	315 ± 30	**387**	**47**
AFA18-02A_44	44	bulk organic sediment	SacA57085	dated	640± 30	**598**	**35**
AFA18-02A_76	76	bulk organic sediment	SacA57086	dated	365 ± 30	**429**	**57**
AFA18-02B_8-8.5	92	bulk organic sediment	SacA57087	dated	165 ± 30	**177**	**86**

AFA18-02B_50.5-51	134.5-135	bulk organic sediment	SacA57088	dated	**post 1950**
AFA18-02B_81.5-82	165.5-170	bulk organic sediment	SacA57089	dated	**post 1950**
AFA18-02B_59.5-63	143.5-147	vegetal macroremains	SacA	**not successful**	Not sufficiently organic carbon
AFA18-02B_81-82	165-170	bulk organic sediment + vegetal macroremains	SacA	**not successful**	Not sufficiently organic carbon
AFA18_02B_66.5	149,5	Fish bone	Microcarbon dating*	**In progress**	
AFA18_02A_61	61	Fish bone	Microcarbon dating*	**In progress**	
AFA18-02A_61	61	bulk organic sediment	SacA	**In progress**	
AFA18-02B_67	150	bulk organic sediment	SacA	**In progress**	
AFA18-02B_35-39	118-122	vegetal macroremains	Microcarbon dating*	**In progress**	
AFA18-02B_51-53	134-136	vegetal macroremains	Microcarbon dating*	**In progress**	
AFA18-02B_82.5-83.5	165.5-166.5	vegetal macroremains	Microcarbon dating*	**In progress**	

*Tab 3 : AFA18-02 core samples for AMS ^{14}C measures; * = ECHoMICADAS - Environnement Climat et Homme « Micro Carbon Dating System » (LSCE-UMR8212).*

A total of 15 samples are prepared for radiocarbon measures (Tab 3). As a result of the rarity of vegetal macroremains, the first 6 samples were dated on bulk organic carbon. However, this preliminary results show an overlap and an inversion of ^{14}C ages, evidencing the limitation of this method for the AFA18-02 core dating, thus preventing the age model building. This age inversion is probably caused by the percolation and contamination of organic carbon in the sediment microporosity along the core. The same dating problem raised for radiocarbon analysis of lacustrine Abhe Lake Sequence presented in Gasse (1975). A new package of ^{14}C analysis is in progress with the aim to solve the dating problem. New ^{14}C measures will be made on fish bones and on vegetal microremains obtained from microsampling method. “Micro Carbon Dating System” methodology developed by LSCE-UMR8212 lab will be enabled to dating the small quantities of organic microremains (from 1.2 mg of vegetal material). Two new ^{14}C measures will be tried on bulk organic carbon samples coming from fish bones layers samples, with the aim to contain reservoir age effect on lacustrine carbonated products.

On AFA18-02 core, XRF major elements data was obtained with a 1mm resolution. Because of the high liquefy sediment, this resolution of measure was not possible over the first ~60 cm on the top of the core (Figure 6).

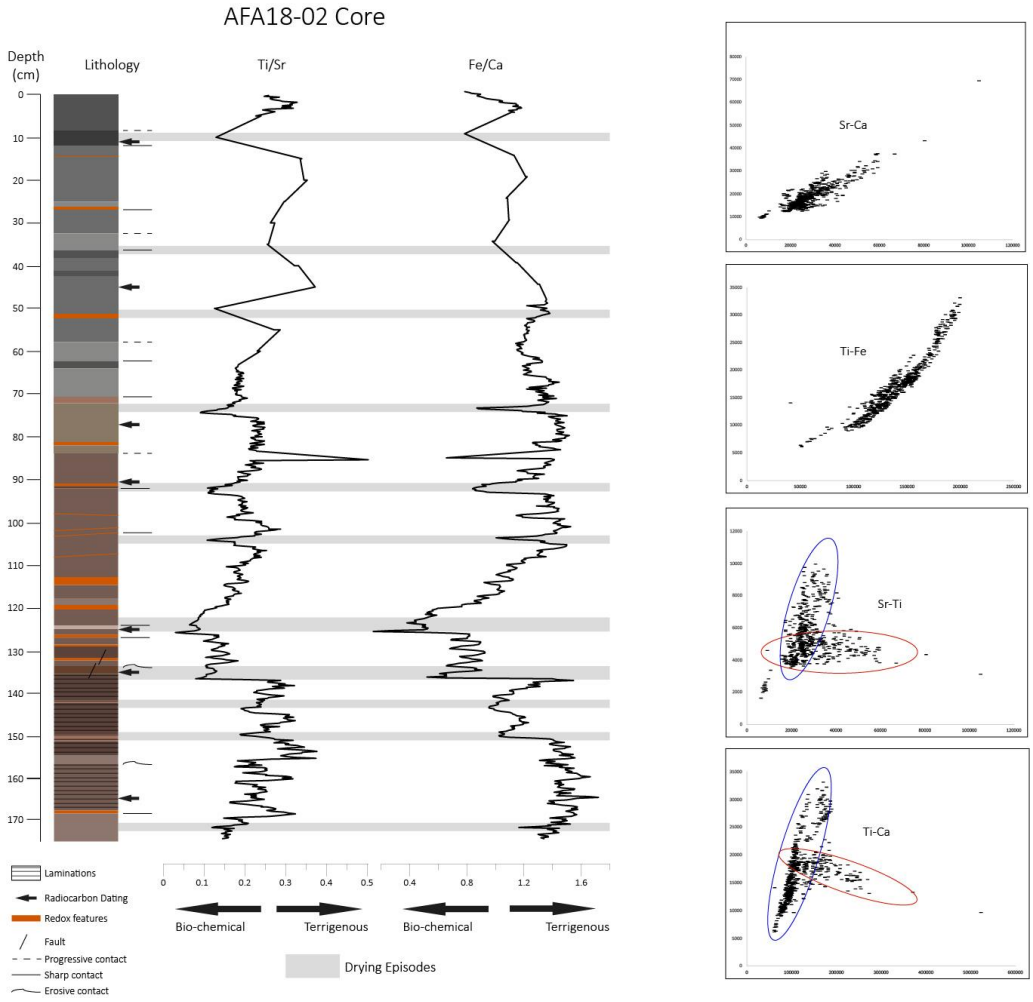

Figure 6 : AFA18-02 core XRF major elements results.

High correlation between plotted Ti and Fe non-mobile elements and between Sr and Ca mobile-elements allow us to differentiate the mineralogical terrigenous elemental markers from the lacustrine primary productivity ones. Thus, Ti/Sr and Fe/Ca elemental ratios are employed as a marker of terrigenous-inputs/biochemical-lacustrine-productivity (Croudace and Rothwell, 2015; **Figure 6**).

Over the laminated clay-silty sedimentary facies (170 - 134 cm) high values of Ti and Fe which gradually decrease until 125 cm when whitish layer with high Ca and Sr values occurs. This carbonated level could correspond to a change in water chemical balance probably triggered by reduction of waterbody extension, thus inducing the formation of an evaporitic layer. Others punctual Ca-Sr rich layers are localised all over the sequence, which are preliminary interpreted as a sort-term drying episodes (**Figure 6**). Fe and Ti values increase gradually after the 125 cm carbonated layer reaching a quite constant values until the top of the core.

Paleolandscape evolution and Geoarchaeology

I - Geomorphological approach as a tool for understand the Human-Paleoenvironment coevolution at the Abhe Lake paleobasin

We present and summarize the geomorphological and geoarchaeological work conducted over the 2018-2019 field season (December 2018 and February 2019) for the *Volcanological and Archaeological Program for Obsidian Research (VAPOR)-Afar.* One of the principal goals of the VAPOR-Afar program is to reconstruct the human-environment paleo-milieu and to refine the Later Stone Age (LSA)/ Neolithic chrono-cultural sequence in the Central Afar region (Ethiopia). In particular, this work is focused on the Abhe Lake paleobasin, which represents a geographic, geologic and hydrologic entity at the centre of the Afar triangle.

In this region, the geomorphological knowledge of sedimentary archives is limited to the works of F. Gasse, conducted in 70s, when she reconstructed the Abhe lake fluctuations between arid and humid periods during the Pleistocene and Holocene transition on the basis of the diatom flora of lacustrine sediments (Gasse, 1977, 1975). These studies on the Abhe Paleolake can give important information about East-African climate change and the activity of the African paleomonsoon in this region. However, much fieldwork remains to be done before we can understand the precise duration and the installation modalities of the arid-humid periods, and many questions remain unanswered: What was the real impact of the climatic change on the paleo-landscape evolution and on the hydrological balance of the Lower Awash Valley and Abhe Lake basin? What kind of sedimentary environments and landscapes were connected to, and formed around, the Lake Abhe during the humid and arid periods? Can these environments host and preserve the remains of LSA or Neolithic occupations? Is there a relationship between the type of deposits and archaeological chronology? What is the impact of the climate and environmental change on prehistoric human occupation around the Abhe Lake between 15 000 and 3 000 years BP?

The new archaeological data collected during the 4 VAPOR-Afar field seasons (2014 to 2018) have become increasingly rich and the new ^{14}C AMS (accelerator mass spectrometry) ages show a longer period of human prehistoric occupation in the central Afar region. The study of the sedimentary environments connected to the remains of these human occupations is necessary to understand the relationship between the human landscape exploitation, and the landscape and climate evolution in the central Afar region. For this reason, during the 2018 field season of VAPOR-Afar program, we have focused our work on the sedimentary archives for the geomorphological and geoarchaeological surveys in the Lower Awash Valley.

Survey was carried out in the Lower Awash Valley during two season: the first, coupled with the coring operations on Afambo and Gemeri lakes (December 2018), and the second one in February 2019.

II - Geomorphology

- Recognition and characterization of pedological horizons

In actual arid or semi-arid regions, the geomorphic study of desert soil can give substantial information about the landscape development and the environmental change. Desert soils are a sensitive products of the global climate change, then they can represent a complementary powerful tool for reconstitution of paleoclimate oscillations in arid regions. Desert soils can also drivers of regional environmental change thanks to: their hydrologic proprieties of water storage, their role in erosion patterns and the soil fauna supported by organic matter.

In Central Afar region the pedologic horizon are almost unknown given by a lack of soil studies. In the Abhe lake basin, only two pedogenic deposit were previously documented: one in Serdo area (Semmel, 1971) et one founded in the BRGM hydrothermal drill (Demange et al., 1971) studied by F. Gasse (1975).

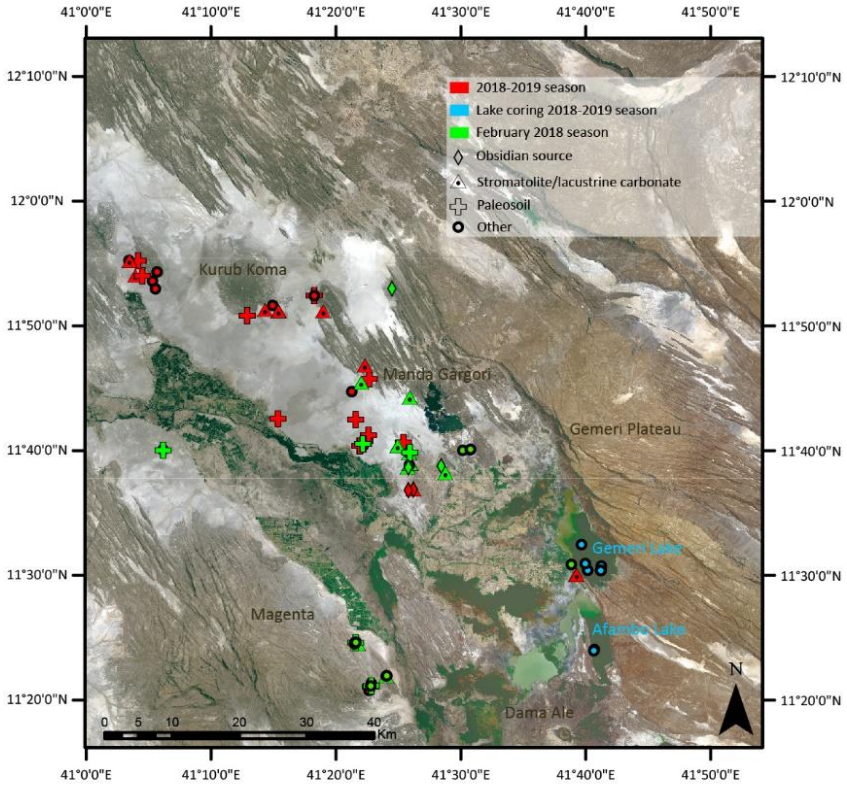

Fig 7 : Geomorphological Survey and Sounding points recorded during 2018-2019 field season (C. Mologni)

A total of 9 paleosoil formations were documented from February 2018 VAPOR-Afar mission. During the last December 2018-February 2019 field season Gandeli Buri, Kurub-05 and Strom_20 paleosoil sequences are documented.

Gandeli Buri_ST1 (11.90024°N; 41.07439°E) shows a clay rich deposit with polygonal peds structure, under one-meter-thick dune formation (**Figure 8**A); close to this, two pedologic horizons are observed interstratified between aeolian layers (11.92058°N ; 41.05689°E; **Figure 8**B).

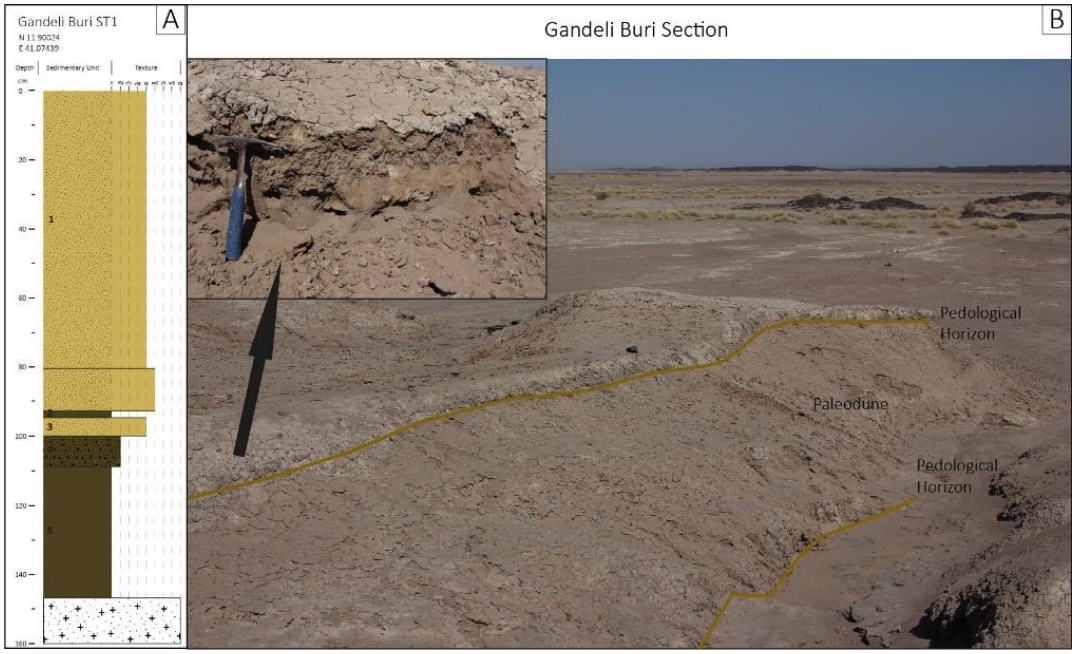

Figure 8 : A) Gandeli Buri ST1 sequence ; B) Gandeli Buri pedological horizons intercalated in a paledune sequence.

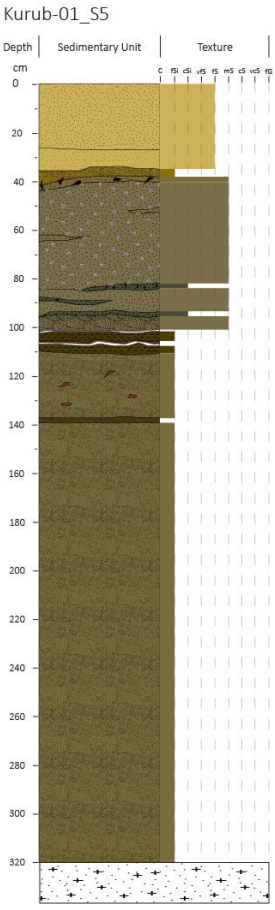

Figure 9 : Kurub-01_S5 sequence.

The continuation of survey in Kurub Bahari area has led to the sampling of paleosoils in Kurub-05_S3, Kurub-01_S5 spits (**Figure 9**), while during Kurub-07 site excavation four different horizons of paleosoil are distinguished (SU18; SU12-29; SU15; SU26; Fig).

The lab analytical strategy provides for grain size analysis, soil micromorphology, bulk XRF analysis and XRD on clay fraction. The application of these crossed methods will provides to the first sedimentologic, geochemical and mineralogical classification of paleosoils in central afar region. Lab analysis will allow to understand the morphogenetic signification of these deposits, distinguishing between palustrine and soil development or pedological crust formations.

➢ <u>Stromatolites, Carbonated crusts and related deposits</u>

During the last 2018-2019 VAPOR-Afar field seasons we continued to describing and sampling the carbonate formations linked to the past lake water-level oscillations. Systematic survey of the Abhé paleolake basin plane and borders has employed and new 16 lacustrine carbonate crusts and stromatolite structures has detected (**Fig 7**; **Tab 4**). Three of these are included in a formation processes of archaeological sites; is the case of Lakora_3, Raso_2 and Stromatolis sites, which will be presented and discussed in detail in the designated section (Part III- Geoarchaeology).
Results of the lake level-related carbonates survey confirms the previous observation about the presence of a stromatolitic group located between 370-390 m a.s.l., and shows a new carbonates group placed around 420 m a.s.l. never documented in the Lower Awash Valley basin. These second carbonated crusts group exceed of ~20 m the maximum level water proposed in Gasse (1975, 1977), and then attested a higher pre-Holocene or Holocene lake level.

For the first group we can differentiate two phases of stromatolitic formation which are separated by a thin sand level (3-4 cm), confirming the presence of a dry episode in the

Middle Holocene. Stromatolis site shows this drying event with an anthropic structure and thicker sandy layer (~20 cm) separating two different stromatolitic generations (Figure 12). The main lake transgression phase is well documented in Strom_20 sample, where the stromatolitic dome is preceded by a clay rich mud layer containing lacustrine bivalves (Unios type; Figure 10).

Figure 10 : Strom_20 sequence picture

^{14}C AMS measurements on two lake level-related carbonates groups and on two stromatolite generations of the first group are in progress.

Feb. 2018 season	2018-2019 season	Material	Latitude	Longitude	Altitude a.s.l.	Age yrs Cal BP
Stromato 1 Sup		stromatolite	41.47886	11.63678		
Stromato 1 Inf		stromatolite	41.47886	11.63678		
Stromato Colline		stromatolite	41.36707	11.75724	389	
Stromato 4		stromatolite	41.42893	11.64448	374	
Stromato 5		stromatolite	41.43233	11.64940		
Stromato 6		stromatolite	41.43233	11.64940		
Stromato 7		stromatolite	41.43058	11.66355	372	5732 ± 69
Stromato 2		stromatolite	41.36707	11.75724		
Stromato 8		stromatolite	41.41640	11.67253	368	
Stromato 9B		stromatolite	41.41602	11.67337	371	
Stromato 9A		stromatolite	41.41602	11.67337	371	
Stromato 10A		stromatolite	41.41558	11.67350	380	9807 ± 81
Stromato 10B		stromatolite	41.41558	11.67350	380	9008 ± 70
						11 073 ± 154 (U-Th)
Stromato 11		stromatolite	41.43165	11.73781	384	
Stromato 13		stromatolite	41.36255	11.40793	381	5920 ± 32
Stromato 14		stromatolite	41.40031	11.36540	372	
	Stromato 16 sup	stromatolite	11.85521	41.23836	374	
	Stromato 16 inf	stromatolite	11.85521	41.23836	374	
	Stromato 17 A	stromatolite	11.67813	41.42272	375	3534 ± 35
	Stromato 17 B	stromatolite	11.67813	41.42272	375	
	Stromato 18	stromatolite	11.67813	41.42272	375	
	Stromato 19	stromatolite	11.67352	41.41557	369	
	Stromato 20 US1	stromatolite	11.90034	41.06560	373	10447 ± 73
	Stromato 20 US4	stromatolite	11.90034	41.06560	373	10530 ± 64

Stromato 20 US5	stromatolite	11.90034	41.06560	373	11125 ± 113
Stromato 22 surface	stromatolite	11.92016	41.05743	373	
Encroutement calcaire1	calcareous crust	11.50027	41.65386	396	
encroutement calcaire2	calcareous crust	11.50089	41.65402	452	
Lakora3 US2 erodé	stromatolite	11.67813	41.42271	375	
Stromato 39A	stromatolite	11.85273	41.31623	376	8848 ± 23
Stromato 39B	stromatolite	11.85273	41.31623	376	
Brèche carbonatée 3	calcareous crust	11.61436	41.43664	427	
Champignons + Croute Calcaire	calcareous crust	41.3058	11.8722		27597 ± 120
Loma Encroutement Calcaire	calcareous crust	41.0427	11.8825		
Stromatolis US1	stromatolite	11.85276	41.25646	376	5627 ± 36
Stromatolis US1 Inf	stromatolite	11.85276	41.25646	376	
Stromato 32	calcareous crust	11.78047	41.37136	418	953 ± 32
OBS Stromato Borawli west flank	stromatolite	11.61374	41.42978	376	
Kur-05 Stromato 34 surface	stromatolite	11.70827	41.35911	375	
Stromato 36 2nd Generation	stromatolite	11.84698	41.21438	374	
Stromato 31	stromatolite	11.85274	41.25632	380	8743 ± 109

Tab 4 : Total of stromatolite or lacustrine carbonated crusts sampled during VAPOR-Afar mission.

III – Geoarchaeology

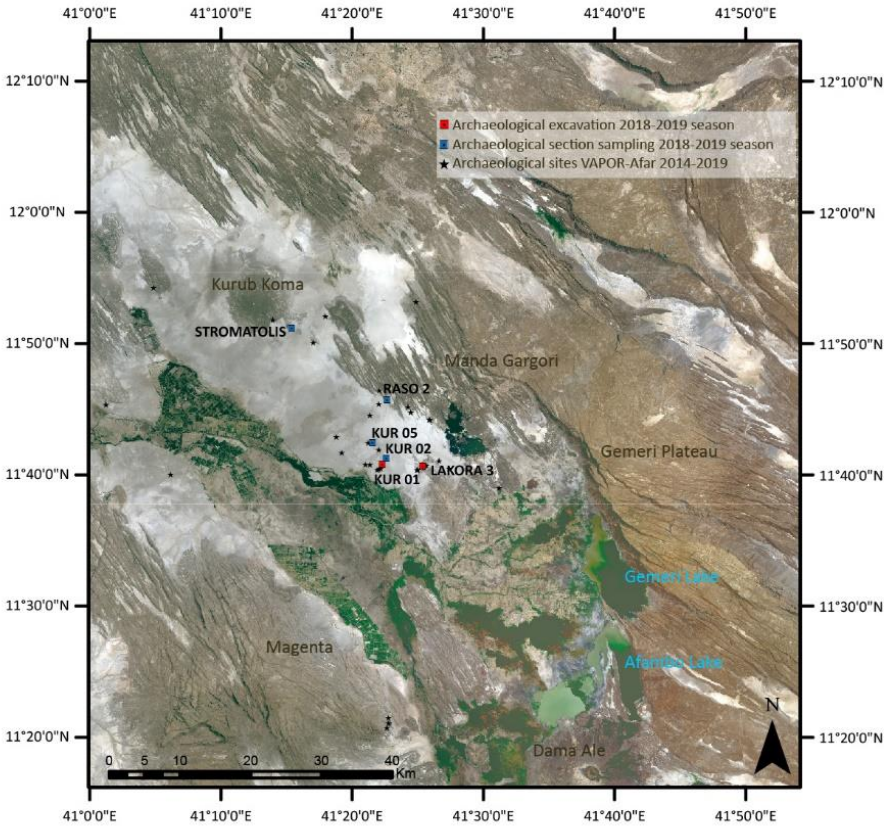

Figure 11 : Archaeological sequences localisation recorded during 2018-2019 field season (C. Mologni)

- 'Stromatolis' archaeological site

Stromatolis site is placed in the northern part of the Kurub plane (Figure 11; 11.85276° N ; 41.25646° E), at the foot of Kurub volcano South slope. The site presents a thin sequence (Figure 12) composed from the top to the bottom by: US1) stromatolite with laminar structure and surface ripple marks; US2) Circular anthropic structure composed by two levels of basaltic stones; US3) pale brown massive fine-sandy layer, well sorted with rare lacustrine shells (*Melanoides tuberculata*); US4) brown clay-fine silt layer, granular to polyedric structure, with rare terrestrial shells; US5) stromatolite domes with columnar structure.

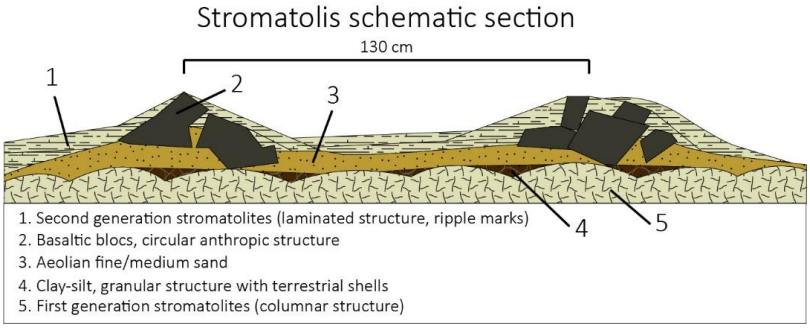

Figure 12 : 'Stromatolis' archaeological site schematic section.

Two separated stromatolite generations (US1 and 5) contain the anthropic structure and the linked sediments (US2-3-4). The structure presents a circular shape and is composed basaltic blocs (**Figure 12**). After the probably early Holocene lacustrine transgression (US5; 8848 ± 23 yr cal BP) and a palustrine deposit (US4) which marked the retreat of lake waters, the US3 sandy layer reflected a drying event where human occupation occurs, probably corresponding to 8.2 ka BP climatic event. Successively, a new transgression phase (US1), finished around 5627 ± 36 yr cal BP, has flooded the structure and preserved the intercalated sediments. ^{14}C mesure from terrestrial shell of US4 gives an age of 8506 ± 49 yr cal. BP.

Figure 13 : View of 3D model of 'Stromatolis' archaeological site

- Raso_S2

Placed on the East border of Kurub Plane (Fig. 5; 11.76201 N; 41.37741 E), the Raso_2 sequence, partially eroded (first upper 30 cm) by a little seasonal oued, presents two main archaeological layers (US 5 and US 1b). The stratigraphic sequence starts from the bottom with a saprolite basaltic alteration level (US 9), followed by a brown silty-clayey layer rich in secondary carbonate pebbles (US8). US7 is characterized by clayey texture and polyedric structure suggesting the occurrence of pedogenic process, despite the reduction of secondary carbonates until US 6. From US 5d, an erosional irregular basal contact marks the shift in sedimentologic formation processes: few decametric rounded basaltic blocs in a gravely matrix are accommodated on channel-like basement morphology, suggesting the installation of fluvial dynamics. The irregular erosional surface is filled by coarse and medium sand (US 5c) indicating a reduction of

sediment transport energy, leading to the sub-horizontal regular surface where the first human occupation occurs. Fine sandy US 5b and 5a contain the majority of the anthropic material and a considerable charcoals amount, which radiocarbon measure giving an age comprise between 10418 – 10743 cal yrs BP. A slight erosional contact separates US 5a and US 4 which changing in sedimentary material could indicate the first lacustrine transgression corresponding to the first early Holocene Abhe lake transgression (Gasse 1975, 1977). Lacustrine reworked sediments continuing until US2 where charcoal dated material give an age of 10515 – 10785 yr cal BP while biogenic carbonates from oncolithe shows an age between 5746 – 5911 yr cal BP. Oncolithe age and elevation coincide with the lake Abhe transgression occurred between 6.8 and 5.5 ka cal BP (Gasse 1975, 1977), thus are considered *in situ*, indicating the littoral lacustrine wave action. While charcoal dated sample from US 2 is considered reworked from underlying US. From US 1b starting the second clayey pedogenic horizon of Raso_2 sequence rich in charcoal and presenting a polyhedric to granular structure. This paleosoil could corresponds to the Middle Holocene retreat of lake Abhe starting around 5.5 ka cal BP. US 1b represent s the upper sedimentary unit of the Raso_2 sequence, similar to US 1b, this layer is bioturbated, slightly coarser and presenting some desiccation faults. On the actual surface an assemblage of lithic artefacts was founded, probably coming from a paleosoil wind deflation erosion.

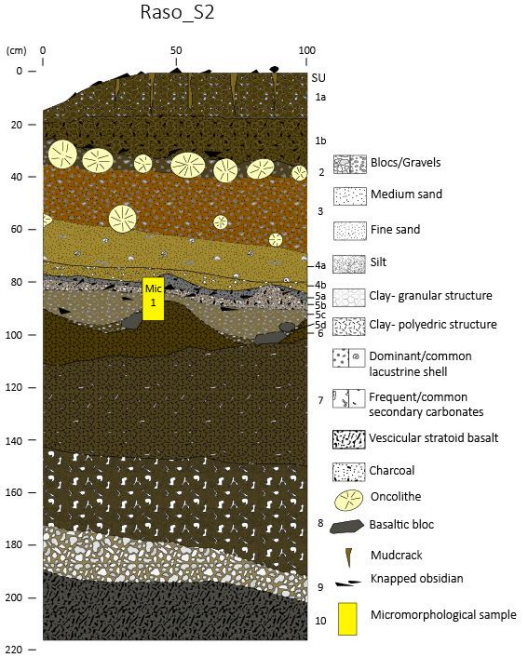

Figure 14 : Raso-S2 archaeological sequence

➢ Lakora-3

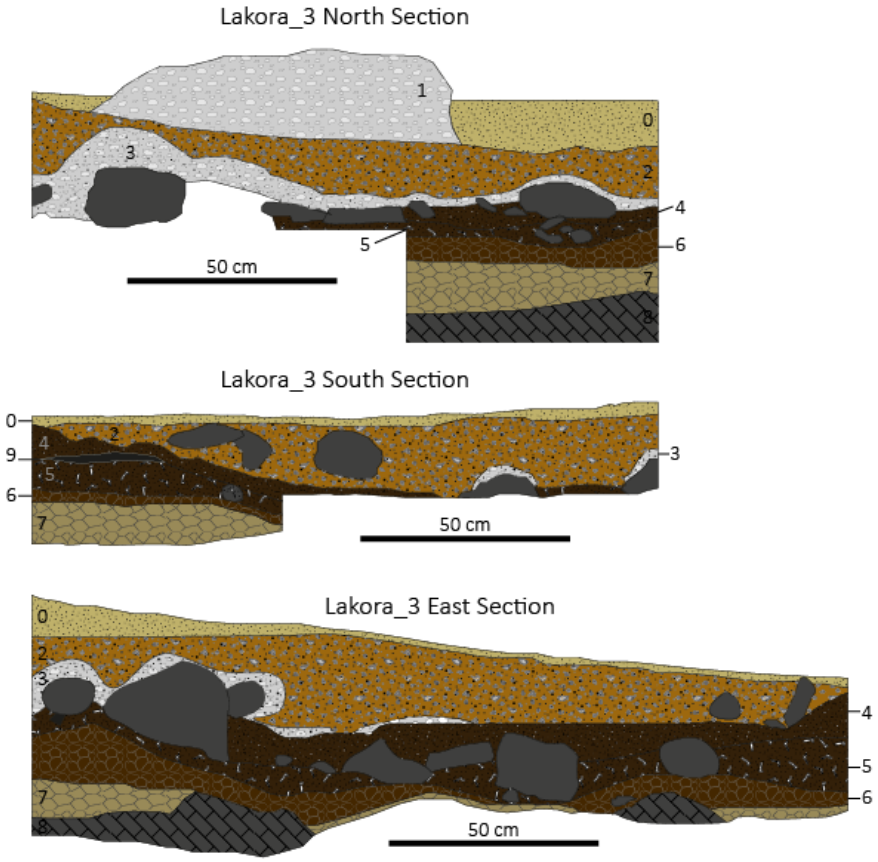

SU	Field Description
0	Surface sedimentary cover. Silt, weakly selected, eroded stromatolites and basaltic inclusions. Loose massive structure.
1	2nd generation stromatolites outcrops.
2	Shell deposit in a silty-sand matrix, weakly selected, with common basaltic gravel inclusions (2 cm). Brown-orange colour, loose massive structure.
3	1st generation stromatolites. Highly weathered with some enveloping lithic tools.
4	Silt, moderately selected, with common basaltic angular gravels inclusions (2 mm), very dark-brown colour and massive to granular loose structure. Few charcoal and presence of obsidian lithic tools.
5	Silt, well selected, with a loose massive to granular structure and very dark-brown colour. Frequent charcoal, frequent fish bones and common obsidian lithic tools.
6	Fine-silt, well selected, with common calcareous and basaltic gravel inclusions (rounded, 2-3 cm). Dark-brown colour and granular structure (thickness of peds: 0.5-1cm). Common terrestrial shell and few obsidian lithic tools
7	Silt-clay well selected, with common basaltic gravel (2mm) and carbonate crusts/eroded stromatolites (<5cm) inclusions. Whitish-brown colour and polyedric structure. Frequent secondary carbonates and terrestrial shells.
8	Basaltic bedrock.
9	(Hearth) Silt, well selected, with common basaltic angular gravels inclusions (2 mm), very dark-brown colour and massive to granular loose structure. Frequent charcoal, frequent fish bones and presence of obsidian lithic tools.

Figure 15 : lakora-03 archaeological sequence

Lakora-3 site is located on the northern slopes of Borawli mountains (Fig 5; 11.67813° N; 41.42271° E) at the south border of Kurub plane with an elevation of 368 m a.s.l. The sedimentary sequence of Lakora-3 is punctually preserved from erosive processes over ~20 m^2 thanks to the stromatolitic cover. A sounding area of 150 x 200 cm was opened; 7 sedimentary units are described of which two containing anthropic material. From the bottom to the top we found (Figure 15): the weathered basaltic bedrock (US 8); a silty-clay whitish-brown colour layer, with polyedric structure, weathered basaltic gravels inclusions (2mm) and carbonated crusts/eroded stromatolites (US 7); dark brown fine silty-clay layer, with granular structure and common terrestrial shells (US 6), probably corresponding to a slope pedogenic

event; a dark-brown silty layer well selected with loose massive granular structure rich in fish bones, charcoal, obsidian lithic artefacts and subangular decametric basaltic blocs (US 5); US4 is moderately selected mainly silty with common basaltic angular gravels inclusions, lithic artifacts and subangular decametric basaltic blocs; US 3 is represented by the first very weathered stromatolite generation, which englobes the upper part of basaltic blocs which are based in US 5 and 4; US 2 corresponding to reworked lacustrine material very rich in melania and bivalve shells which are englobed in a silty-sand brown-orange matrix presenting a loose massive structure; finally US 1 is represented by a second stromatolitic generation which emerges to the actual cover surface. The two stromatolitic generation coud correspond to the two Holocene lacustrine phases evidenced in Gasse (1975, 1977) and recognised in Stromatolis and Raso-2 sites. From US 5 archaeological level a radiocarbon age on charcoal given an age comprise between 10737 and 11163 yr cal BP.

- Kurub-07

The site of Kurub-07 was excavated over a 34m2 surface area. This open-air site is exposed on the slopes of a large dune complex in the SW of the Kurub Bahari plain and several kilometers north of the current Awash River delta.

43 SU were described during three seasons of fieldwork on the basis of excavation and pedo-stratigraphic observations from site sections. We present here only the SU observed on the K_trench section, which is representative of the stratigraphic and site formation processes and of the main archaeological layers (Figure 16).

SU18 represents the continuous sedimentary basement of the sequence characterized by dark-brown prismatic structured clays rich in authigenic gypsum which has been interpreted as a palustrine pedogenised deposit. This layer is dated on bulk organic carbon to 7587-6174 cal. BP. A paleodune complex represented by SU41 and 13 composed of cross-laminated and well sorted fine-sand follows. At the interface between SU 41 and 13 we find a phase of occupation characterized by few lithic artifacts, faunal remains and charcoal. The following archaeological level SU15 is dated between 3914-3647 and 3830-3587 cal. BP. SU15 is a silty-clayey polyhedral structured layer rich in secondary carbonate nodules with abundant flat-lying broken ceramics, semi-articulated faunal remains, charcoal and lithics. SU12, marked by a more structured matrix, by the lack of secondary carbonates and the persistence of anthropic material is dated to 3638-3477 and 3568-3407 cal. BP. This pedogenic event is localized in SU12 and 29 and dated to 3638-3407 and 3636-3476 cal. BP. SU9/14 are composed of consolidated or non-consolidated aeolian sand and produced some pottery fragments, wild and domestic fauna, charcoal, lithics and groundstone, namely on or just below the surface, and cap the underlying pedogenic horizons. The most recent anthropic layer is a polymorphous oven structure (ST1) cutting into SU12, 42, 43 and 18 in the south end of the site (K-L/10-9). The oven, which is the first of its kind for the period and region has been dated on charcoal to between 3600 and 3300 cal. BP.

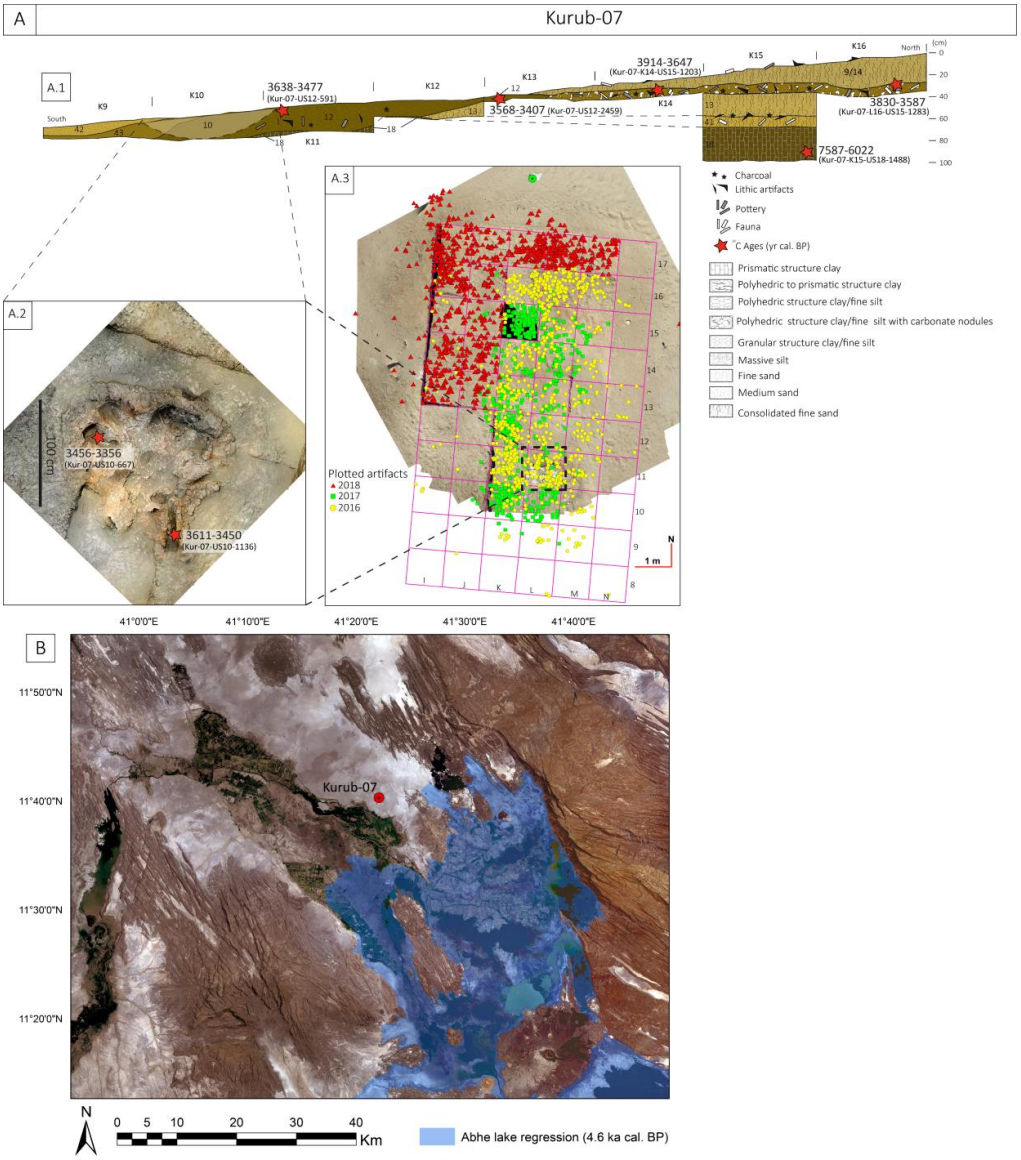

*Figure 16 : **a.1**) Kurub-07 trench K archaeological sequence with calibrated ages localisation; **a.2**) orthophoto of anthropic structure (ST10, oven) from Kurub-07 site with calibrated ages; **a.3**) Kurub-07 site artefacts and ST10 localisation; **b**) Abhe lake regression phase model at 4.6 ka cal. BP and Kurub-07 site localisation.*

References

Blaauw, M., 2010. Methods and code for 'classical' age-modelling of radiocarbon sequences. Quaternary Geochronology 5, 512–518. https://doi.org/10.1016/j.quageo.2010.01.002

Bronk Ramsey, C., 2001. Development of the Radiocarbon Calibration Program. Radiocarbon 43, 355–363. https://doi.org/10.1017/S0033822200038212

Croudace, I.W., Rothwell, R.G. (Eds.), 2015. Micro-XRF Studies of Sediment Cores, Developments in Paleoenvironmental Research. Springer Netherlands, Dordrecht. https://doi.org/10.1007/978-94-017-9849-5

Demange, J., Di Paola, G.M., Lavigne, J., Lopoukhine, M., Stieltjes, L., 1971. Etude Géothermique du Territoire Français des Afars et des Issas. B.R.G.M.

Gasse, F., 2000. Hydrological changes in the African tropics since the Last Glacial Maximum. Quaternary Science Reviews 19, 189–211.

Gasse, F., 1977. Evolution of Lake Abhe (T.F.A.I.), from 70,000 BP. Nature 265, 42–45.

Gasse, F., 1975. L'évolution des lacs de l'Afar Central (Ethiopie et T.F.A.I.) du Plio-Pléistocène à l'Actuel. Recostitution des paléomilieux lacustres à partir de l'étude des Diatomées. Université de Paris VI, Paris.

Gasse, F., Street, F.A., 1978. Late Quaternary lake-level fluctuations and environments of the northern Rift Valley and Afar region (Ethiopia and Djibouti). Palaeogeography, Palaeoclimatology, Palaeoecology 24, 279297299–295325.

Hoelzmann, P., Keding, B., Berke, H., Kröpelin, S., Kruse, H.-J., 2001. Environmental change and archaeology: lake evolution and human occupation in the Eastern Sahara during the Holocene. Palaeogeography, Palaeoclimatology, Palaeoecology 169, 193–217.

Kuper, R., Kröpelin, S., 2006. Climate-controlled Holocene occupation in the Sahara: motor of Africa's evolution. Science 313, 803–807.

Reimer, P.J., Bard, E., Bayliss, A., Beck, J.W., Blackwell, P.G., Ramsey, C.B., Buck, C.E., Cheng, H., Edwards, R.L., Friedrich, M., Grootes, P.M., Guilderson, T.P., Haflidason, H., Hajdas, I., Hatté, C., Heaton, T.J., Hoffmann, D.L., Hogg, A.G., Hughen, K.A., Kaiser, K.F., Kromer, B., Manning, S.W., Niu, M., Reimer, R.W., Richards, D.A., Scott, E.M., Southon, J.R., Staff, R.A., Turney, C.S.M., van der Plicht, J., 2013. IntCal13 and Marine13 Radiocarbon Age Calibration Curves 0–50,000 Years cal BP. Radiocarbon 55, 1869–1887. https://doi.org/10.2458/azu_js_rc.55.16947

Shanahan, T.M., McKay, N.P., Hughen, K.A., Overpeck, J.T., Otto-Bliesner, B., Heil, C.W., King, J., Scholz, C.A., Peck, J., 2015. The time-transgressive termination of the African Humid Period. Nature Geoscience 8, 140–144. https://doi.org/10.1038/ngeo2329

Tierney, J.E., Lewis, S.C., Cook, B.I., LeGrande, A.N., Schmidt, G.A., 2011. Model, proxy and isotopic perspectives on the East African Humid Period. Earth and Planetary Science Letters 307, 103–112. https://doi.org/10.1016/j.epsl.2011.04.038

Trauth, M.H., Maslin, M.A., Deino, A.L., Junginger, A., Lesoloyia, M., Odada, E.O., Olago, D.O., Olaka, L.A., Strecker, M.R., Tiedemann, R., 2010. Human evolution in a variable environment: the amplifier lakes of Eastern Africa. Quaternary Science Reviews 29, 2981–2988. https://doi.org/10.1016/j.quascirev.2010.07.007

BII.3 Prospections geomorphologiques et sondages pédologiques dans la vallée du Gobaad - PSPCA 2018

Prospections geomorphologiques et sondages pédologiques dans la vallée du Gobaad

Carlo Mologni

Dans le cadre de la dernière mission PSPCA 2018, le volet de travail géomorphologique as comporté une série de prospections, de sondages et de prélèvements sédimentaires avec l'objectif d'affiner la compréhension du lien entre l'évolution paléohydrologique du bassin du Lac Abhé et la formation/érosion d'archives sédimentaires périphériques non-lacustres contenant du record archéologique. Dans cette contribution sont synthétisées les objectives, les observations et les résultats de terrain obtenus en Janvier 2018.

L'importance des travaux geomorphologiques dans la vallée du Gobaad

Dans le bassin du Gobaad la connaissance géomorphologique des archives sédimentaire est reliée principalement au travaux de F. Gasse (1975, 1977) dont les fluctuations climatiques et environnementales sont reconstituées à l'aide de l'étude des flores diatomiques contenues dans les dépôts de l'ancien Lac Abhé. Grace à son travail, on as aussi une idée des oscillations altimétriques des lignes littorales lacustres suite aux changements de l'intensité de la mousson sur la région Afar entre 30 ka BP et l'actuel. Toutefois la durée précise des phases humides/arides dans la région de l'Afar Central à la fin du Pléistocène et pendant l'Holocène reste encore peu connue, puisque la plupart des études paléoclimatiques continentaux modernes sont basés sur la région des Grand Lacs Ethiopiens, au sein du rift African (Chalié and Gasse, 2000; Gasse et al., 1989; Gillespie et al., 1983; Lamb et al., 2002; Legesse et al., 2002), et sur les Hauts Plateaux Ethiopiens (Lamb, 2001, 2001; Lamb et al., 2018, 2007a, 2007b; Marshall et al., 2011, 2009; Tiercelin et al., 2008; Wagner et al., 2018). Au-delà des problématiques strictement paléoclimatiques, certaines questions d'ordre géomorphologique, et connectées aux questionnements archéologiques du projet, restent ouvertes : Quel a été le réel impact de changements climatiques sur l'évolution des paléopaysages et des géomorphologies autour du Lac Abhé ? En d'autre termes, quel type d'environnements sédimentaires ont pu se former, et être connectés au Lac Abhé pendant les respectives périodes humides et arides ? Quel type d'environnement sédimentaire a pu été l'objet d'occupation humaine préhistorique, et sous quels paramètres géographiques ? Est-ce qu'il y a une cohérence chronologique-spatiale entre les déports lacustres résiduels, les dépôts sédimentaires périphériques au paleolac et le record archéologique ? Au final, est-ce-que les changements climatiques à l'Holocène ont pu avoir un rôle dans l'émergence des premières sociétés de production et dans l'installation/abandon des groupes Humains sur rives du paleolac Abhé entre 15 et 3 ka BP ?
Grace aux travaux de recherches archéologiques combinés aux enquêtes géomorphologiques effectués dans ces dernières années dans le cadre du projet PSPCA (Cauliez, 2017, 2016, 2015), aujourd'hui on dispose d'un grand nombre d'âges et d'observations pedostratigraphiques sur les sondages archéologiques effectués au long de la Vallée du Gobaad. Ceci constitue la base pour un approche analytique un qui vise à la clarification des questionnemment ci-dessus proposés.
L'étude approfondis des séquences sédimentaires archéologiques est aujourd'hui conseillé pour mieux comprendre les relations mutuelles entre l'Homme et le Climat au Pléistocène supérieur et à l'Holocène.

Considérations sur le contexte géologique, hydrologique et paléoclimatique de la Vallée du Gobaad

Le bassin du Lac Abhé est situé au long de l'axe du graben de Tandaho-Gobaad (NE-SO), un soubassement basaltique constitué par des coulées stratoïdes (4.4-2.5 Ma) disloquées par des failles dont les rejets visibles atteignent fréquemment les 1000m (Corti et al., 2015; J. Varet, 2018; Varet, 1978). A l'intérieur de ce dense réseaux de failles, d'appareils volcaniques et des coulées basaltiques fissurales plus récentes apparaissent : du volcanisme acide localisée principalement sur les massifs d'As Eyla et Aysilo constitué par de rhyolites et obsidienne ; une série intermédiaire constitués de basaltes (Basaltes du Golfe) ; un deuxième épisode de volcanisme acide uniquement localisé sur le massif d'Aysilo ; une dernière émission de trapps (J. Varet, 2018). Sur ce substrat volcanique se posent les formations sédimentaires quaternaires formés pendant les phases de transgression et régression lacustre. Pendant les périodes humides au Pléistocène supérieur et à l'Holocène, le bassin du Gobaad et de la basse vallée de l'Awash ont été submergées par un Hyper- (29-17,000 BP et 10-8,000 BP), Mega- (7,500-4,500 BP) et Macro (2,500-0 BP) Lac, dont

l'extension maximale as rejoint les 6000 km^2 (4000 km^2 dans la basse vallée de l'Awash et 2000 km^2 dans le secteur du Gobaad à Djibouti).
Actuellement, cette région reçoit entre 200 et 400 mm de précipitations par an et souffre d'une évaporation de 3000mm/an. Les surfaces d'eaux en Afar Central (Lac Abhé, Gemeri et Afambo) sont alimentées per les apports en débit fluide de la rivière Awash et ses affluent (3000 hm^3/an), qui prennent les sources sur les Hauts Plateaux Ethiopien, où s'enregistre 200mm/mois des précipitations entre mars et septembre. Le Lac Abhé est et a été donc sujet à des fluctuations de niveau rapides et importantes dépendant, avant tout, du climat régnant sur les Hauts Plateaux Ethiopiens et principalement par l'intermédiaire de l'Awash et de ses affluents. Le rôle du Gobaad, dans le bilan hydrologique actuel et du passé du bassin du Lac Abhé, reste donc marginal. Toutefois, ce n'est pas seulement l'Awash qui bénéficie de crues 'extraordinaires', ou des crues succèdent à plusieurs années de sécheresse, mais aussi les bassins alimentés par des circulations souterraines, comme Le Gobaad (Vinet et al., 2012). Le substrat géologique de la plaine du Gobaad est favorable aux circulation souterraines, ceci est confirmée par l'importante présence sources chaudes situés au long de la faille bordière Sud du Gobaad (sources peu chaudes entre 26° et 46° C), des failles bordières Nord (avec des températures comprises entre 35° 61° C°) et à l'intérieur du graben où ils se trouvent les plus connus cheminées du Lac Abhé qui atteignent de températures autour des 98.5 et 99.5° C (Fig 1; Demange et al., 1971).
Le fond de la plaine du Gobaad s'élève entre 240 et 420 m sur 40 km, grossièrement en direction E-W. La partie en aval représente l'ouverture orientale du Lac Abhé. Grace à sa pente (4,5‰) les oueds Gobaad et Degadlé ont des cours fixés, alors que l'Awash (avec une pente autour du 0,6‰) comble son cours et forme des marécages. Ceci as permis une érosion limitée et du coup une très grande richesse en sédiments quaternaires.

Figure 1 : Partie deltaïque de la plaine du Gobaad : en premier plan les cheminées hydrothermales et sur le fond le Lac Abhé.

Stratégie de travail et premiers résultats de terrain

Le travail géomorphologique effectué en Janvier 2018 s'est déroulé selon deux axes principaux : a) le premier concernant des prospections sélectives au long des escarpements basaltiques aux marges de la Vallée du Gobaad avec l'objectif de documenter, caractériser et cartographier les dépôts et les morphologies des anciens littoraux lacustres ; b) le deuxième as concerné la description pédostratigraphique et l'échantillonnage sédimentaire (en vrac et en bloc) de

séquences archéologiques déjà connues au sein du projet PSPCA, avec l'objectif de mener des analyses plus approfondies liés aux problématiques ci-dessus présentés.

a) Les dépôts lacustres et littorales

Diffèrent types de dépôts lacustres ont été reconnus, chacun avec un significat précis. La variabilité de ces dépôts dépende des paramètres spatiaux et de leur environnement de croissance. Cet environnement est défini à partir de leur positionnement dans la colonne d'eau dans le lac. À la base, on trouve les dépôts diatomiques, qui représentent les eaux de fond de lac. Déjà amplement décrites en Gasse (1975), les diatomites de la région présentent diffèrent facies plus ou moins argileuses. Ces dépôts représentent les réceptacles de la sédimentation par décantation dans le lac, ceci implique la présence de faciès plus détritiques, mais aussi la présence des résidus produits par l'activité biologique lacustre, comme les ossements de poisson. Les diatomites toutefois, ne représentent pas des marqueurs de rivage, ou de limites d'extension des paleolacs au Pléistocène/Holocène. En effet, ces dépôts suivent la topographie du fond du lac et ne se développent pas en zone littorale (Fig 2A).

Figure 2 : Les formations diatomitiques du bassin du Gobaad : A) Diatomites à la base du versant du massif de Aysilo. Leur structure suive la topographie du versant. B) Séquence diatomitique à Nord de l'oued Degadlé. C) Vue des diatomites holocènes à Nord de l'oued Degadlé.

Le côté Nord du bassin du Gobaad est très riche en diatomites, en particulier la zone de Barogali-Degadlé, où une succession épaisse environ 5 m est observable sur plusieurs kilomètres d'extension de l'Est à l'Ouest (Fig 2B, C) : 1) à la base des diatomites très altérées et argileuses couvrent le substrat Plio-Pléistocène constitué par des sols argileux gypsiques. Ces diatomites appartenant probablement à une phase pléistocène de transgression lacustre ; 2) des dalles calcaires tabulaires scellent ce dépôt à diatomite ; 3) au-dessus, sur environ 150 cm d'épaisseur, se développe un dépôt

à limons-sableux brun-vertes ; 4) suite à une transition constituée par une couche à poupées calcaires d'origine pédologique et une couche sableuse à coquilles type *Melanoides tuberculata*, 5) d'autres diatomites (~150 cm) délimitent la fin supérieure de la séquence. Du bas vers le haut est représentée une phase lacustre, suivie par un assèchement du lac, et ensuite une réoccupation des eaux lacustres représenté par un développement diatomitique (Fig 2B).

Cette séquence correspond aux observations reportées en Gasse (1975), où les diatomites de base représentent le troisième évènement lacustre au Pléistocène (ABHE III), la dalle calcaire marque la fin de cet évènement humide (après 20.8 ka BP), les limons représentent une phase d'asséchement probablement autour de 17 ka BP, le niveau à *Melanoides tuberculata* indique une période dont les eux du lacs en transgression étaient peu profondes, et au final les diatomites supérieures qui signent l'occupation du lac à l'Holocène. Sur la route qui amène aux rivages actuels du Lac Abhé est observable en semi-continuité l'extension de ces diatomites Holocènes et les encroutements calcaires qui témoignent les niveaux des lacs historiques.

Des niveaux constitués exclusivement de coquilles *Melanoides tuberculata* ont été aussi observés. Ceci indiquent des eaux peu profondes (max ~4-5 m ; Murray, 1975).

Figure 3 : Les dépôts stromatolitiques de Aysilo : A) vue du plateau intermédiaire du versant Sud du massif d'Aysilo (370-400m) avec des structures stromatolitiques in situ (taches blanches) ; sur le fond les sommets du massif (~500m). B) Particulier des structures stromatolitiques du plateau intermédiaire du massif d'Aysilo. C) Vue du plateau intérmediaire d'Aysilo avec des stromatolites in situ (premier plan), et plaine du Gobaad (arriere plan). D) Fragments de stromatolites et galets basaltiques en position secondaire, roulés.

Au cours de cette mission, la recherche de morphologies et dépôts littoraux lacustres a été effectué principalement sur les versants sud du massif de Aysilo. A partir de la plaine alluviale du Gobaad (~325m) les versants du massif d'Aysilo se présentent assez abrupts jusqu'à environ 370m d'altitude, où un plateau assez vallonné prend la place (Fig 3A). Sur ces versants quelque résidus de diatomites est observable, avec de lignes d'abrasion lacustre. Ensuite, une autre pente assez abrupte reprend sa montée jusqu'au sommet du massif situé à environ 500m (Fig 3A). Sur le plateau vallonné intermédiaire, autour de 370-400 m, plusieurs dépôts stromatolitiques *in situ* ont été observées et documentées (Fig3B, C). Ceci sont des constructions carbonatées qui se forment suite à l'activité biologique de cyanobactéries, qui se situe de norme dans des eaux douces superficielles (1-2 m de profondeur ; Krumbein, 1983; Reid, 2011; Riding, 2007). Les stromatolites représentent un indice de stabilité environnementale et un bon marqueur des paléo-littoraux lacustres. En conséquence ces dépôts indiquent que sur ces plateaux au sein du massif d'Aysilo il y a eu un rivage lacustre qui a

perduré pour une période assez longue. En remontant le versant, des dépôts colluviaux contenant de galets basaltiques et de fragments de stromatolites roulées ont été observées (Fig 3D). Ensuite, plus en haut, vers les sommets du massif, des lignes d'abrasion lacustre ont été distinguées.
Grace à ce travail de prospections, des nouveaux points ont été ajoutés à la reconstruction de la paléogéographie du lac au Pléistocène/Holocène dans le bassin du Gobaad. Toutefois la recherche de dépôts pédologiques périphériques associés à ces niveaux d'extension lacustre doit être effectuée au-delà de ces hauts rivages >400m.

a) Les séquences à paléosols/paléodunes

Un des objectifs du travail géomorphologique au sein du projet PSPCA est d'améliorer la compréhension des contextes sédimentaires et des processus de formation des sites archéologiques fouillés dans le bassin du Gobaad pour mieux les caler dans leur contexte paléoenvironnementale et paléoclimatique. La plupart de sites archéologiques connues sont contenus dans des séquences pédologiques intercalées ou couvertes par des dunes fixes. Dans la vallée du Gobaad l'origine et la signification environnementale précise de ces séquences sédimentaires est encore peu connue. Pour cette raison, à partir de la campagne PSPCA 2018, une ré-investigation et un échantillonnage des séquences archéologiques a été commencée, afin de mener d'analyses de granularité, micromorphologiques, XRF et DRX sur les sédiments. Pour le moment deux séquences archéologiques ont été décrites et échantillonnes : la séquence du site de Tewqo Dhaba et la sequence du site d'Antakari 3.

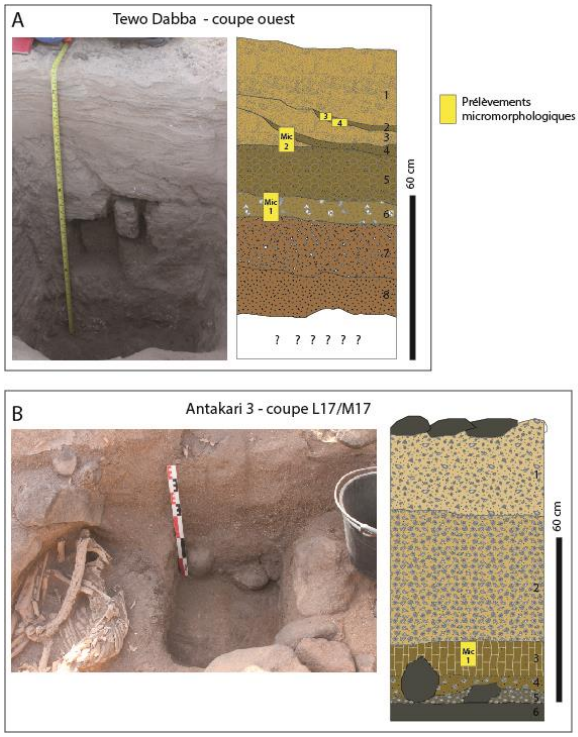

Figure 4 : Sondages géomorphologiques dans des sites archéologiques du Gobaad et relative localisation des prélèvements sédimentaires : A) Site de Tewko Dhaba ; B) Site de Antakari 3.

Le site de Tewqo Dhaba, connu depuis 2008 et éponyme du faciès céramique Tewqo Dhaba, se situe dans une dune dans la plaine du Gobaad, au sud du massif Aysilo. En janvier 2017 a été l'objet d'un sondage qui as eu comme objectif le prélèvement d'échantillons pour effectuer des datations absolues par OSL et ^{14}C (Cauliez, 2017). En Janvier 2018 le sondage effectué l'année précèdent a été ré-ouvert et les observations stratigraphiques sur la coupe Ouest ont données du bas vers le haut la séquence suivante (Fig 4A) : US8 - une couche à sable moyenne-grossière brun-rougeâtre avec des graviers (3-4mm) abondantes, qui est probablement correspondante au dépôt observable à la base de la dune qui a été raviné par l'écoulement d'un oued à régime saisonné ; US7 - des sables moyennes-fines brun-rougeâtres avec des inclusions calcaires abondantes (0,5-1 cm) ; US6 - des sables moyennes-fines brunes avec d'abondantes coquilles type *Melanoides tuberculata* ; US5 - d'argiles sableuses brun foncé et massif ; US4, 3, 2, 1 - une dune fixe à sable fine contenant deux couches argileuses sub-horizontales dans le sens de la pente qui terminent au milieux des dépôts éoliens. Des échantillons en vrac ont été collectés de chaque US, des blocs micromorphologiques ont été prelevés de l'US3, US2.1, 2.2 et de l'US 2.

Le tumulus d'Antakari 3, plus imposant monument funéraire connu à ce jour dans la Corne de l'Afrique, a fait l'objet de plusieurs campagnes de fouilles en 2008, 2009, 2011, 2016, 2017 et 2018. Le site a livré d'importantes informations paléoanthropologiques grâce à l'étude de nombreux individus provenant de cette sépulture collective (S. Hérouin, M. Matu), et une étude paléoenvironnnamentale sur les restes de poisson est en cours (L. Coudert). Toutefois une étude systématique et approfondis concernant les processus de formation sédimentaires de la séquence archéologique n'a été jamais effectué. Pour cette raison, en Janvier 2018, le site a été l'objet d'un sondage profond jusqu'au substrat basaltique, afin d'amener des observation pedostratigraphiques approfondis et avec l'objectif d'étudier en laboratoire les relatif dépôts.

Le sondage a été effectué dans le carré M17 et les observations/prélèvements sédimentaires ont été effectués sur la coupe L17/M17 (Fig 4B). Du bas vers le haut : US5 - Posé sur le substrat basaltique se développe une couche à sables moyennes-grossières brun rougeâtre foncé, massif avec de traits ferrugineux secondaires ; US4 - suive une couche à sables moyennes-fines brunes cimentées, avec d'abondantes coquilles de type *Melanoides tuberculata* ; US3 - le dépôt devient de plus en plus fin avec du sable-limoneux brun foncé avec une structure grumeleuse à polyédrique et avec d'abondantes coquilles de type *Melanoides tuberculata*. Ces premières unités sédimentaires englobent quelque bloc basaltique qui pose sur le substrat. Ces blocs sont déconnectés et ne semblent pas suivre l'organisation de la structure à blocs basaltiques anthropique construite dans les couches supérieures. US2 - la séquence se poursuit avec le paquet sableux à coquilles qui contient la plupart du record archéologique aujourd'hui en train de fouille. Cette couche correspond avec les US 304 et 305 de la fouille archéologique. US1 - La dernière couche supérieure correspond à l'US 302 de la fouille archéologique, qui est ensuite scellé par une couverture de bloc basaltiques d'origine anthropique. Des prélèvements sédimentaires en vrac ont été collectés dans les couches inférieures et un bloc micromorphologique a été prélevé de la couche 3. La couche 3, présente des faibles traits de développement pédologique associés à d'éléments aquatiques lacustres, qui rappellent l'US3 du sondage à Tewqo Dhaba.

References :

Cauliez, J., 2017. PSPCA – Programme 320 Premières Sociétés de Production dans la Corne de l'Afrique. Projet quadriennal 2014-2017. Rapport des travaux conduits en 2017 (sur financements 2016) + Opérations projetées pour la nouvelle quadriennale 2018-2021. (Rapport des travaux conduits en 2017 (sur financements 2016) + Opérations projetées pour la nouvelle quadriennale 2018-2021). CNRS – Laboratoire TRACES – UMR 5608 – Toulouse.

Cauliez, J., 2016. PSPCA – Programme 320 Premières Sociétés de Production dans la Corne de l'Afrique. Projet quadriennal 2014-2017. Rapport des travaux conduits en 2016 (sur financements 2015) – Deuxième année de quadriennale. CNRS – Laboratoire TRACES – UMR 5608 – Toulouse.

Cauliez, J., 2015. PSPCA – Programme 320 Premières Sociétés de Production dans la Corne de l'Afrique. Projet quadriennal 2014-2017. Rapport des travaux conduits en 2015 – Deuxième année de quadriennale. CNRS – Laboratoire TRACES – UMR 5608 – Toulouse.

Chalié, F., Gasse, F., 2000. Late Glacial Holocene diatom record of water chemistry and lake level change from the tropical East African Rift Lake Abiyata (Ethiopia). Palaeogeogr. Palaeoclimatol. Palaeoecol. 187, 259–283.

Corti, G., Bastow, I.D., Keir, D., Pagli, C., Baker, E., 2015. Rift-Related Morphology of the Afar Depression, in: Billi, P. (Ed.), Landscapes and Landforms of Ethiopia. Springer Netherlands, Dordrecht, pp. 251–274. https://doi.org/10.1007/978-94-017-8026-1_15

Demange, J., Di Paola, G.M., Lavigne, J., Lopoukhine, M., Stieltjes, L., 1971. Etude Géothermique du Territoire Français des Afars et des Issas. B.R.G.M.

Gasse, F., Lédée, V., Massault, M., Fontes, jean-C., 1989. Water-lake fluctuations of lake Tanganiyka in phase with oceanic changes during the last glaciation and deglaciation. Nature 342, 57–59.

Gillespie, R., Street-Perrot, A., Switsur, R., 1983. Post-glacial arid episodes in Ethiopia have implications for climate prediction. Nature 306, 680–683.

J. Varet, 2018. Geology of Afar (East Africa), Springer. ed, Regional Geology Reviews.

Krumbein, W.E., 1983. Stromatolites — the challenge of a term in space and time. Precambrian Res. 20, 493–531. https://doi.org/10.1016/0301-9268(83)90087-6

Lamb, A.L., Leng, M.J., Lamb, H.F., Telford, R.J., Mohammed, M.U., 2002. Climatic and non-climatic effects on the δ18O and δ13C compositions of Lake Awassa, Ethiopia, during the last 6.5ka. Quat. Sci. Rev. 21, 2199–2211. https://doi.org/10.1016/S0277-3791(02)00087-2

Lamb, H.F., 2001. Multi-proxy records of Holocene climate and vegetation change from Ethiopian crater lakes, in: Biology and Environment: Proceedings of the Royal Irish Academy. JSTOR, pp. 35–46.

Lamb, H.F., Bates, C.R., Bryant, C.L., Davies, S.J., Huws, D.G., Marshall, M.H., Roberts, H.M., 2018. 150,000-year palaeoclimate record from northern Ethiopia supports early, multiple dispersals of modern humans from Africa. Sci. Rep. 8. https://doi.org/10.1038/s41598-018-19601-w

Lamb, H.F., Bates, C.R., Coombes, P.V., Marshall, M.H., Umer, M., Davies, S.J., Dejen, E., 2007a. Late Pleistocene desiccation of Lake Tana, source of the Blue Nile. Quat. Sci. Rev. 26, 287–299. https://doi.org/10.1016/j.quascirev.2006.11.020

Lamb, H.F., Leng, M.J., Telford, R.J., Ayenew, T., Umer, M., 2007b. Oxygen and carbon isotope composition of authigenic carbonate from an Ethiopian lake: a climate record of the last 2000 years. The Holocene 17, 517–526. https://doi.org/10.1177/0959683607076452

Legesse, D., Gasse, F., Radakovitch, O., Vallet-Coulomb, C., Bonnefille, R., Verschuren, D., Gibert, E., Barker, P., 2002. Environmental changes in a tropical lake (Lake Abiyata, Ethiopia) during recent centuries. Palaeogeogr. Palaeoclimatol. Palaeoecol. 187, 233–258.

Marshall, M.H., Lamb, H.F., Davies, S.J., Leng, M.J., Kubsa, Z., Umer, M., Bryant, C., 2009. Climatic change in northern Ethiopia during the past 17,000 years: A diatom and stable isotope record from Lake Ashenge. Palaeogeogr. Palaeoclimatol. Palaeoecol. 279, 114–127. https://doi.org/10.1016/j.palaeo.2009.05.003

Marshall, M.H., Lamb, H.F., Huws, D., Davies, S.J., Bates, R., Bloemendal, J., Boyle, J., Leng, M.J., Umer, M., Bryant, C., 2011. Late Pleistocene and Holocene drought events at Lake Tana, the source of the Blue Nile. Glob. Planet. Change 78, 147–161. https://doi.org/10.1016/j.gloplacha.2011.06.004

Murray, H.D., 1975. Melanoides tuberculata (Müller), Las Morras Creek, Bracketville. Bullettin Am. Malacol. Union 43.

Reid, R.P., 2011. Stromatolites, in: Hopley, D. (Ed.), Encyclopedia of Modern Coral Reefs. Springer Netherlands, Dordrecht, pp. 1045–1051. https://doi.org/10.1007/978-90-481-2639-2_152

Riding, R., 2007. The term stromatolite: towards an essential definition. Lethaia 32, 321–330. https://doi.org/10.1111/j.1502-3931.1999.tb00550.x

Tiercelin, J.-J., Gibert, E., Umer, M., Bonnefille, R., Disnar, J.-R., Lézine, A.-M., Hureau-Mazaudier, D., Travi, Y., Keravis, D., Lamb, H.F., 2008. High-resolution sedimentary record of the last deglaciation from a high-altitude lake in Ethiopia. Quat. Sci. Rev. 27, 449–467. https://doi.org/10.1016/j.quascirev.2007.11.002

Varet, J., 1978. Geology of Central and Southern Afar (Ethiopia and Djibouti Republic). Editions du Centre National de la Recherche Scientifique, Paris.

Vinet, F., Adi, J., Cherel, J.-P., Colas, A., Pasquet, M., Gutherz, X., 2012. RAPPORT SUR LES CRUES DE L'OUED GOBAAD A AS EYLA (REPUBLIQUE DE DJIBOUTI, AOUT 2010) PROCESSUS, IMPACTS ET REMEDIATION. Université Montpellier3/Sud Hémisphere.

Wagner, B., Wennrich, V., Viehberg, F., Junginger, A., Kolvenbach, A., Rethemeyer, J., Schaebitz, F., Schmiedl, G., 2018. Holocene rainfall runoff in the central Ethiopian highlands and evolution of the River Nile drainage system as revealed from a sediment record from Lake Dendi. Glob. Planet. Change 163, 29–43. https://doi.org/10.1016/j.gloplacha.2018.02.003

BII.4 Rapport des travaux Géomorphologiques - PSPCA 2019

Rapport des derniers travaux Géomorphologiques/Géoarchéologiques

PSPCA 2019

Carlo Mologni & Laurent Bruxelles

Dans le cadre de la dernière mission PSPCA 2019, le volet de travail géomorphologique as comporté une série de prospections, de sondages et de prélèvements sédimentaires avec l'objectif d'affiner la compréhension du lien entre l'évolution paléohydrologique du bassin du Lac Abhé et la formation/érosion d'archives sédimentaires périphériques non-lacustres contenant du record archéologique.

L'importance des travaux geomorphologiques dans la vallée du Gobaad

Dans le bassin du Gobaad la connaissance géomorphologique des archives sédimentaire est reliée principalement au travaux de F. Gasse (1975, 1977) dont les fluctuations climatiques et environnementales sont reconstituées à l'aide de l'étude des flores diatomiques contenues dans les dépôts de l'ancien Lac Abhé. Grace à son travail, on as aussi une idée des oscillations altimétriques des lignes littorales lacustres suite aux changements de l'intensité de la mousson sur la région Afar entre 30 ka BP et l'actuel. Toutefois la durée précise des phases humides/arides dans la région de l'Afar Central à la fin du Pléistocène et pendant l'Holocène reste encore peu connue, puisque la plupart des études paléoclimatiques continentaux modernes sont basés sur la région des Grand Lacs Ethiopiens, au sein du rift African (Chalié and Gasse, 2000; Gasse et al., 1989; Gillespie et al., 1983; Lamb et al., 2002; Legesse et al., 2002), et sur les Hauts Plateaux Ethiopiens (Lamb, 2001, 2001; Lamb et al., 2018, 2007a, 2007b; Marshall et al., 2011, 2009; Tiercelin et al., 2008; Wagner et al., 2018). Au-delà des problématiques strictement paléoclimatiques, certaines questions d'ordre géomorphologique, et connectées aux questionnements archéologiques du projet, restent ouvertes : Quel a été le réel impact de changements climatiques sur l'évolution des paléopaysages et des géomorphologies autour du Lac Abhé ? En d'autre termes, quel type d'environnements sédimentaires ont pu se former, et être connectés au Lac Abhé pendant les respectives périodes humides et arides ? Quel type d'environnement sédimentaire a pu été l'objet d'occupation humaine préhistorique, et sous quels paramètres géographiques ? Est-ce qu'il y a une cohérence chronologique-spatiale entre les déports lacustres résiduels, les dépôts sédimentaires périphériques au paleolac et le record archéologique ? Au final, est-ce-que les changements climatiques à l'Holocène ont pu avoir un rôle dans l'émergence des premières sociétés de production et dans l'installation/abandon des groupes Humains sur rives du paleolac Abhé entre 15 et 3 ka BP ?

Grace aux travaux de recherches archéologiques combinés aux enquêtes géomorphologiques effectués dans ces dernières années dans le cadre du projet PSPCA, aujourd'hui on dispose d'un grand nombre d'âges et d'observations pedostratigraphiques sur les sondages archéologiques effectués au long de la Vallée du Gobaad. Ceci constitue la base pour un approche analytique un qui vise à la clarification des questionnement ci-dessus proposés.

Les paléorivages du Lac Abhé et l'emplacement de sites archéologiques

Les travaux de repérage, description et interprétation des morphologies, des dépôts sédimentaires marqueurs des anciens rivages lacustres correspondants aux phases de transgression et de régression ont continué au cours des opérations de terrain en Janvier 2019. Différentes zones ont été prospectés : sur le horst de faille au Sud de As Eyla, sur les versant nord du massif de Ara le Koma, sur les versants du massif d'Aysilo et plus au Nord-Est dans le Diksa Déré. Une grande variabilité de marqueurs littoraux a été constatée et documentée en deux familles : les marqueurs morphologiques et les marqueurs sédimentaires. Dans les premiers on trouve les coupures de pente en correspondance e surfaces d'abrasion lacustre (Fig 1B), ou la formation de terrasses rocheuses reconnues à l'intérieur d'un canyon de déversement vers le bassin d'Hanlé (Fig 1D) ; les deuxièmes sont représentés par de deltas de type Gilbert (Fig 1B), ou par des formation microbialitiques (stromatolites et oncolites ; Fig 1A, C), lesquelles, une fois complètement érodées, laissent leur empreinte fossile sur la surface de croissance en donnant une forme à « champignon » (Fig 1E).

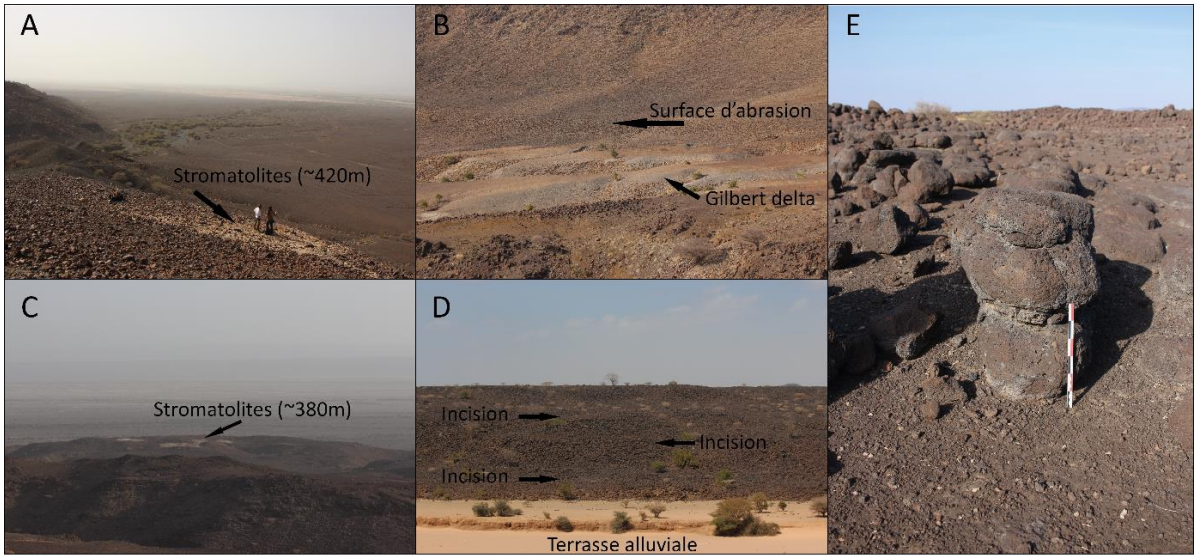

Figure 1 : marqueurs littoraux morphologiques et sédimentaires : A) planché stromatolitique sur les versant Nord du Massif d'Ara le Koma (~420m) ; B) Surface d'abrasion lacustre associée à delta de type Gibert ; C) planché stromatolitique sur les versants Sud du Massif d'Aysilo (~380m) ; D) terrasses rocheuses d'incision en bordure du canyon de déversement vers le bassin d'Hanlé ; E) morphologie à « champignon », témoin d'une ancienne dôme stromatolitique érodée en proximité du site archéologique d'Antakari 3.

Certains éléments littoraux repérés sur le terrain ont été échantillonnés avec l'objectif de définir une chronologie précise des fluctuations lacustres Holocènes. En attendant ces âges, un travail de tri, de calibration et de recalcule des altitudes (MNT 5m) des données publiées dans la thèse de F. Gasse (1975) a permis de proposer une courbe mise à jour des fluctuations du paleolac Abhé sur les derniers ~11 ka BP (Fig2). La confrontation de cette courbe avec le placement chronologique et altitudinale des sites archéologiques datés dans le bassin du Gobaad a permis de caler chronologiquement plusieurs formes littorales non-datables reconnues sur le terrain, et de reconstituer la relation entre l'emplacement spatiale des sites archéologiques et les pulsations lacustres Holocènes (Fig2).

En ce qui concerne la variation du niveau du lac Holocène trois phases de transgression ont été observées. La première (Abhé IV ; selon la terminologie en Gasse 1975) est divisé en deux sous-phases : Abhé IV.a avec sa première évidence à 10.6 ka cal BP (342m), son pic entre 10.4 et 9.8 ka cal BP (410-430m) et sa fin entre 9.8 et 9.7 ka cal BP (~370m) ; la deuxième (Abhé IV.b) qui oscille entre 371 et 362 m sur plus d'un millénaire (9.6 – 8.2 ka cal BP). En moins de 200 ans on observe une chute abrupte du niveau du lac à 240m qui semble continuer jusqu'à 7 ka BP ou une première évidence de remontée du lac à 327m ouvre la phase Abhé V. Le niveau du lac reste stable entre 6.7 et 5.4 ka cal BP (360 - 365 m), subi un abaissement d'environ 20m entre 5.4 et 4.6 ka cal BP (346 m) pour après régresser probablement au même niveau documenté à 8.2 ka cal BP (240). La remontée du lac à l'Holocène récent, et correspondante à la phase Abhé VI (Gasse 1975), est documenté à partir de 2.8 jusqu'à 1.5 ka cal BP (max 314m). Ces variations de niveaux du lac Holocènes seront confirmées ou modifiées dans les années à venir grâce aux récentes opérations de terrain et au programme de datations d'échantillons provenant des formes sédimentaires littorales.

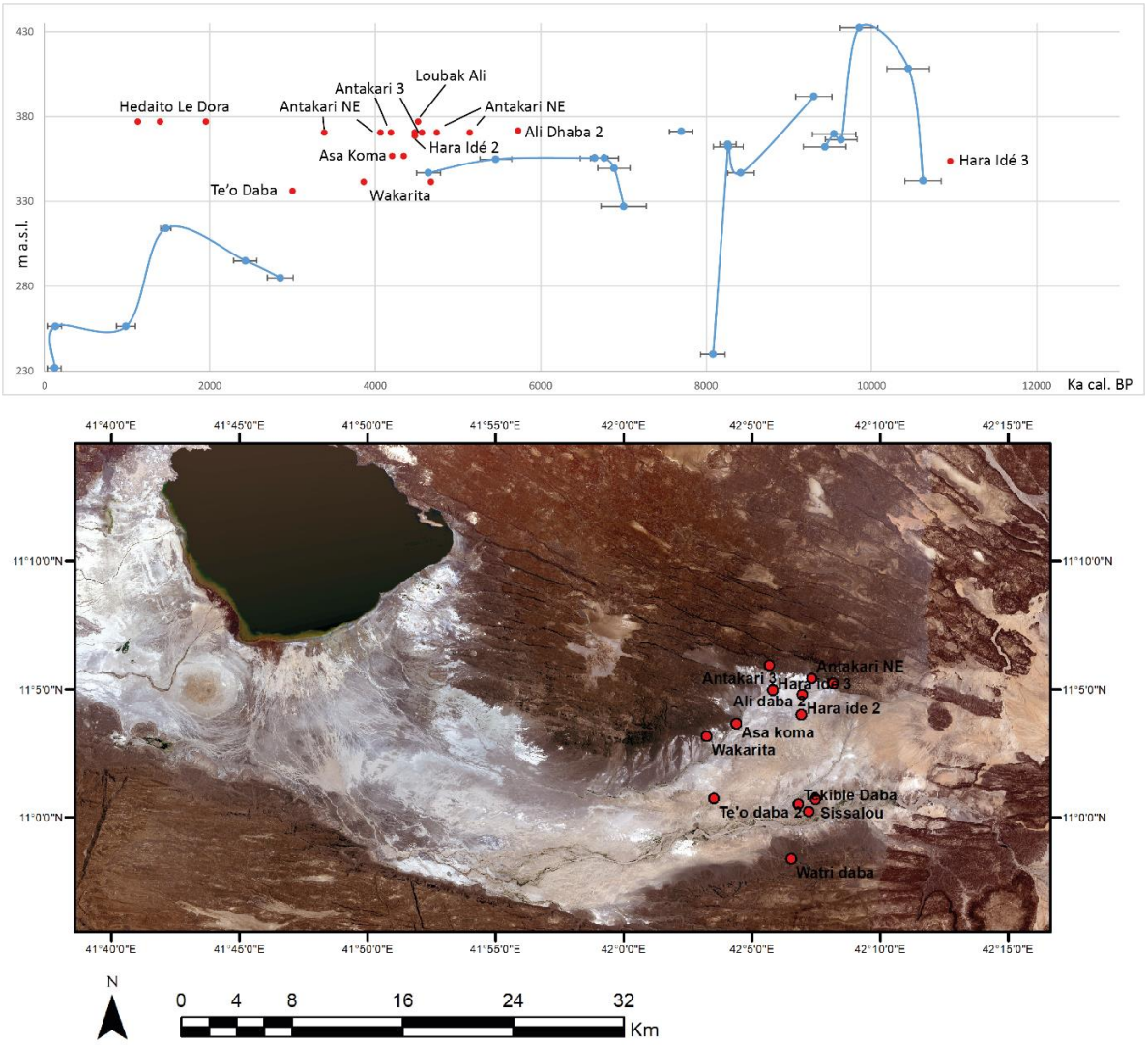

Figure 2 : En haut courbe de fluctuations lacustres du lac Abhé à l'Holocène d'après les âges publiées en Gasse (1975) calibrées et les altitudes recalculées, avec localisation altitudinale et chronologique des sites archéologiques datés dans le cadre du projet PSPCA. En bas localisation spatiale des sites archéologiques datés dans le cadre du projet PSPCA

Investigation géoarchéologque du site Antakari 3

Avec l'objectif de comprendre plus finement les processus de formation anthropiques/naturels et afin d'établir une chronologie du début de la mise en place, des phasages de la structure funéraire d'Antakari-3, une campagne d'investigation géo-archéologique intrasite a été mise en place au cours des missions PSPCA 2018/2019. Pendant ces campagnes deux sondages profonds (qui atteignaient le substrat basaltique) ont été réalisés au sein de la structure avec l'objectif de couvrir toute la séquence sédimentaire : le premier au centre de la structure dans le carré M17 et le deuxième en bordure de la structure en M7. Positionnés au long du même transect (bande M) ces deux sondages ont permis d'un regard préliminaire sur la variabilité latérale de la morphologie des dépôts qui constituent la structure et de reformuler la séquence des Unités Sédimentaires (US). Un troisième carré de fouillé à été investigué (Q16) afin de préciser la stratigraphie de l'entrée du monument funéraire. Ci-dessous sont présentés les observations stratigraphiques et les descriptions pedo-sédimentaire des trois sondages.

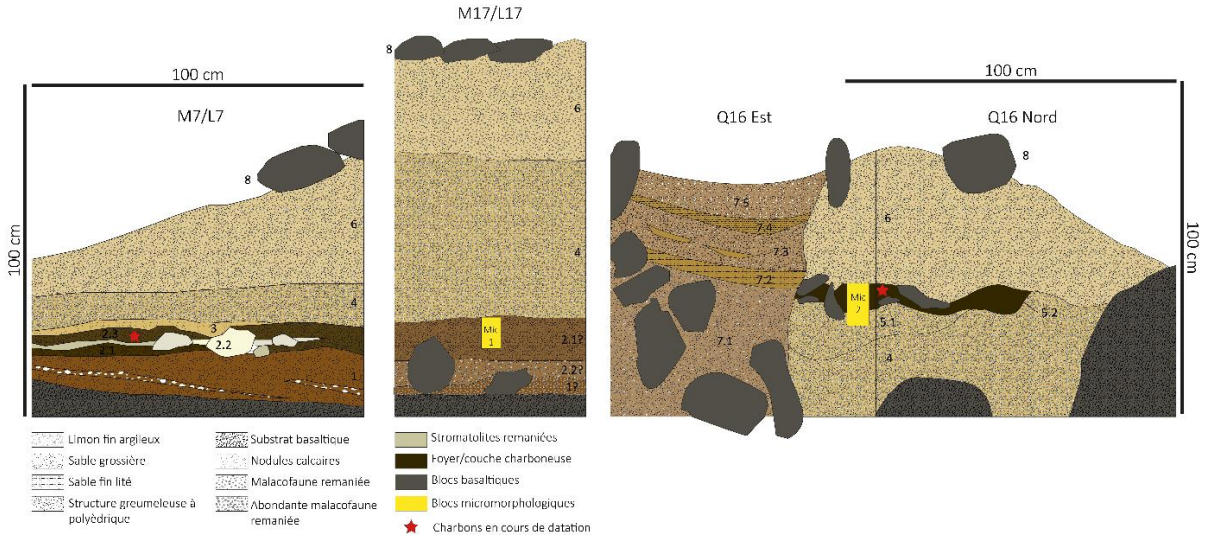

Figure 3 : Coupes stratigraphiques des sondages présentés et discutées dans le texte.

Coupe M7/L7 (Fig 3)

Sur le substrat basaltique se pose l'US1 caractérisé par de sables grossières massives prises dans une matrice plus limoneuse brun-rougeâtre, deux lentilles sédimentaires subhorizontales riches en nodules carbonatés (1-2 cm) traversent cette US. Il s'agit d'un sol d'altération basaltique formé avant l'édification du monument. L'US 2.1 est composé par des limons-argileux brun à structure grumeleuse, à polyédrique avec des charbons de bois et quelque coquille mélanoide. Antérieure aux dépôts anthropogénique, l'US2.1 représente le développement d'un petit évènement pédogénique. L'US2.2, composée principalement par de stromatolites sub-arrondies en position secondaire souvent altérées par décarbonatation indique la mise en place d'un ou plusieurs phases lacustres suivies par une régression activation d'un réseau de ruissellement et le développement d'un petit horizon pédologique (US2.3). Au sein de cette dernière US un charbon de bois a été prélevé pour des dations 14C en AMS afin d'obtenir un âge *post-quem* du début de l'édification du monument funéraire. Suite à une couche très mince de sable fin bien trié (US3), la séquence sédimentaire se poursuit avec un premier épais apport de sédiment anthropique (US4) de sable grossier à structure massive riche en malacofaune souvent fragmentée et avec quelque cailloux basaltique (4-5 cm) à sa base. L'US5 est suivie par un deuxième apport anthropique (US6) présentant une texture légèrement plus fine (sables moyens-grossières) et une fragmentation plus prononcée de la composante coquillière. Une surface de dalles et blocs basaltiques selle la séquence qui correspond us dernier élément structural du monument anthropique.

Coupe M17/L17 (Fig 3)

Localisé au centre de la structure anthropique le sondage en M17 présente du bas vers le haut les Unités suivantes : US1 ? - Posé sur le substrat basaltique se développe une couche à sables moyennes-grossières brun rougeâtre foncé, massif avec de traits ferrugineux secondaires probablement correspondant au sol d'altération basaltique reconnait plus au sud dans le sondage e M7. US2.2 ? - suive une couche à sables moyennes-fines brunes cimentées, avec d'abondantes coquilles de type *Melanoides tuberculata*. Considéré le caractère *in situ* du matériel lacustre, cette unité pourrait correspondre aux US2.1, 2.2 du sondage en M7., toutefois la corrélation stratigraphique précise de ces unités sur la longueur de tout le monument sera possible au moment des opérations de connexion des deux sondages prévues dans la prochaine campagne de fouille ; US2.3 - le dépôt devient de plus en plus fin avec du sable-limoneux brun foncé avec une structure grumeleuse à polyédrique et avec d'abondantes coquilles de type *Melanoides tuberculata*. Ces premières unités sédimentaires englobent quelque bloc basaltique qui pose sur le substrat. Ces blocs sont déconnectés et ne semblent pas suivre l'organisation de la structure à blocs basaltiques anthropique construite dans les couches supérieures. US4 - la séquence se poursuit avec le paquet sableux à coquilles qui contient la plupart du record archéologique aujourd'hui en train de fouille. Cette couche correspond avec les US 304 et 305 de la fouille

archéologique. US1 - La dernière couche supérieure correspond à l'US 302 de la fouille archéologique, qui est ensuite scellé par une couverture de bloc basaltiques d'origine anthropique. Des prélèvements sédimentaires en vrac ont été collectés dans les couches inférieures et un bloc micromorphologique a été prélevé dans l'US2.1.

Coupe Q16 Est (Fig 3)

A la marge Est du monument funéraire d'Antakari 3, suite aux opérations de fouille dédiées au dégagement de l'entrée de la structure reconnaissable par deux dalles basaltique positionnées verticalement, deux coupes ont été relevées et étudiées dans le détail. Dans le carré Q16 la fouille n'a pas pu atteindre la base et la partie inférieure de la séquence sédimentaire (US 1, 2, 3), en conséquence toutes les US présentent un caractère anthropogénique. Du bas vers le haut ont été observées le US4 et 6 séparées par les US5.1 et 5.2 qui présentent plusieurs faciès de combustion. En particulier l'US5.2 avec sédiment limoneux charbonneux brun-noir englobant quelque caillou basaltiques thermo-altéré, suggère la présence d'une structure de combustion. Au sein du foyer des charbons ont été échantillonnés afin d'effectuer des datation ^{14}C qui permettront donc de définir en chronologie absolue la fin du premier apport anthropique (US4) et le début du deuxième apport anthropique (US6). Un bloc micromorphologique a été prélevé au long des US 5.1 et 5.2 afin de documenter au mieux la structure de combustion. Ces deux premières phases d'apport sédimentaires avec la structure de combustion associée, sont recoupées sur tout leur épaisseur. Un troisième apport sédimentaire anthropique comble donc cette ouverture, qui coïncide donc avec l'entrée du monument funéraire : les US7.1 et 7.2 pourraient représenter une première phase de remplissage, les US7.3 et 7.4 une deuxième et l'US7.5 une troisième. Les deux dalles basaltiques verticales qui marquent le positionnement de de l'entrée sont postérieures à ces apports sédimentaires.

Considérations de reconstitution du contexte paléopaysagère autour du site d'Antakari 3

Le croisement entre les observations géoarchéologiques et la reconstitution des paléorivages lacustres en relation aux sites archéologique fouillées dans les Gobaad (Fig 2), permet d'avancer quelque considération sur les processus de formation sédimentaire du site d'Antakari 3 sur l'évolution de son contexte paléopaysagère avant et au cours de son occupation Humaine.
Le matériel lacustre *in situ* non-anthropique localisé à la base du monument (US2.2) correspondrait donc au matériel accumulé en zone littorale (entre 360-370m) pendant la transgression entre 6.8 et 4.7 ka BP. Suite au début de la régression lacustre à ~4.7 ka BP, un mince paléosol s'est développé (US2.3) suivi probablement par un phénomène de désertification abrupte (US3). C'est à partir de 4560 yrs cal. BP qui est attesté la première occupation anthropique du site d'Antakari 3. Sur la base des données acquises jusqu'à maintenant, au moment du début de l'édification du monument funéraire le rivage lacustre en phase de régression se trouvait autour 1,7 Km de distance de l'emplacement du site. L'US2.2 plus différents marqueurs littoraux (Fig 1E) localisées dans les alentours du site archéologique, témoignent de la présence *in situ* de matériel lacustre littoral (stromatolites, mélange de coquilles dans une matrice de sables moyens-grossiers). En considérant ces observations et tenant compte de la rapidité de régression des rivages au début de l'aridification Holocène (~2 Km en ~100 ans) c'est envisageable que le matériel utilisé pour l'édification du monument funéraire (US4) se trouvait en ce moment disponible autour du site.
Les datations prévues sur les charbons provenant des US2.2 et 5.2 permettront de préciser la chronologie de début d'édification du site et de son phasage.

Evaluation de la couverture sédimentaire quaternaire sur le Massif d'Aysilo

Le forte taux d'érosion et la forte altération chimique des accumulation sédimentaires et des roches silicatées en zone tropicale (Bastian et al., 2017) peut expliquer la manque d'archives sédimentaires sur les horsts du semi-graben de Tendaho-Gobaad. La problématique de la conservation d'archive sédentaires en dehors de la basse plaine du Gobaad est cruciale pour la documentation de sites archéologiques contemporains aux hauts niveaux lacustres Holocènes (>370m ; >420) dans le bassin du Gobaad. Suite à l'analyse des modèles de reconstitution paléohydrologique du Lac Abhé plusieurs lignes de rivage sur les versants Sud du Masssif D'Aysilo ont été localisé. Les images satellites et les prospections de terrain ont confirmé cette hypothèse avec le repérage et la documentation de plusieurs couvertures stromatolitiques déjà observées en 2018. Ces larges couvertures carbonatées représentent pas seulement un marqueur

fiable des anciennes zones littorales et des archives paleo-climatiques à haute résolution, mais aussi des éléments de protection des accumulations sédimentaire pré-transgression lacustre des phénomènes érosifs postérieurs.
C'est pour cette raison qu'en Janvier 2019, 6 sondages et des repérages de surface ont été effectués (Fig 4) avec l'objectif de tester les accumulations sédimentaires potentielles contenant des niveaux archéologiques conservées sous la couverture stromatolitique.

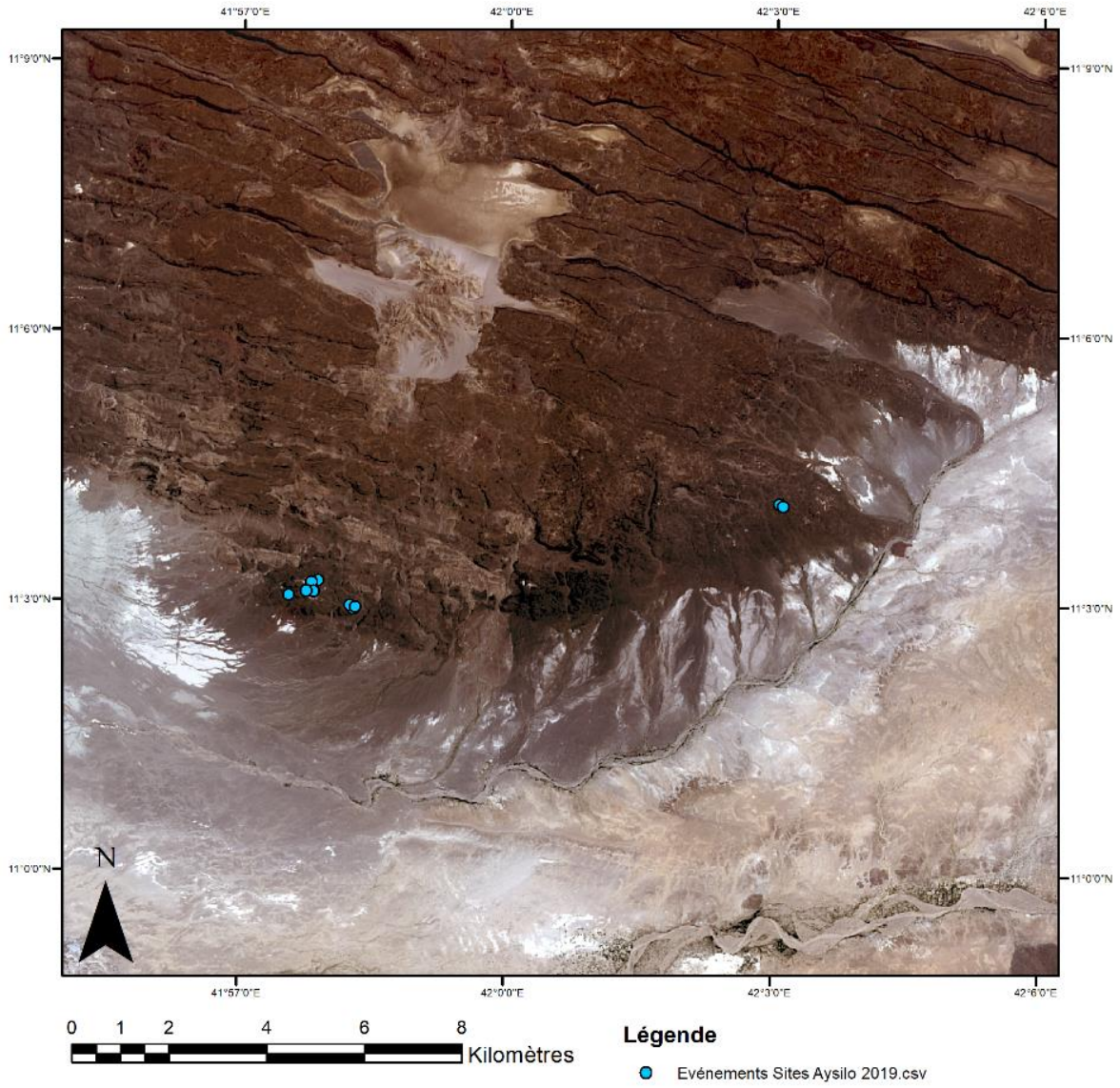

Figure 4: Localisation des sondages et de repérages de surface effectuées pendant la mission PSPCA 2019.

L'emplacement des sondages a été choisi à partir l'estimation visuelle de l'épaisseur de la couverture sédimentaire par rapport au substrat basaltique et à partir la présence ou absence de matériel anthropique en marge des couvertures carbonatées (indicateur d'un niveau archéologique érodé). Les observation stratigraphiques et pedo-sedimentaires des sondages effectués montrent une variabilité avec : des colluvions de matériel lacustre (Fig 5A), des couches coquilleres asurmontés par des stromatolites remaniées (Fig 5B), ou par des oncolites en position primaire (Fig 5C). Les accumulations sédiantaires sous les formations lacustres peuvent varier selon l'emplacement : des paléosols argileux à structure polyedrique surmonté par des lignes de blocs basaltiques (Fig 5A), des sols d'altératon basaltique (Fig 5B), ou

des sols silteux riches en gravillons. Des rares évidences archéologiques ont été observées dans ces formations sédimentaires (site Aysilo 5)

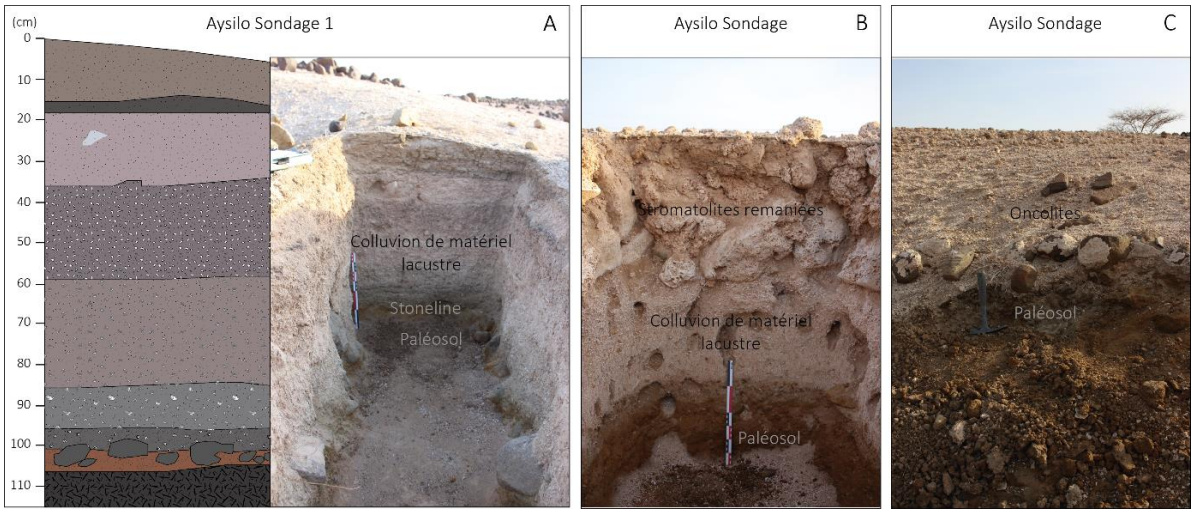

Figure 5: A) coupe stratigraphique et photo du Sondage Aysilo1; B, C) Exemple de sondages effectuées sur le massif d'Aysilo pendant la mission PSPCA 2019.

La totalité de sondages a permis de reconnaitre une homogénéité de conservation d'archives sédimentaires pédologiques ou détritiques antérieures aux formations lacustres. Des datations absolues sur la couverture stromatolitique et sur les formations sédimentaires sous-jacentes sont envisagées au cours de la prochaine année du projet. Toutefois, à partir des données sur l'évolution paléhydrologique à l'Holocène quelque considération chronologique est avancée. Les formations carbonatées lacustres du Massif d'Aysilo sont localisées entre 380 et 390m, altitude correspondante aux lignes de rivage comprises entre 10.4 et 8.2 ka BP. Ces dépôts pédologiques se sont donc probablement formés au cours d'une période antérieure aux grandes transgressions lacustres Holocènes.

Analyse geoarchéologique et micromorphologique de la sequence Hara Ide 3

(en Anglais)

General stratigraphy and preliminary interpretation

The operations of excavation of the Hara-Ide-3 site and correlations with Hara-Ide-3-ST8 sounding and Hara-Ide-1-section (Fig. 6) have permitted to describe and differencing five sedimentary phases A, B, C, D, E. The pedosedimentary description of this sequence is presented above and synthetized in the Tab. 1.

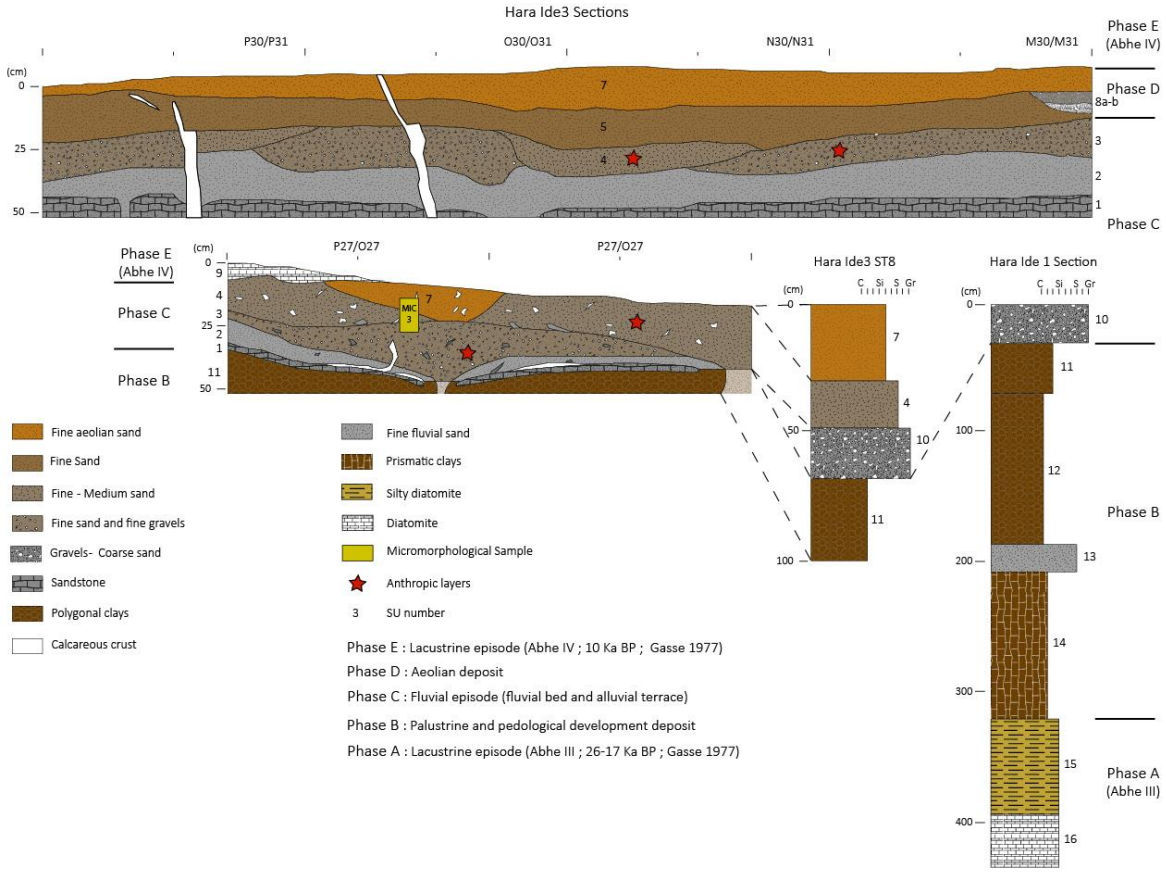

Figure 6 : Lithostratigraphy of the Site Hara Ide 3 with correlations with Hara Ide3 ST8 and Hara Ide 1 section.

Phase	Sedimentary Unit (SU)	Fieldwork pedosedimentary description
A	16	With clay-silts horizontay microlaminated (diatomite formation)
	15	Pale brown silts, well sorted (diatomite formation)
B	14	Brown very well sorted clay, well developed prismatic structure, with rarely silty and sandy inclusions.
	13	Grey fine sand, well sorted and micro-cross-laminated. Some shell fragments (~1mm)
	12	Brown clay, well sorted, polygonal structured and sand inclusions.
	11	Brown silty clay deposit, well sorted, polygonal structured and abundant coarse sand and gravel (5mm – 1cm).

C	10	Gravel (<2 cm), poorly sorted, massive structured in a coarse sandy matrix.
	1	Grey diagenised fine sand, very well sorted and crossed-undulated micro-laminae (<1mm).
	2	Grey fine sand, very well sorted and crossed-undulated micro-laminae (<1mm).
	3	Consolidated pale-brown fine/medium sand, well sorted texture and massive structure. Some gravel (2-3 mm), abundant carbonate nodules (5mm-1cm) and SU1 fragments inclusions. Rare charcoal, bone fragments and ostrich egg shells.
	4	Pale brown-grey fine sand, well sorted, massive-to-granular structure, abundant carbonated nodules. Carbonated gravel inclusions (1-2 cm) at the base of the unit. Rare charcoal, bone fragments and ostrich egg shells.
D	5	Brown fine sand, well sorted, massive structure, with structure with abundant calcareous nodules and some clasts at the base of the unit
	6	Brown fine sand, well sorted, massive structure.
	7.1/7.2	Brown-reddish fine sand, very well sorted, massive structure with abundant calcareous nodules (3 mm – 1 cm)
	8a	Dark brown consolidated fine sand, with charcoal inclusions.
	8b	Whitish ash, some charcoal and bones.
E	9	Withe clay-silts horizontay microlaminated (diatomite formation)

Tab 1 : Fieldwork pedosedimentary description of Hara Ide sequence

From the bottom to the top the phase A is composed by an offshore biogenic diatomite formation (SU16) followed by silty diatomite unit (SU15) characterized by pale brownish colour and then attesting a lowering in lake water column depth. Phase B is generally composed by brownish clayey deposit intercalated by massive fine sand event probably of alluvial origin (SU13). At the base of this Phase, SU14 presents a strong prismatic clay aggregation which turns upwards in a coarser clayey unit characterized by polygonal structure. This sedimentary Phase likely correspond to the retreat of the lake shoreline correlated to the development to a palustrine deposit (SU14), a slight reactivation of the local hydrographic system (SU13) is followed by a pedogenic event (SU12 and 11).

Sedimentary Phase C start with an erosive event and by the deposition grey gravel and sand which vary laterally according to the topography of the studied area. Over the archaeological site, the beginning of this Phase is characterized by a diagenised laminated and well sorted fine/medium sandy unit SU1, followed by fine sand laminated layer (SU2). This deposit indicates a fluvial deposit of medium to low energy flow, probably corresponding to the activity of a lateral stream. Next to the actual main hydrographic network (Hara Ide 1 Section; Fig. 6), deposits are coarser and composed by gravels embedded in a coarse sand matrix (SU10), attesting a higher energy flow. The end of the sedimentary Phase C is characterized by a well sorted fine to medium sand without any evident structure (massive deposit; SU3 and 4). SU3 is coarser with some gravels and calcareous pebbles inclusions. It's in these sedimentary units that prehistoric Human occupation have been attested. Indeed, Human bones, charcoals and ostrich egg shells has been founded and documented. A more precise description and sedimentogenetic interpretation of SU4 and SU3 has been possible thanks to micromorphological analyses presented in the next paragraph.

Phase D is characterized by massive and very well sorted fine sand probably of aeolian origin (SU5 to SU7). Macroscopical evidences which permits to difference these upper layers from the main archaeological units are the absence of coarse inclusions or of secondary nodules and the pale reddish colour of the matrix. A more recent site occupation is attested by the presence of anthropic hearths which cuts the upper levels (ex. SU8a-b).

The Hara-Ide-3 is sealed by whitish diatomite deposit attesting a more recent lacustrine transgression (SU9) corresponding to the sedimentary phase E. All the Hara-Ide-3 sequence is traversed by a vertical and horizontal calcareous crusts, probably linked to the dissolution and re-precipitation of secondary carbonates coming from the upper $CaCO_3$-rich lacustrine deposits.

Micromorphological description and interpretation

With the aim to better understand the sedimentary formation processes of the upper Phase C, and thus the sedimentary context of the prehistoric occupation of the Hara Ide 3 site, three micromorphological blocs have been collected from the sections. Here is presented the micromorphological description and interpretation of the Sample HI-3_MIC3 (Fig. 6) which covers the Sedimentary Units 3 4 and 7. A synthetic description is presented in Tab. 2, although the results are discussed below. Micromorphological description follows the guidelines proposed by Stoops (2003).

Coarse fraction

Sample	SU	µm	Qz	Basalt	Olivine	Plg	Pyrx	Gr	Ca	OM	Bone	Shell
HI-3_MIC3	3	20-300	****	/	**	*	**	***	***	/	/	/
	4	10-200	****	/	**	*	*	**	***	/	/	/
	7.1	20-200	***	/	**	**	**	****	*	/	/	*
	7.2	20-100	***	/	**	**	**	*	*	/	/	/

Groundmass

Sample	SU	c/f distribution pattern	c/f ratio	c/f limit	Sorting	Distribution	Orientation
HI-3_MIC3	3	coarse monic/close fine enaulic	70/30	10	moderately	random	random
	4	coarse monic	80/20	7	well	random	random
	7.1	coarse monic	90/10	10	Very well	random	random
	7.2	coarse monic	90/10	15	Very well	random	random

Microstructure and voids

Sample	SU	Peds	Separation/ pedality degree	Accomoda-tion	Porosity	%	Microstructure
HI-3_MIC3	3	porous crumbs	/	/	Complex packing voids/channels/chambers	30	Intergrain microaggregate
	4	No peds	/	/	Simple packing voids/channels	40	single grain
	7.1	No peds	/	/	compound packing voids/channels/vughs planes	40	single grain
	7.2	No peds	/	/	simple packing voids	50	single grain

Pedofeatures

Sample	SU	Type	Localisation	Nature	Colour/birefringence	Quantity	Remarks
HI-3_MIC3	3	typic disorthic nodules	groundmass	micrite	High birifrangent		Fig VI.13i
	4	typic disorthic nodules	groundmass	micrite	High birifrangent	***	Fig VI.13g

	7.1	Dendritic orthic nodules	groundmass	Fe-Mn	Red	**	Fig VI.13f Fig VI.13d
	7.1	typic disorthic nodules	groundmass	micrite	High biriffrangent	**	
	7.1	Crescent infillings	channels	silt	/	*	Fig VI.13e bioturbation

Tab 2 : Sinthetized micromorphological description of HI-3_Bloc3

From the bottom to the top, the three SU sampled in the HI-3_MIC3 are well recognised in this section (Fig. 7):

SU3 is characterized by a subangular coarse fraction moderately sorted mainly ranged between 20 and 300 µm (Fig 7d), with a slight developed intergrain microaggregate microstructure which includes several porous crumbs with a strong micritic b-fabric. The porosity network is organised as a mix of Complex Packing Voids and abundant channels and chambers. Pedofeatures are mainly represented by abundant and coarse micritic disorthic nodules (2mm to 1 cm), however, no calcitic features on voids are observed.

SU4 presents a more sorted subangular coarse fraction without fine fraction peds. The porosity acquires a simple packing voids pattern, and the pedofeatures follow the same characteristics of SU3 (Fig 7g, h).

With the SU7.1 the coarse fraction became very well sorted with a rounded to sub-angular shape of grains. Porosity is mainly represented by a simple packing voids. The specific markers of this unit are the abundance of Fe-Mn Dendritic orthic nodules (Fig 7d), mainly concentred at the limit between SU 7.1 and SU4, and the pronounced bioturbation (Fig 7e).

Finally, SU7.2 presents a slightly smaller and very well sorted rounded to sub-angular coarse fraction without evident pedofeatures.

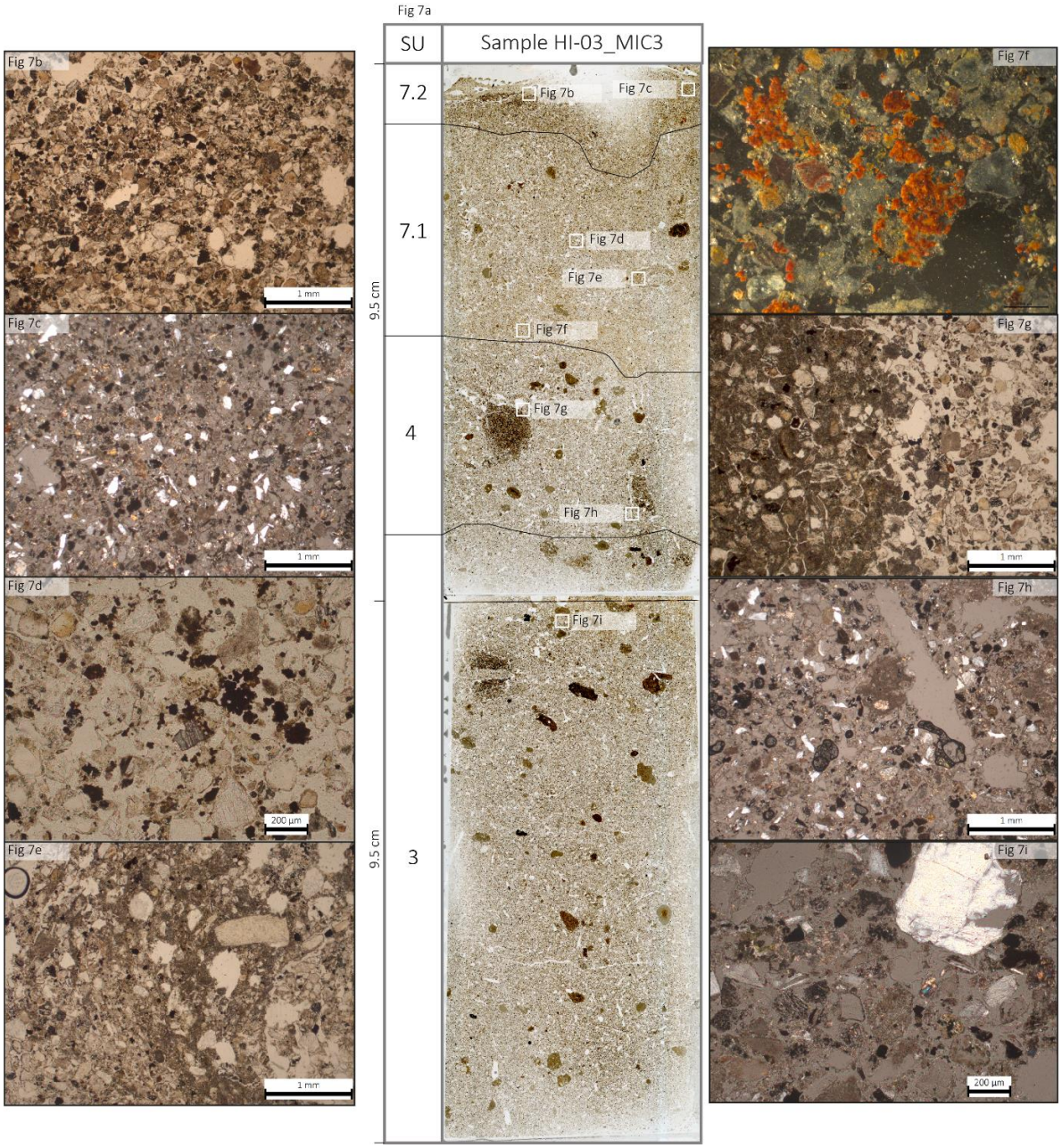

Figure 7 : Sample HI-03_MIC3 : ***a)*** *Plane Polarised Light (PPL) scan of thin section and localisation of Sedimentary Units and microphotos; PPL* ***b)*** *and crossed polarized light (XPL)* ***c)*** *microphotos of SU7.2 groundmass;* ***d)*** *PPL microphoto of Fe-Mn dendritic orthic nodules of SU7.1;* ***e)*** *PPL microphoto of increscent infilling due to bioturbation process;* ***f)*** *Oblique Incident Light microphoto of Fe-Mn dendritic orthic nodules of SU7.1;* ***g)*** PPL microphoto of micritic nodule; **h)** XPL microphoto of channel and chamber in SU4; **i)** XPL microphoto of graundmass of SU3.

In all four SU (3, 4, 7.1, 7.2), the predominance of sorted heavy and resistant minerals (garnet, quartz) and the low quantities of fresh weathering basalt products (plagioclases, olivine, pyroxenes) exclude the direct sedimentary transfer hypothesis linked to gravity-induced or fluvial processes from the proximal basaltic horsts. This mineralogical assemblage rather suggests a reworked allochtonous material from heavily weathered and sorted origin. Additionally, the absence of specific groundmass structure excludes the primary deposition of fluvial sedimentation which characterize the lower Phase C (SU1 and 2). These mineralogical and groundmass characteristics of well sorted sub-anguar and rounded coarse material which rarely exceed the 200 µm can be attributed to aeolian-type sedimentary transfer, as an evidence even observed in paleo-dune deposits of Kurub-07 site (Fig 7d). From the bottom to the top of the thin section a slight diminution in grain size together with the completely lack of the fine fraction point out to the

increase of aeolian transfer processes through the top, particularly for the Sus 7.1 and 7.2 (Phase D). Here, the absence of secondary precipitation of carbonates as a coatings or infillings around voids or grains and the absence of micritic nodules suggest a slightly pronounced hydromorphic processes on this part of the sequence. Only Fe-Mn nodules are observed at the beginning of Phase D. Macroscopically, precipitation of post-depositional carbonates linked to the installation of upper lacustrine sediment of Phase E are evident as a thick carbonated sub-vertical crusts which cross the sediments of Phases C and D. Excluding these crust formations, chemical post-depositional processes seem not affected the archaeological deposit. Over the Phase C physical reworking of sediments seems to be limited to few centimeters because of the carbonate crust fragmentation and deplacement (Fig 6). Only the upper part of Phase D has been partially affected by actual and sub-actual aeolian deflation.

Chronostratigraphic correlation of the Hara-Ide-3 sequence and its paleoenvironmental significance

This preliminary sedimentological and geoarchaeological investigation of the Hara Ide site, combined to new radiocarbon ages have permitted to propose a chronostratigraphic framework of the sequence and to provide a preliminary paleoenvironmental interpretation of sedimentary formation processes described in the previous paragraph.

The lower clayey and silty diatomites of the Phase A likely correspond to the lacustrine transgression of Lake Abhe named Abhe-III by Gasse (1977, 1975) which was dated between ~31 and ~25 ka cal. BP. Clayey deposits of the Phase B are slightly pedogenised attesting a lacustrine regression accompanied by the development of a palustrine deposit intercalated by a low energy fluvial stream (SU 13). Soil development corresponding to SU 11 suggest the regression of lake waters over this basin area. Interruption of humid conditions around 20 ka BP is largely attested in East Africa as a strong reduction of hydrological activity sometimes bringing to the drying of large lakes (Lamb et al., 2018). Aggradation of fluvial deposits (SU 10 and 11) could be interpreted as a slight resurgence of humid conditions before the installation of aeolian sedimentation of SU3, 4, 5, 6, 7 attesting an abrupt drying environment likely corresponding to the Younger Dryas arid event (YD; ~13 to 11.6 ka; Alley, 2000; Garcin et al., 2007). Radiocarbon ages confirm this hypothesis with two dates at 13572 ± 71 and 13471 ± 40 yr cal. BP from SU3. Aeolian sedimentation together with prehistoric occupation continues until the SU7, which was dated around ~11 ka cal. BP. The Hara Ide 3 sequence ends with the Lake Abhe-IV transgression which attaints for the first time this level (~360 m a.s.l.) around ~10.5 ka cal. BP (Fig 2). Accordingly, the diatomite deposit (offshore and depth water column deposit) of SU9 was dated at ~10 ka cal. BP when the lake has attained his maximal level (~420m a.s.l.; Fig. 2)

Références :

Alley, R.B., 2000. The Younger Dryas cold interval as viewed from central Greenland. Quaternary science reviews 19, 213–226.

Bastian, L., Revel, M., Bayon, G., Dufour, A., Vigier, N., 2017. Abrupt response of chemical weathering to Late Quaternary hydroclimate changes in northeast Africa. Scientific Reports 7, 44231. https://doi.org/10.1038/srep44231

Chalié, F., Gasse, F., 2000. Late Glacial Holocene diatom record of water chemistry and lake level change from the tropical East African Rift Lake Abiyata (Ethiopia). Palaeogeography, Palaeoclimatology, Palaeoecology 187, 259–283.

Garcin, Y., Vincens, A., Williamson, D., Buchet, G., Guiot, J., 2007. Abrupt resumption of the African Monsoon at the Younger Dryas—Holocene climatic transition. Quaternary Science Reviews 26, 690–704. https://doi.org/10.1016/j.quascirev.2006.10.014

Gasse, F., 1977. Evolution of Lake Abhe (T.F.A.I.), from 70,000 BP. Nature 265, 42–45.

Gasse, F., 1975. L'évolution des lacs de l'Afar Central (Ethiopie et T.F.A.I.) du Plio-Pléistocène à l'Actuel. Recostitution des paléomilieux lacustres à partir de l'étude des Diatomées. Université de Paris VI, Paris.

Gasse, F., Lédée, V., Massault, M., Fontes, jean-C., 1989. Water-lake fluctuations of lake Tanganiyka in phase with oceanic changes during the last glaciation and deglaciation. Nature 342, 57–59.

Gillespie, R., Street-Perrot, A., Switsur, R., 1983. Post-glacial arid episodes in Ethiopia have implications for climate prediction. Nature 306, 680–683.

Lamb, A.L., Leng, M.J., Lamb, H.F., Telford, R.J., Mohammed, M.U., 2002. Climatic and non-climatic effects on the δ18O and δ13C compositions of Lake Awassa, Ethiopia, during the last 6.5ka. Quaternary Science Reviews 21, 2199–2211. https://doi.org/10.1016/S0277-3791(02)00087-2

Lamb, H.F., 2001. Multi-proxy records of Holocene climate and vegetation change from Ethiopian crater lakes, in: Biology and Environment: Proceedings of the Royal Irish Academy. JSTOR, pp. 35–46.

Lamb, H.F., Bates, C.R., Bryant, C.L., Davies, S.J., Huws, D.G., Marshall, M.H., Roberts, H.M., 2018. 150,000-year palaeoclimate record from northern Ethiopia supports early, multiple dispersals of modern humans from Africa. Scientific Reports 8. https://doi.org/10.1038/s41598-018-19601-w

Lamb, H.F., Bates, C.R., Coombes, P.V., Marshall, M.H., Umer, M., Davies, S.J., Dejen, E., 2007a. Late Pleistocene desiccation of Lake Tana, source of the Blue Nile. Quaternary Science Reviews 26, 287–299. https://doi.org/10.1016/j.quascirev.2006.11.020

Lamb, H.F., Leng, M.J., Telford, R.J., Ayenew, T., Umer, M., 2007b. Oxygen and carbon isotope composition of authigenic carbonate from an Ethiopian lake: a climate record of the last 2000 years. The Holocene 17, 517–526. https://doi.org/10.1177/0959683607076452

Legesse, D., Gasse, F., Radakovitch, O., Vallet-Coulomb, C., Bonnefille, R., Verschuren, D., Gibert, E., Barker, P., 2002. Environmental changes in a tropical lake (Lake Abiyata, Ethiopia) during recent centuries. Palaeogeography, Palaeoclimatology, Palaeoecology 187, 233–258.

Marshall, M.H., Lamb, H.F., Davies, S.J., Leng, M.J., Kubsa, Z., Umer, M., Bryant, C., 2009. Climatic change in northern Ethiopia during the past 17,000 years: A diatom and stable isotope record from Lake Ashenge. Palaeogeography, Palaeoclimatology, Palaeoecology 279, 114–127. https://doi.org/10.1016/j.palaeo.2009.05.003

Marshall, M.H., Lamb, H.F., Huws, D., Davies, S.J., Bates, R., Bloemendal, J., Boyle, J., Leng, M.J., Umer, M., Bryant, C., 2011. Late Pleistocene and Holocene drought events at Lake Tana, the source of the Blue Nile. Global and Planetary Change 78, 147–161. https://doi.org/10.1016/j.gloplacha.2011.06.004

Stoops, G., 2003. Guidelines for Analysis and Description of Soil and Regolith Thin Sections.

Tiercelin, J.-J., Gibert, E., Umer, M., Bonnefille, R., Disnar, J.-R., Lézine, A.-M., Hureau-Mazaudier, D., Travi, Y., Keravis, D., Lamb, H.F., 2008. High-resolution sedimentary record of the last deglaciation from a high-altitude lake in Ethiopia. Quaternary Science Reviews 27, 449–467. https://doi.org/10.1016/j.quascirev.2007.11.002

Wagner, B., Wennrich, V., Viehberg, F., Junginger, A., Kolvenbach, A., Rethemeyer, J., Schaebitz, F., Schmiedl, G., 2018. Holocene rainfall runoff in the central Ethiopian highlands and evolution of the River Nile drainage system as revealed from a sediment record from Lake Dendi. Global and Planetary Change 163, 29–43. https://doi.org/10.1016/j.gloplacha.2018.02.003

Bibliography

Bird, E. C. F. (2008). *Coastal Geomorphology: An Introduction*. Wiley, Chichester, England ; Hoboken, NJ, 2nd ed edition. 22

Gasse, F. (1975). *L'évolution des lacs de l'Afar Central (Ethiopie et T.F.A.I.) du Plio-Pléistocène à l'Actuel. Recostitution des paléomilieux lacustres à partir de l'étude des Diatomées*. PhD thesis, Université de Paris VI, Paris. 33